Grant agreement no. 776479

COACCH

CO-designing the Assessment of Climate CHange costs

H2020-SC5-2016-2017/H2020-SC5-2017-OneStageB

D2.3 Impacts on infrastructure, built environment, and transport

Work Package:	2
Due date of deliverable:	M 22 (September/2019)
Actual submission date:	16/10/2019
Start date of project: 01/DEC/2017	Duration: 42 months
Lead beneficiary for this deliverable:	Global Climate Forum (GCF)
Contributors:	Daniel Lincke, Jochen Hinkel (GCF), Kees van Ginkel, Ad Jeuken (Deltares), Wouter Botzen, Max Tesselaar (VU), Enrico Scoccimarro (CMCC), Predrag Ignjacevic (VU)

Dissemination Level		
PU	Public	
CO	Confidential, only for members of the consortium (including the Commission Services)	
CI	Classified, as referred to in Commission Decision 2001/844/EC	

Disclaimer

*This project has received funding from the European Union's Horizon 2020 research and innovation programme under the Grant Agreement No **776479.***

Version log

Version	Date	Released by	Nature of Change
0.1	13/05/2019	Daniel Lincke (GCF)	First draft
0.2	20/08/2019	Daniel Lincke (GCF)	Finished GCF section on coastal impacts
0.3	24/09/2019	Daniel Lincke (GCF)	Preliminary version for internal review
1.0	07/10/2019	Daniel Lincke (GCF)	First public version
1.1	16/10/2019	Daniel Lincke (GCF)	Revised public version

Suggested citation:

Lincke, D., Hinkel, H., van Ginkel, K., Jeuken, A., Botzen, W., Tesselaar, M., Scoccimarro, E., Ignjacevic, P. (2018). D2.3 Impacts on infrastructure, built environment, and transport Deliverable of the H2020 COACCH project.

*This project has received funding from the European Union's Horizon 2020 research and innovation programme under the Grant Agreement No **776479.***

Table of Contents

*This project has received funding from the European Union's Horizon 2020 research and innovation programme under the Grant Agreement No **776479.***

Deliverable Summary

This document describes the impact assessment on infrastructure, built environment, and transport that has been conducted in order to inform the COACCH project. The assessment uses state-of-the art models for coastal and river flooding as well as a new model for flood impacts to transport networks and computer impacts for Europe at **higher spatial resolution** (NUTS2) compared to previous studies.

Future impacts (short-term to long-term) under **varying socio-economic scenarios** are computed for the RCP/SSP scenario combinations selected with stakeholders in WP1. In addition, coastal flood impacts are assessed for a high end scenario with global coastal average sea-level rise of 170cm until 2100, to illustrate the effects of such a very improbable, but not impossible, high end sea-level rise. For adaptation two different strategies have been analysed: a follow current pratice strategy and a no adaptation strategy where no (further) adaptation measures are taken.

Coastal floods can have most severe effects to infrastructure in the EU with expected **annual damages of €13 trillion (high end sea-level rise)** respectively €4.5 trillion (RCP 8.5), if no further adaptation measures are taken. However, i**nvestment into adaptation can reduce these impacts drastically** (two to three orders of magnitude), but adaptation to rising sea-level might cost between €15 billion and €40 billion every year in 2100.

For river flooding, this deliverable introduces local-level river flood damage model CLIMRISK-RIVER which is further integrated into CLIMRISK, a climate-economy IAM. The risk of river flooding in the EU is expected to rise from €9.5 billion in 2010 to between **€70-80 billion in 2080** for most assessed RCP-SSP scenario combinations. However, an extreme outcome may arise for a future development aligned with RCP8.5-SSP5, for which projections show expected **annual damage of €255 billion**. The results show significant spatial inequalities of river flood risk, stressing the importance of using local level river flood estimates in estimating the impacts of climate change for implementing timely local flood adaptation policies in the EU.

The deliverable further introduces the newly developed line-based model OsdaMage for assessing flood impacts to road infrastructure. By applying this model with river floods, we find that flood impacts to road infrastructure are in general 1-2% of the total flood damages. This shows that flood impacts to road infrastructure have been overestimated in previous studies.

*This project has received funding from the European Union's Horizon 2020 research and innovation programme under the Grant Agreement No **776479.***

1 Introduction

This document will assess climate risks due to increased coastal and river flooding for the infrastructure, built environment, and the transport sector according to the protocol defined in D1.6 using the scenarios defined in D1.5. European (and global) scale impacts and economic costs of rising sea-level and associated rising extreme water levels (storm surges) on the built environment will be assessed using the DIVA model. The assessment includes the impacts of gradual land loss due to submergence and erosion as well as the impact of increased damage to coastal built environment provoked by extreme sea-level events.

European scale impact and costs of river flooding on the built environment will be assessed by adding direct and indirect damages on built environment and infrastructure drawing from latest studies in this field (e.g. BASE, CLIMRISK) to the latest result from JRC's LISFLOOD-FP modelling. Main outputs are estimates of annual expected flooding damage in different scenarios, at resolutions ranging from 12 by 12 kilometre scale to NUTS2 level for Europe.

For road infrastructure, the traditional grid-based approach is complemented by a new object-based approach, in order to develop better damage estimates. For this purpose, also a new set of road-specific damage curves was developed. Main outputs are estimates of annual expected damages of river floods in different scenarios for infrastructure networks on a European scale. These results are available at the road segment level as well as aggregated on NUTS-3, and any higher NUTS aggregation level.

*This project has received funding from the European Union's Horizon 2020 research and innovation programme under the Grant Agreement No **776479.***

2 Methodology

2.1 Models overview

For the assessment of impacts of increased coastal flooding as a consequence of sea-level rise the DIVA model was used (Hinkel, 2014). River flooding was assessed using the models GLOFRIS (Ward et al., 2016; Winsemius et al., 2017) and LISFLOOD (Alfieri et al., 2016a, 2016b). In addition to the grid-based impact assessments with GLOFRIS and LISFLOOD, a new line-based impact model for road infrastructures is introduced (Koks et al., 2019), called OSdaMage. The main components of each model are outlined in Table 1.

Table 1: Main components of flood risk models in this deliverable

Lead	Model	Exposure units	Adaptation	Hazard	Output resolution	Output variables	Indirect economic damages (WP 3-4)
GCF	DIVA	Built environment (Incl. infra-structure)	Current protection + future protection (No further protection: keep dike heights, BAU protection: keep current practice)	Gradual loss of land due to SLR	NUTS2	Annual cost	Yes, together with UniGraz
				SLR + Coastal floods	NUTS2	EAD	
VU	GLOFRIS	Built environment (Incl. infra-structure)	Current protection, Keep dike heights, future protection	River floods	50*50km, and NUTS2	EAD	Yes, together with UniGraz
Delta-res	LISFLOOD + FIAT	Road infra-structures (grid-based)	Current protection + future protection (keep dike heights, keep protection level)	River floods	100*100m, NUTS3, NUTS2, country	EAD	
Delta-res	LISFLOOD + OSdaMage	Road infra-structures (line-based)	Current protection + future protection (keep dike heights, keep protection level)	River floods Proof-of-concept coastal floods	100*100m, NUTS3, NUTS2, country	EAD	Input for tipping point analysis (WP3)

2.2 DIVA

DIVA (Dynamic Interactive Vulnerability Assessment) is a global coastal impact model is used to produce impacts and cost projections at global and sub-global levels (Vafeidis et al., 2008; Hinkel and Klein 2009; Hinkel et al. 2013, 2014). DIVA is an integrated model of coastal systems that assesses biophysical and socio-economic impacts of SLR and socio-economic development. It includes a global database which represents the world's coasts (excluding Antarctica), using more than 12,000 linear segments with more than 100 parameters per segment. The DIVA model focuses on various aspects including coastal erosion impacts and adaptation (Hinkel et al., 2013), coastal wetland change (Spencer et al., 2016) and coastal flood impacts and adaptation (Hinkel et al., 2014).

*This project has received funding from the European Union's Horizon 2020 research and innovation programme under the Grant Agreement No **776479.***

DIVA has been used in numerous application and several EU projects (Impact2C, RISES-AM) to investigate the implications of sea-level rise.Earlier assessments by the World Bank and the Asian Development Bank include global analysis of flood impacts (Nicholls et al., 2010), protection cost (Nicholls et al., 2018), as well as regional scale analysis (East Asia, Nicholls et al, 2013) and national analysis (Kebede et al., 2010)).

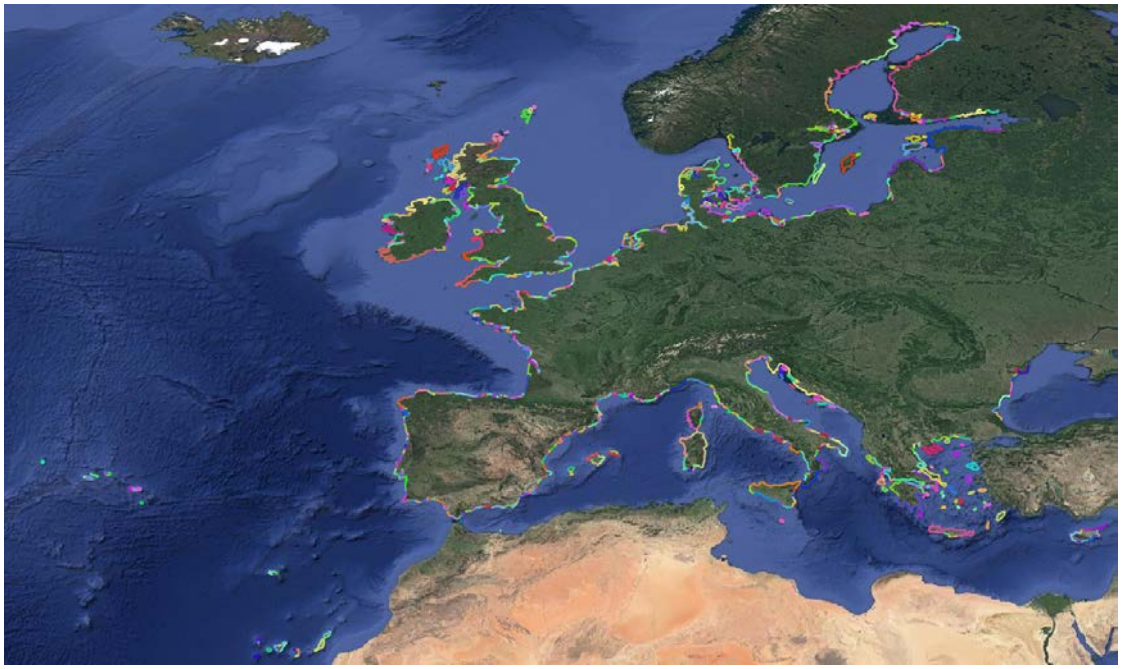

Figure 1: Coastline segments of the EU28 in the DIVA database.

DIVA is driven by climatic (sea-level rise) and socio-economic scenarios (drivers). The impact assessment comprises a number of modules representing physical processes and economic costings, as well as different adaptation strategies. DIVA divides the worlds coast into 12,148 segments with variable length but homogeneous characteristics, and is equipped with a database that contains about 80 biophysical and socio-economic parameters for each segment. Of these segments, 1,445 represent the coastline of the EU28 (Figure 1) with a total length of 52,800 km.

Here we will focus on flooding and protection against flooding. We use the same flood model as Hinkel et al. (2014). For each segment of the coastline a stylized model of the floodplain is generated (Figure 2). Flood risk is considered in terms of expected annual damage to assets, expected annual number of people flooded. Following (Messner et al., 2007) a logistic depth-damage function is applied to assets (giving the fraction of assets damaged for a given flood depth) with a 1-m flood destroying 50% of the assets. Adaptation costs in terms of the dike and other defence investments and the additional maintenance costs to maintain the new defences. The maintenance costs can be significant and are important to consider as it is important that such maintenance is included in long-term plans.

*This project has received funding from the European Union's Horizon 2020 research and innovation programme under the Grant Agreement No **776479.***

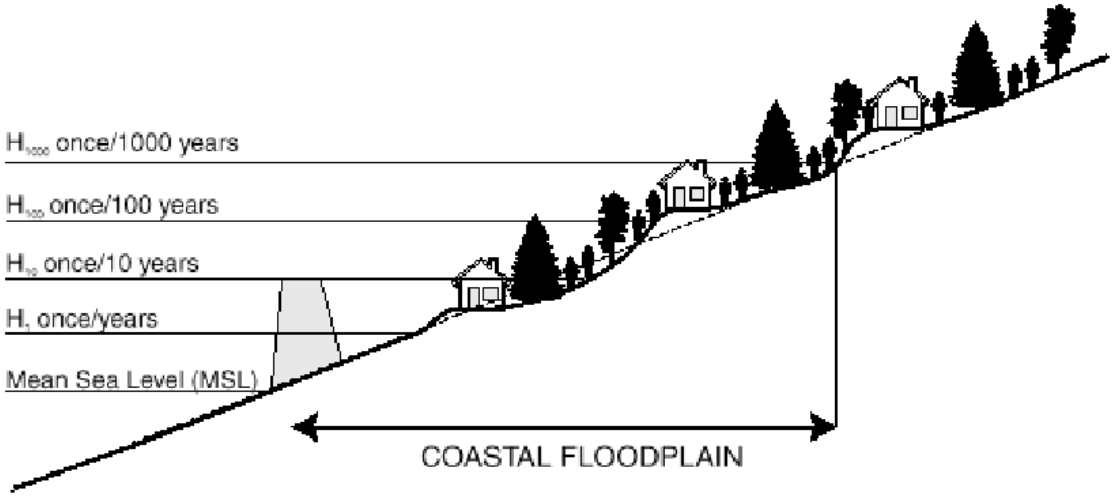

Figure 2: Stylized model of the floodplain as used in the DIVA model.

The datasets and assumptions that have been used to populate the database and to configure the stylized floodplain model are listed in Table 2.

Table 2: Datasets and assumptions that have been used to populate the coastline segment database for the simulations in this report.

Parameters/Module	**Assumption/Dataset**
Hazard (mean sea-level)	HadGEM-ES2 steric SLR and glacier melting, different ice-sheet (Greenland, Antarctica) melting assumptions
Hazard (extreme water levels)	GTSR (Muis,2016)
Exposure	SRTM 0.3*0.3 arcsec based elevation GRUMP based population GDPC based assets
Flood protection	Stylized assumption on existing protection (Sadoff,2015), Keep existing dike heights (No additional adaptation), Keep existing protection (BAU adaptation)
Vulnerability	Depth-damage functions (Hinkel,2014)

For adaptation, Hinkel et al. (2014) follow earlier studies, such as Hoozemans et al. (1993) and Nicholls (2004), and consider a common protection approach using (stylized) dikes. The initial DIVA approach to adaptation was based on a demand for safety function (Yohe and Tol, 2002) which attempts to model human behaviour based on empirical observation. As only limited data from very well protected areas is available to calibrate, this leads to future overprotection (Hinkel et al., 2014). Other protection strategies have been used within DIVA, such as cost-benefit-optimal protection (Lincke and Hinkel, 2018) or keeping the expected damages constant (Nicholls et al., 2018). However, here we apply the simpler model from (Sadoff,2015),

*This project has received funding from the European Union's Horizon 2020 research and innovation programme under the Grant Agreement No **776479.***

which captures the coastal essence of FLOPROS (Scussolini et al., 2016). Expert judgement protection levels for big urban agglomerations are combined with protection level estimates based on GDP per capita and population density for other regions.

2.3 GLOFRIS and LISFLOOD

In this deliverable, two river flood models are used: GLOFRIS and LISFLOOD. For LISFLOOD, both a grid based and an object-based approach (OSdaMage) are used. The differences between these models are described along the three components that determine flood risk: hazard, exposure and vulnerability (Table 3).

Table 3: Risk components of the GLOFRIS, LISFLOOD-grid, and LISFLOOD-OSdaMage models

Component	**GLOFRIS**	**LISFLOOD + grid based damage**	**LISFLOOD + object based damage (OSdaMage)**
Hazard (climate forcing)	EU-WATCH for baseline (Weedon et al., 2011). CMIP5 GCMs for future projections (Taylor et al., 2012)	Only baseline	EUROCORDEX (12 models)
Hazard (hydrology)	PCR-GLOBWB-DynRout (Van Beek & Bierkens, 2009; Van Beek et al., 2011) 1 * 1 km resolution	LISFLOOD-FP-2018 100 * 100 m resolution	LISFLOOD-FP-2018
Grid vs. object-based exposure	*Grid-based*	*Grid-based*	*Object-based (lines)*
Exposure	Urban density taken from HYDE database (Klein Goldewijk et al., 2011)	LUISA-2012 (Rosina et al., 2018) All land cover classes (section 3.2) and for road and rail infrastructures only (section 3.5)	OpenStreetMap (OpenStreetMap contributors, 2019) Only for road infrastructure
Flood protection	FLOPROS (Scussolini et al., 2016)	Updated FLOPROS (Jongman et al. 2014)	Updated FLOPROS (Jongman et al. 2014)
Vulnerability	JRC-damage functions (Huizinga, 2007, 2017)	JRC-damage functions (Huizinga, 2007, 2017)	New damage functions (only for road infrastructure)

GLOFRIS

Flood risk is generally estimated as an expected annual damage (EAD), as this provides a more average statistic for flood risk management than the absolute damage that occurs for a certain exceedance probability of a river. The EAD is calculated by taking the integral of the probabilities where protection standards are exceeded, multiplied by the damage that a certain exceedance level causes. This integral can be written as in equation 1, if the flood hazard extremes are determined

*This project has received funding from the European Union's Horizon 2020 research and innovation programme under the Grant Agreement No **776479.***

on an annual basis.

$$R = \int_{p=0}^{1} D\theta\,(p)dp \qquad (1)$$

In equation 1, R is the annual expected damage; D is an impact modelled for land inundation, which can consist of both direct and indirect damages, and specific flood characteristics such as duration, depth and extent, with an annual probability of exceedance *p*[1/T]; θ represents the vulnerability of an area to flood inundation, specifically determined by socio-economic factors which are fixed-in-time. Therefore, equation 1 contains the classic setup of flood risk as a combination of hazard, exposure and vulnerability. We will now explain in detail how each of these components is implemented in the GLOFRIS model cascade (Ward et al., 2017; Winsemius et al., 2016), which will be used for estimating the EAD for river floods in NUTS 2 regions in Europe under climate change and socio-economic scenarios. The GLOFRIS flood damage and EAD estimates serve as input in other COACCH tasks, including the integration of river flood risk in the Integrated Assessment Model CLIMRISK (see section 2) and for analyses with the Dynamic Integrated Flood Risk and Insurance (DIFI) Model for work packages 3 and 4.

Flood hazard

It can be seen in Figure 3 that most steps in the GLOFRIS model cascade are to determine the hazard component of the EAD. All steps above the impact modeling are included for this purpose. The model simulates river discharge levels that occur with certain probabilities, which are expressed as return periods (2, 5, 10, 25, 50, 100, 250, 500 and 1000 years). For the baseline flood risk, the daily water level per river basin corresponding to each return period is estimated by forcing PCR-GLOBWB (Van Beek & Bierkens, 2009; Van Beek et al., 2011), using yearly time-series data of maximum flood volumes for 1960-1999, which are taken from the EU-WATCH project (Weedon et al., 2011). Then, for each cell a Gumbel distribution is fitted through this time-series, in order to estimate flood volumes for the selected return periods.

For future flood hazard projections, the GLOFRIS framework can be run with bias corrected meteorological data from the CMIP5 Global Circulation Models (Taylor et al., 2012), as provided by the ISIMIP project (Hempel et al., 2013). Each of these models are compatible with representative concentration pathways (RCPs), which depict developments of greenhouse gas concentrations in the atmosphere (van Vuuren et al., 2011). Similar to deriving the baseline flood risk, future projections are based on averages over 40-year time slices (i.e. 2010-2049 for 2030; 2030-2069 for 2050; 2060-2099 for 2080).

Impact modeling

The previously derived flood hazard is combined with exposure and vulnerability data in order to derive the potential impact of flooding (UNISDR, 2015). Included impacts are, amongst others, the affected population and GDP, and urban exposure, which is determined as the fraction of each grid cell with urban land cover.

*This project has received funding from the European Union's Horizon 2020 research and innovation programme under the Grant Agreement No **776479.***

To estimate the exposure to flood hazard, the urban density data for the baseline is taken from the HYDE database (Klein Goldewijk et al., 2011), which contains the urban fractions of each grid cell. Each grid cell is then assigned the economic value of assets depending on national GDP per capita in 2010 (van Vuuren et al., 2007). Note that the baseline for socio-economic data is 2010, whereas the estimated baseline for flood hazard is centered around 1980. As the GLOFRIS baseline is 2010, the assumption is made that flood hazard remained more or less constant over the period 1980-2010, which is a necessary choice as a result of data limitations regarding the EU-WATCH project. Future developments in urban densities and asset values are projected in the IMAGE model (Stehfest et al., 2014), which uses data from the Shared Socio-Economic Pathways (SSPs) (Riahi et al., 2017) taken from IIASA's SSP database. Future economic values of urban areas are then estimated by multiplying the projected urban population with the national per capita GDP, also taken from the SSP database.

The potential damage a flood event can cause for each urbanized grid cell is then computed based on modeled inundation depth, urban density, economic value, and global flood depth-damage functions per occupancy type taken from Huizinga et al. (2017). The global flood depth-damage functions consist of stage-damage curves, and account for the vulnerability of assets to floods of various depths. The included stage damage functions are based on the JRC global functions database (Huizinga et al., 2017), which are differentiated per continent.

Finally, a flood can only occur when river discharge levels exceed the protection standards, i.e. when a dike is supposed to withstand water levels of a 100-year return period, water levels associated with a 50-year return period cannot cause flooding. In GLOFRIS, the protection standards are taken from the modeling layer of the FLOPROS dataset (Scussolini et al., 2016), which offers protection standards on a regional scale. For the results shown in section 3, flood protection standards are assumed to remain constant, which means that for regions where flood hazard increases in the future, the dike heights are raised accordingly to keep the flood hazard constant, whereas for regions where flood hazard decreases, the flood protection standards will be higher in the future.

Based on the previous, an exceedance probability curve can be constructed, where for each of the return periods the associated expected damage is plotted. The EAD can then be determined as the area under this curve, where it is cut off at the regional protection standard in place.

LISFLOOD

The LISFLOOD model combined with the grid-based damage assessment is roughly similar to the GLOFRIS model. The most important differences (for the model implementations in this study) are:

- The river discharges in LISFLOOD are derived from observed discharges from 1990-2016, whereas the GLOFRIS discharges are based on observations from 1960 to 1999

*This project has received funding from the European Union's Horizon 2020 research and innovation programme under the Grant Agreement No **776479.***

- The inundation module of LISFLOOD simulates inundations on a 100 by 100 m^2 resolution, whereas GLOFRIS simulates inundations on a 1 by 1 km^2 resolution.
- LISFLOOD does not calculate new inundation maps for each combination of RCP, evaluation year and climate model. Instead, it locally shifts the likelihood of the inundations of the 5 * 5 km^2 hydrological model (Alfieri et al., 2015) for each combination.
- LISFLOOD calculates the grid-based damage over all LUISA land use classes (results in section 3.2) whereas this implementation of GLOFRIS only calculates the damage to urbanized areas. In addition, we present results of LISFLOOD and LUISA where we only report the grid-damage to road infrastructures, as well as the impacts as estimated with the new line-based OSdaMage model (results in section 3.6).

2.4 CLIMRISK-RIVER

Integrated assessment models (IAMs) of climate and the economy are commonly used to project the future economic impacts of climate change and to assess the benefits of climate policy aimed at reducing the greenhouse gas emissions. Nevertheless, such models have received various criticisms, including those related to the aggregated spatial dimension of the models, the incomplete representation of climate change risks, and the fact that the damage functions that translate global warming into economic impacts are outdated and require improving.

We improve upon the estimates of the economic impacts of climate change by developing a river flood risk model CLIMRISK-RIVER and introducing it into an existing climate-economy integrated assessment model. Figure 4 gives the conceptual structure of the CLIMRISK-RIVER model. It operates on a local scale and can project climate change-related river flood damage for various socioeconomic, climate and flood adaptation scenarios. CLIMRISK-RIVER consists of river flood damage functions on a 0.5° *0.5° grid cell level that cover the entire globe. In addition, it accounts for local human adaptation through the use of recently developed local flood protection standard data. The flood damage function estimates allow the user to explore the local river flood impacts of climate change for any user defined climate change and socioeconomic scenario.

*This project has received funding from the European Union's Horizon 2020 research and innovation programme under the Grant Agreement No **776479.***

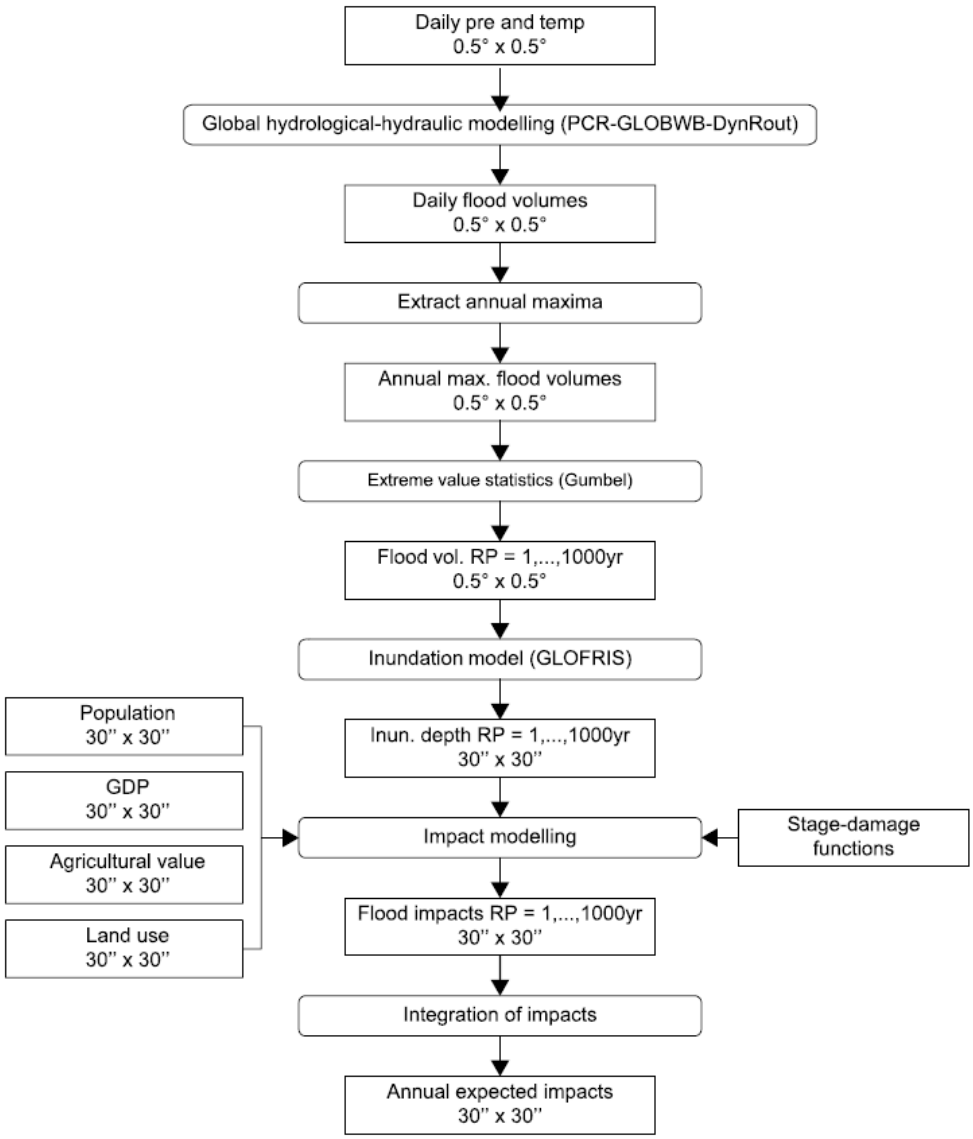

Figure 3: flowchart of the main dataflow and models used in GLOFRIS

The main goal in developing CLIMRISK-RIVER is to produce validated damage functions for different protection standard assumptions that can be fed with temperature, precipitation and GDP estimates from any climate or socioeconomic scenario combination. The input for the flood risk model is based on the GLOFRIS model (see 3.3), a global framework for flood risk assessment that works on a detailed spatial scale 30" * 30" and includes all main river basins worldwide (Winsemius et al., 2016). The main ingredients of the new flood damage functions for CLIMRISK-RIVER are as follows:

- **Risk**: Expected annual damage (EAD), as explained in the subsection **GLOFRIS**
- **Vulnerability**: Flood protection standards
- **Hazard**: Climate projections
- **Exposure**: Economic projections

*This project has received funding from the European Union's Horizon 2020 research and innovation programme under the Grant Agreement No **776479.***

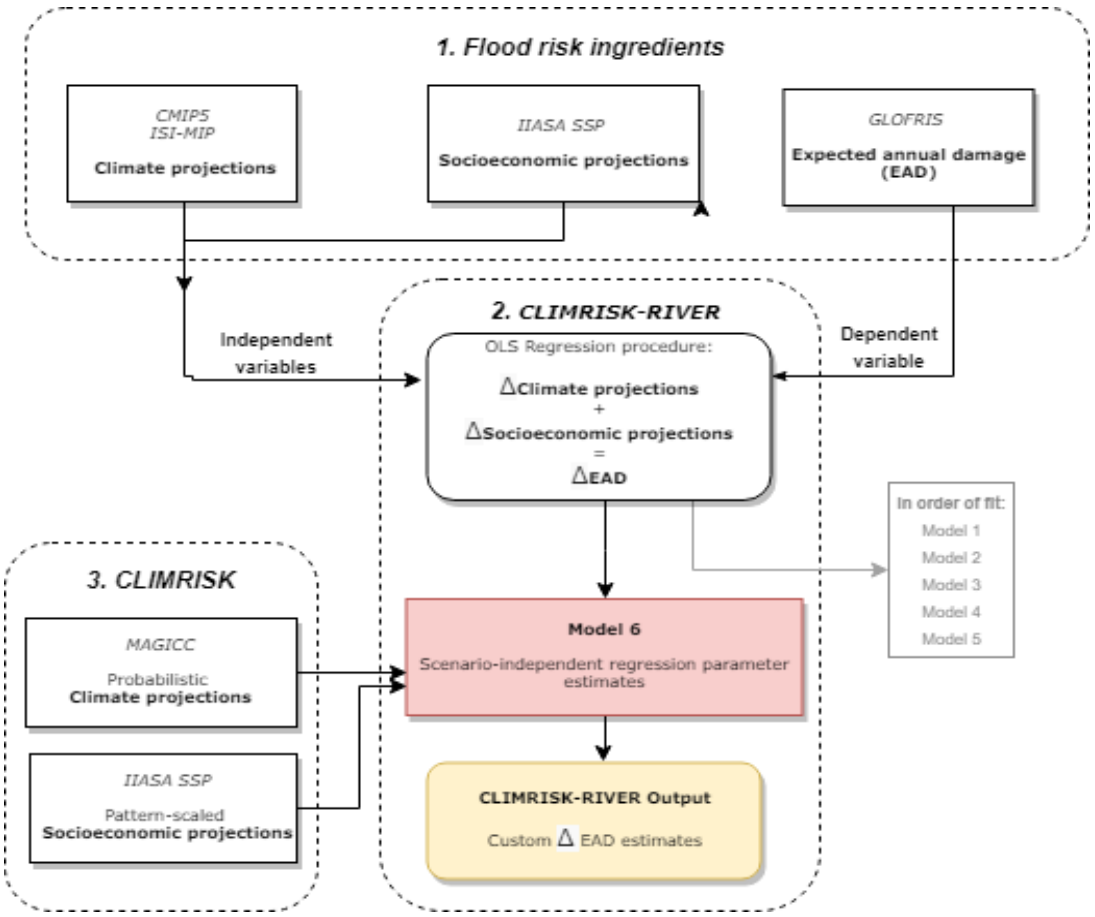

Figure 4: Structure of the CLIMRISK-RIVER model

Vulnerability: Flood protection standards

To obtain more reliable estimates of annual expected river flood risk, the current flood protection standards must be taken into account. The flood protection standards enter the flood risk model through the EAD function whereby damages of rivers with return periods lower than the available protection standards are assumed to be zero.

A comprehensive global database - **FLOPROS** - of observed and modelled current river protection standards has recently been compiled (Scussolini et al., 2016). The flood protection data are available at the state level and any given cell receives protection equal to its estimated state protection level. The river protection data are currently available for 2,683 states in the world in the form of river return periods against which the state is protected. However, in estimating the annual expected flood damage in the future, we also need estimates of future flood protection standards that depend on adaptation decisions about flood protection investments. The FLOPROS data consists of two dimensions:

*This project has received funding from the European Union's Horizon 2020 research and innovation programme under the Grant Agreement No **776479.***

- **Current Height Standards** (*BaselineStd*), which assume that the protection standards are maintained at the baseline *height* in the future and allow the river flood risk to vary over the course of the century. This scenario does not imply any additional river flood adaptation.
- **Current Level Standards** (*CurrentStd*), which assume that the protection standards are maintained at the baseline *level* in the future, keeping the flood probability constant. This scenario does imply additional river flood adaptation as the flood protection standards are upgraded according to the varying natural factors in order to maintain constant flood probability. Regardless of the constant flood probability, the flood-related damage could still vary with the amount of exposed assets and the severity of flooding.

Hazard: Climate Projections

As in many climate IAMs, surface air temperature is among the primary climate variables of interest and serves as the main proxy for climate change. We are also interested in the effect of precipitation on the river flood risk. Precipitation has, until now, not been introduced into an IAM damage function and it is important to assess its relative impact on river flood risk in light of newly available local precipitation data.

Whereas the climate forcing data in CLIMRISK is generated through MAGICC with the use of pattern scaling, the forcing data in GLOFRIS contains daily gridded estimates of surface temperature and precipitation. These are generated using different ESMs, interpolated to 0.5° * 0.5°, and they are bias corrected using observations from 1960 to 1999 for the EU-WATCH project. These same estimates are then used to force the PCR-GLOBWB global water and hydrological model (Sutanudjaja et al., 2017). The EU EU-WATCH forcing observations are also used to generate the baseline flood risk. To create the climate input variables necessary for the river flood damage functions, daily temperatures were converted to annual mean temperature and daily precipitation to total annual precipitation. Since the GLOFRIS model produces estimates for three periods centered around years 2030, 2050 and 2080, mean annual surface temperature and total annual precipitation estimates were averaged over the years 2010-2050, 2030-2070 and 2060-2100. Finally, differences of precipitation and temperature with respect to the baseline period average climate were taken in order to fit the MAGICC climate projection units. For temperature, the difference is expressed in absolute value of ℃ while for precipitation, the percentage change of precipitation with respect to baseline period is required.

Exposure: Economic Projections

Exposure, for which we use GDP as proxy, is another important determinant of total flood damage because it captures the extent of assets that are prone to flooding. The

*This project has received funding from the European Union's Horizon 2020 research and innovation programme under the Grant Agreement No **776479.***

GDP data used to estimate the flood damages in GLOFRIS are also derived from the IIASA SSP Database (Riahi et al., 2017).

The GDP estimates are a subset of the IIASA SSP database, and they were used to generate the GLOFRIS estimates and are, for the sake of consistency, required for generating the flood damage functions. The scenarios used include SSP1, SSP2, SSP3, SSP4 and SSP5 estimates for years 2010, 2030, 2050 and 2080.

Damage Functions

An important step in CLIMRISK-RIVER development is the formulation of the flood damage functions which depend on model resolution and included dependent and explanatory variables. The model scale refers to the area that a particular damage function coefficient covers. Depending on input data availability, the scale can range between highly local 30”×30” grid cells and global. The primary candidates for the model scale in CLIMRISKRIVER are 0.5˚×0.5˚ grid cell and river basin level. The main advantage of basin level functions is simplicity. The main disadvantage, however, is the loss of model fit as heterogeneous grid cell data are aggregated into a single function over a potentially large basin area. The opposite is true of a grid cell level function. As we prefer the higher explanatory power of the grid cell level functions over the smaller total number of function estimates, we set the scale to grid cell level to make full use of local input data. The scale of results is still entirely up to the user who can explore various scenario combinations at different levels of aggregation.

The next step concerns the choice of the dependent and explanatory variables. The main goal of the regressions that follow is to project the ΔEAD_t, that is, the difference in EAD of cell between any given year t and the baseline. We opted for the difference in EAD over absolute EAD because we are only interested in the impact of climate change-related flood risk and therefore must control for the baseline flood risk that is inherently present in the model. However, the EAD estimates in GLOFRIS represent the absolute expected annual damage within a certain 40-year period, and therefore we must therefore express the EAD estimates as differences with respect to the baseline period EAD. This means that ΔEAD_0 refers to 1980 and is zero for all cells. For the available data, t represents a time period mid-point for which the GLOFRIS estimates were made, namely, $t \in [2010,2030,2050,2080]$. Six models, labelled as Models 1-6, are evaluated as CLIMRISK-RIVER candidates (Figure 5).

*This project has received funding from the European Union’s Horizon 2020 research and innovation programme under the Grant Agreement No **776479.***

1. $\Delta EAD_{GF,t} = \beta_1 \Delta GDP_t$
2. $\Delta EAD_{GF,t} = \beta_1 \Delta GDP_t + \beta_2 \Delta T_t$, where $\Delta T_{i,j,t}$ represents the difference between temperature in year t and 2010.
3. $\Delta EAD_{GF,t} = \beta_1 \Delta GDP_t + \beta_2 \Delta T_t + \beta_3 \Delta T_t^2$
4. $\Delta EAD_{GF,t} = \beta_1 \Delta GDP_t + \beta_2 \Delta T_t + \beta_3 \Delta T_t^2 + \beta_4 \Delta P_t$, where $\Delta P_{i,j,t}$ represents the difference in between precipitation in year t and 2010
5. $\Delta EAD_{GF,t} = \beta_1 \Delta GDP_t + \beta_2 \Delta T_t + \beta_3 \Delta T_t^2 + \beta_4 \Delta P_t + \beta_5 \Delta P_t^2$
6. $\Delta EAD_{GF,t} = \beta_1 \Delta GDP_t + \beta_2 \Delta T_t + \beta_3 \Delta T_t^2 + \beta_4 \Delta P_t + \beta_5 \Delta P_t^2 + \beta_6 \Delta T_t \Delta P_t$, where $\Delta T_{i,j,t} \Delta P_{i,j,t}$ represents the interaction term between temperature and precipitation change.

Figure 5: CLIMRISK-RIVER candidates

The best performing model selected as the final **CLIMRISK-RIVER** model is Model *6*:

$$\Delta EAD_{GF,t} = \beta_1 \Delta GDP_t + \beta_2 \Delta T_t + \beta_3 \Delta T_{t2}$$

$$+\beta_4 \Delta P_t + \beta_5 \Delta P_{t2} + \beta_6 \Delta T_t \Delta P_t$$

where β_1 is the effect of a $1 billion increase in GDP, ΔGDP_t is the difference in GDP between year t and 2010, β_2 is the effect of a 1° C increase in surface air temperature, ΔT_t represents the difference in mean surface air temperature between the 40-year period centered around t and 1980, β_3 is the squared term of surface air temperature, ΔT_t^2 is the difference in squared surface air temperature between the 40-year period centered around t and 1980, β_4 is the effect of a 1% increase in total annual precipitation, ΔP_t is the percentage difference in the 40-year mean of total annual precipitation between the period centered around year t and 1980, β_5 is the squared term of total annual precipitation, ΔP_t^2 is the percentage difference in the 40-year mean of total squared annual precipitation between the period centered around year t and 1980, β_6 is the effect of a 1% increase in total annual precipitation conditional on a 1° C increase in surface air temperature and $\Delta T_t \Delta P_t$ is the interaction term between difference in mean surface air temperature and the percentage difference in mean total annual precipitation between the period centered around year t and 1980.

This model was selected so as to take advantage of the explanatory power of precipitation when estimating EAD. Precipitation could capture the effect that wetter (or drier) regions could have on frequency of flooding. In addition, the interaction between temperature and precipitation could capture the interaction between, for example, hotter and wetter regions both of which could lead to an increase in flood risk higher than estimated by temperature and precipitation alone.

This functional form is similar to the RICE damage form, where quadratic climatology terms are used to capture extreme effects of high temperature. There is no constant

*This project has received funding from the European Union's Horizon 2020 research and innovation programme under the Grant Agreement No **776479.***

term in the regression as the function passes through the origin, and the left and right side terms are zero in the baseline year. The specific units for temperature and precipitation explained above were selected so as to match the MAGICC model output. MAGICC generates differences in annual surface temperature in degrees Celsius and percentage difference in annual precipitation with respect to any particular base year.

2.5 CLIMRISK

The flood risk model CLIMRISK-RIVER (CLIMRISK-RIVER) can be introduced into any climate-economy IAM that operates on a local 0.5˚ × 0.5˚ or larger scale. For our purposes, we have chosen to integrate it into the existing CLIMRISK model (Estrada & Botzen, 2018). CLIMRISK is a global model that assesses the dynamic economic impacts of climate change at the local scale (0.5˚x0.5˚) for various socioeconomic and climate change projections. This is done by combining local GDP exposure information with climate projections obtained using pattern scaling of the MAGICC/SCENGEN climate model (Meinshausen et al., 2011). Regional impact functions are derived from RICE model estimates of the GDP impacts of temperature changes and encompass a broad range of economic sectors. The result is a global, dynamic, integrated assessment model that projects climate damages on a local, regional and global scale. CLIMRISK makes use of similar inputs present in CLIMRISK-RIVER:

1. **Risk:** Economic impacts
2. **Hazard:** Climate projections
3. **Exposure:** Economic projections

Risk: Economic Impacts

CLIMRISK relies on the regional damage functions originally developed in the RICE model (Nordhaus & Yang, 1996), with improved estimates in the recent years (Nordhaus, 2017). These regional damage functions encompass a broad range of economic impacts. Following the RICE model, the impact functions take into account the losses suffered by major economic sectors such as agriculture but also the cost of sea-level rise, adverse impacts on health, non-market damages and catastrophic damages (Nordhaus, 2014). The damage function in CLIMRISK is as follows:

$$D_{r,t} = \alpha_r T_t + \beta_r T_{t2}$$

where α_r and β_r represent the regional temperature coefficients that measure the impact of global temperature increase (in degrees Celsius) on climate related regional economic damage, $D_{r,t}$, measured in billions of dollars (2015 PPP).

When converted to a grid cell level, the regional damage function becomes local:

$$D_t = \alpha_r T_t + \beta_r T_{t2}$$

where α_r and β_r represent the regional temperature coefficients that measure the impact of local temperature increase on climate related local economic damage D_t in

*This project has received funding from the European Union's Horizon 2020 research and innovation programme under the Grant Agreement No **776479.***

cell . T_t is the difference in temperature in the cell in year t with respect to the baseline year, 1900. The total economic impacts of climate change in year t in cell are therefore I_t:

$$I_t = Y_t D_t S_{r,t}$$

where Y_t represents the projected output for cell in year t and $S_{r,t}$ represents the scaling factor that ensures that projected damages are exactly the same regardless of whether the regional damage functions are driven by global or grid cell temperatures.

In addition to the local impacts based on the RICE damage functions, CLIMRISK also introduces urban damages into the model. Urban areas are likely to experience higher damage due to climate change than non-urban areas as output tends to be more concentrated in an urban environment. Since the grid cell scale is still likely to cover an area larger than a particular urban city, the total output in an urban cell is divided between the non-urban (20%) and urban (80%) part of the cell. The damage function for the non-urban part of a particular urban cell follows the general CLIMRISK damage function given above, whereas the urban part of the urban cell follows the following function:

$$D_t^{T,U} = 0.9(\frac{T_t + U_t}{2.5})^2$$

where T_t and U_t represent changes in annual temperature in each grid point due to global and local climate change, respectively. The combined damage from the non-urban and urban part of the urban cell represents the total expected damage for that cell in a given year *t*.

Hazard: Climate projections

For the global and regional probabilistic estimates of climate change, CLIMRISK uses the MAGICC version 6 software (Meinshausen et al., 2011). MAGICC represents a reduced-complexity model of climate change and is widely used in the research community to project future climate impacts. It also relies on the technique of pattern scaling to produce local estimates of temperature and precipitation change. The MAGICC projections used in CLIMRISK are the difference in annual mean temperatures (in degrees Celsius) and precipitation (in mm) with respect to 1900. CLIMRISK imposes a triangular probability distribution for the climate sensitivity parameter. This particular distribution is centered around a lower limit of 1.5°C, an upper limit of 4.5°C and a mean value of 3°C for climate sensitivity (Stocker et al., 2013). The triangular distribution of temperatures is the source of uncertainty in the CLIMRISK model and by representing it using a probability distribution the IAM is able to produce estimates that encompass the likely ranges of change commonly found in the literature. As precipitation realizations directly depend on temperature realizations in MAGICC, the triangular distribution covers both climate variables in the model. In this report, only the median (50^{th} percentile) realizations are used for all scenario combinations. Finally, CLIMRISK also accounts for the Urban Heat Island (UHI) effect whereby the urban areas experience higher local temperatures due to

*This project has received funding from the European Union's Horizon 2020 research and innovation programme under the Grant Agreement No **776479.***

climate change than rural areas (Estrada et al., 2017).

Exposure: Economic projections

The economic projection data in CLIMRISK is the same as in CLIMRISK-RIVER. Please refer to the CLIMRISK-RIVER subsection for more information on how this data is constructed.

2.6 LISFLOOD-OSdaMage

Stakeholders involved in the COACCH codesign process expressed a strong interest in transport impacts of climate change (COACCH Deliverable 1.3). Traditional grid-based approaches to flood risk modelling give little insight in the network properties of road disruptions. Therefore, for the COACCH project, Deltares developed an object-based, continental scale flood risk model for European road infrastructure: OSdaMage, building on a model proposed by Koks et al. (2019). The results of this object-based model will be compared to the results of the 'traditional' grid-based models (Figure 6). The focus of this section will be on introduction of the new object-base model.

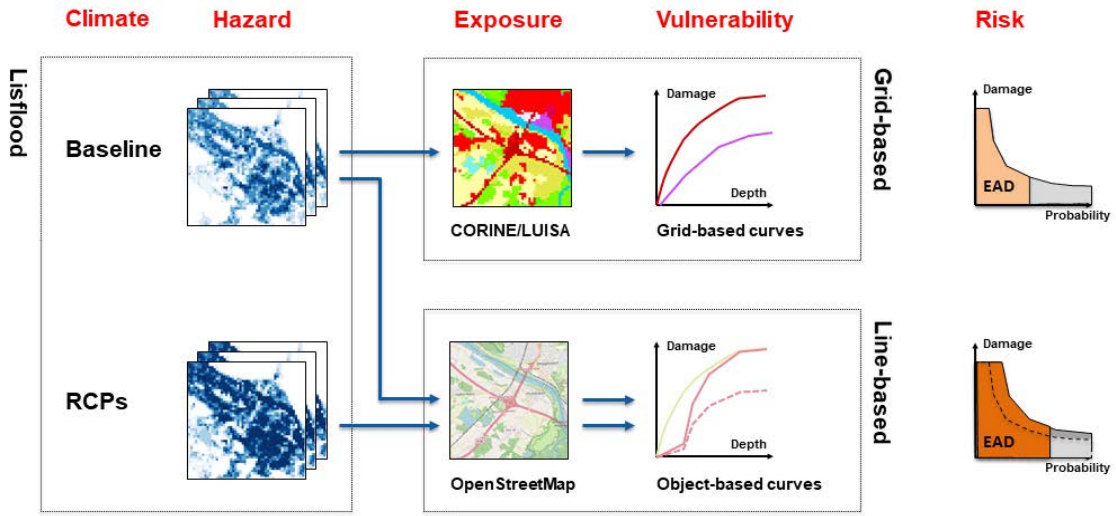

Figure 6: Flood risk using a grid-based and object (line)-based approach

Background and motivation

In the last decade, the field of continental and global scale river flood risk models rapidly developed. These models, such as the aforementioned Lisflood and GLOFRIS, are typically grid-based. First, grid cell inundations are calculated using hydrologic or hydraulic routing procedures. Then, these inundation maps are overlaid with land cover maps, such as the LUCAS, CORINE or LUISA land cover maps for Europe (Figure 7). For each land cover type, typical percentages of land use are tabulated. For example, a residential area has 70% of buildings, 20% of roads and 10% of green recreational spaces. Damage per grid cell is typically calculated using a depth-damage

*This project has received funding from the European Union's Horizon 2020 research and innovation programme under the Grant Agreement No **776479.***

curve. This curve relates the water depth to an expected amount of damage, for each land use type (Figure 8).

Although these grid-based impact models have been very useful for providing continental and global scale risk analysis, they fall short in representing damage to transport infrastructure (Jongman et al., 2012). The grid-based approaches try to estimate the (potential) percentage of infrastructure land use in each grid cell. However, transport network infrastructure such as roads or railways are relatively narrow line elements and take only a small percentage of the grid sizes typical for continental scale modelling: 1 by 1 km^2 (GLOFRIS) or 100 by 100 m^2 (LISFLOOD).

Another disadvantage of grid-based approaches is the loss of the network character of transport networks when rasterizing road or rail datasets. This deprives the modeller of the possibility to study cascading effects of infrastructure disruptions, whereas these might be highly relevant. In many cases, the economic effects from reduced accessibility of regions and passenger and freight delays costs exceed the direct asset losses by far. In contrast, object-based models create the opportunity to study these network effects on top of the assessment of direct asset losses. An additional benefit of object-based modelling is that the object-specific metadata can be used to improve the damage estimate. For example, for estimating damage to roads it is highly relevant to know the road type (e.g. motorway, secondary road, track) and the number of lanes (e.g. 2*4 motorway or 1.5 lane rural road). Also, for each intersection between a road and an inundated grid cell, one wants to know whether one is dealing with unintentionally flooded road, or with a bridge. In the case of a bridge, there very well could be no damage at all. A final example is the of metadata on road electrification (lighting, signalling) available in some datasets, which can be used to reflect the very different road designs between countries. Motorway designs in densely populated and prosperous regions may be much more sophisticated than motorway designs in remote rural areas, which has a large impact on potential damage during flood events.

In earlier days, the grid-based approach could be justified by incomplete vector datasets such as road and rail networks and lacking computational power to take a more detailed approach. However, vector-based dataset such as OpenStreetMaps are now nearly complete, and computational power does not have to be a limiting factor anymore. For continental scale modelling, one could with some effort structure the risk assessment as an ‘embarrassingly parallel’ computational problem, so that it can be solved using state-of-the-art parallel processing techniques. This technique is applied in the OSdaMage model.

Study set-up

Figure 6 gives a stylized overview of the difference between a raster-based and vector based approach to flood risk modelling. Risk is defined as the combination of hazard, exposure and vulnerability. Flood hazard maps for the baseline scenario and

*This project has received funding from the European Union’s Horizon 2020 research and innovation programme under the Grant Agreement No **776479.***

different RCPs are created using the JRC-LISFLOOD model. In a traditional grid-based flood risk assessment, exposure is derived from a land use raster whereas vulnerability per land cover type is described by damage curves. Risk (usually in terms of expected annual damage) can be calculated by integration over the damage estimates from floods with different return periods (i.e. likelihood of flood occurrence). Such an assessment can be done using a tool like Delft-FIAT[1].

In the OSdaMage model, the exposure rasters are replaced by the vector dataset of roads, drawn from OpenStreetMap[2]. To enable a fair methodological comparison with the traditional raster-based approaches, one model run is done where the raster damage curves (Huizinga et al., 2007, 2017) are translated to a vector representation by multiplication the raster damage (€/m^2) by road width (m) to obtain a unit road length damage curve (€/km). This is referred to as the adapted Huizinga (HZ*) function. However, for this study, also a new set of damage curves is developed, which makes benefit of the additional metadata on road type, lane number, presence of bridges and road lighting.

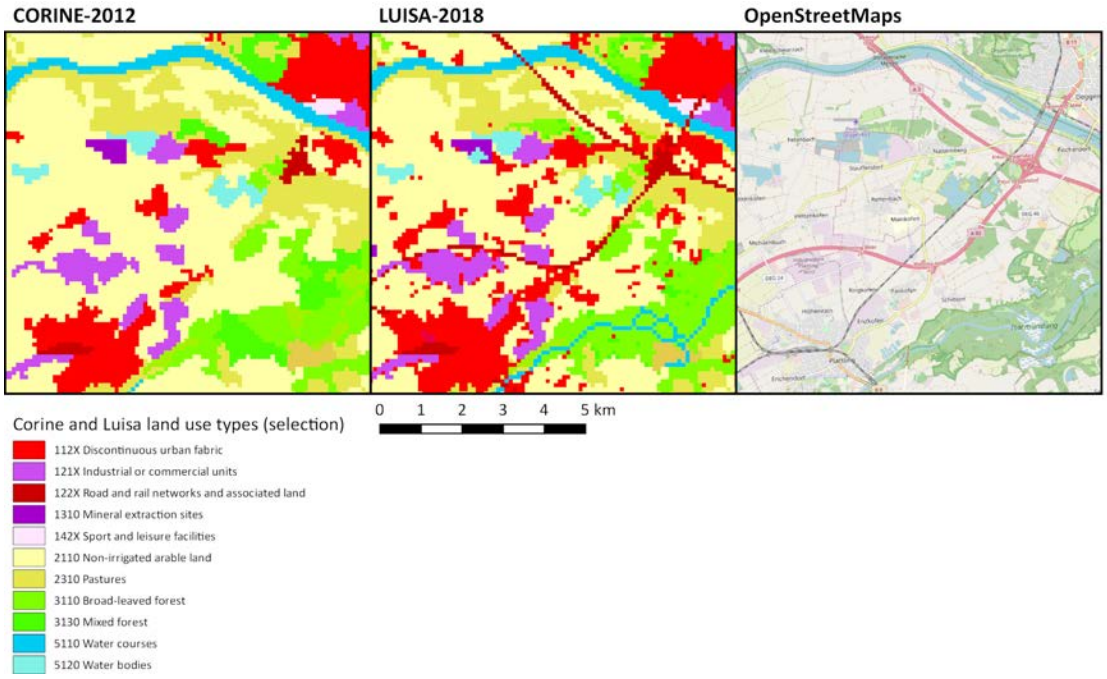

Figure 7: Comparison of CORINE, LUISA and OpenStreetMap land cover maps

Stylized overview of model

The method used for OSdaMage elaborates on the Global Multihazard Transport Risk Analysis (GMTRA) model by Koks et al. (2019, the Python code of which is freely

[1] Slager and Wagenaar (2016). Delft-FIAT documentation (webpage). https://publicwiki.deltares.nl/display/DFIAT/Delft-FIAT+Home (last accessed on May 24, 2019)

[2] OpenStreetMap (2019). Online database. (last accessed on May 24, 2019)

*This project has received funding from the European Union's Horizon 2020 research and innovation programme under the Grant Agreement No **776479.***

available on GitHub[3]. OSdaMage has three key-components (Figure 8). First, a pre-processing step where the (very large) OSM planet file is split in small chunks. For this particular European implementation we split the so-called OSM 'Europe dump file' (OpenStreetMap Contributors, 2019) on the level of NUTS-3 regions (~1330 extracts). The second component is the main model, which runs in parallel for the individual NUTS-3 extracts. The main model fetches and simplifies the road network from the extracts, intersects all individual road segments with the flood hazard maps, and calculates the damage for each return period. The third component is a post-processing step, where the results of the individual extracts are reassembled, GDP correction is done and the expected annual damage is calculated.

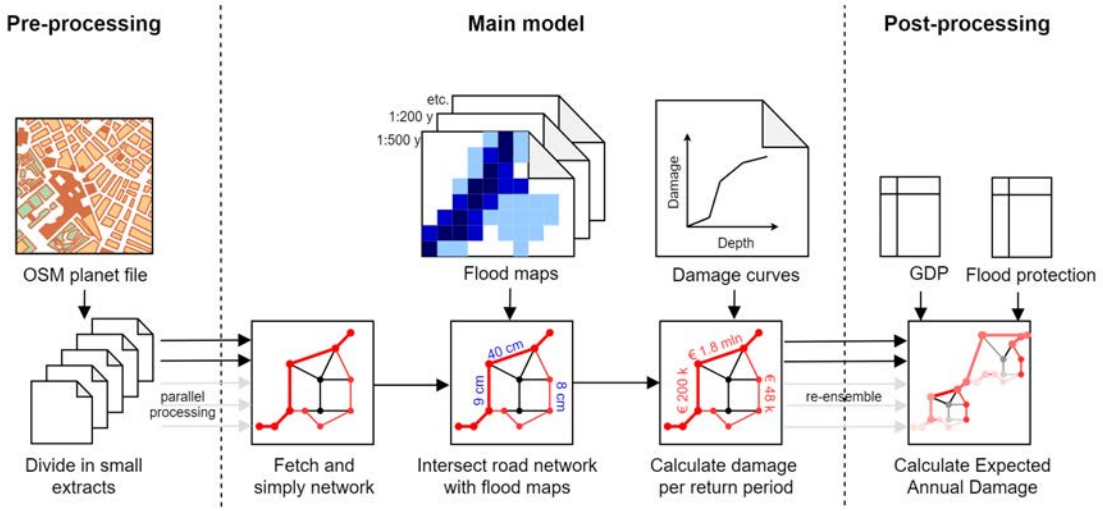

Figure 8: stylized overview of the OSdaMage model

Pre-processing

The pre-processing step is similar to Koks et al. (2019) GMTRA-model, as documented on GitHub[4] . The only difference is that for this study, we extracted small chunks of the OSM 'Europe dump file' of 7 january 2019 (OpenStreetMap Contributors, 2019), on the NUTS-3 level using the NUTS-2016 classification from EUROSTAT[5]. The results of this extraction are saved in the .osm.pbf file format.

Additionally, we calculated the most frequent number of lanes per road type per EU member state, to complete any missing lane data during the damage estimations.

Main model

[3] Koks, E. (2019). Global Multihazard Transport Risk Analysis. Open-source code on https://github.com/ElcoK/gmtra.

[4] Koks, E. (2019). Global Multihazard Transport Risk Analysis. Open-source code on https://github.com/ElcoK/gmtra. Preprocessing documentation on: https://github.com/ElcoK/gmtra/tree/master/docs/source

[5] European Commission (2019). EUROSTAT. https://ec.europa.eu/eurostat/web/nuts/background

*This project has received funding from the European Union's Horizon 2020 research and innovation programme under the Grant Agreement No **776479.***

The parallel processing activities of the model are coordinated by main.ipynb. This script basically only calls the function region_loss_estimation for individual region extracts.

The function Region_loss_estimation structures the loss estimation for one region:
First, it calls fetch_roads which fetches the road network from the .osm.pbf file. Then it calls cleanup_fetch_roads which corrects shortcomings of the preprocessing step (erratic clipping of NUTS-3 regions completely surrounded by other NUTS-3 regions and cutting roads that extent over the NUTS-3 region to avoid double accounting). Next, the road geometries are simplified to 0.00005 degree, which is less than 5 m for Europe. Then, the infra type metadata of OSM is simplified to 7 main categories (motorways, trunks, primary roads, secondary roads, tertiary roads, other roads, tracks), using settings defined in the Excel sheet Mapping_maxdamage_curves.xlsx.
Then, it masks and vectorizes the six flood rasters using create_hzd_df.
Now, the script iterates over all the road segments and calculates the intersections using intersect_hazard. This adds the following data to each road segment: total length; inundated length; average water depth over the inundated part.
Before moving to the loss calculation, the script corrects for any missing lane-metadata. For any road for which the number of lanes is not known, the mode (most frequently occuring) number of lanes per road type is used.
Now the script again iterates over all road segments (and over all damage curves) to do the actual loss calculation using road_loss_estimation. This script has several inputs:

- The road segment containing the inundated length, average water depth and meta-data such as road type and number of lanes
- An interpolator object representing the depth-damage function as defined in the Excel-sheet

Using these inputs, the script calculates for each road segment the damage for each combination of inundation raster (6 return periods: RP10, RP20, RP50, RP100, RP200 and RP500) and damage curve (7x; C1-C7, see section 2.6.3), i.e. 42 results[6]. These are added as new metadata columns to the road segment. However, rather than calculating one single value for each combination, it also has to account for the uncertainty in the max damage estimates. This is done by calculating the minimum, maximum and the 3 linearly scaled in-between values of the max damage estimate. As a result, each road segments has 42 damage tuples containing (min, 25%, 50%, 75% and max damage estimates).

Post-processing (baseline)

In the post-processing step, the expected annual damage (EAD) is calculated and the data is prepared for visualisation.

[6] Parts of these are zero, because not each damage function is applicable on the same road type. For example, there are 4 new damage curves + the HZ' = 5 curves for motorways, and only 2 new damage curves + HZ' = 3 curves for other roads.

*This project has received funding from the European Union's Horizon 2020 research and innovation programme under the Grant Agreement No **776479.***

EAD can be calculated for each individual road segment using the function EAD region segmentwise. This script iterates over each road segment by taking the damage estimates of each six return periods, and integrating over the likelihood of their occurrence. During this integration procedure, it accounts for the flood protection as tabulated by Jongman et al. (2014). For an illustration of the integration procedure and associated assumptions see the next section.
Since all damage estimates were corrected to represent EU-28 average values, one can now correct for local deviations from EU-28 average GDP per capita. This is done by linearly scaling the damage estimates, as proposed by Doll and Essen (2008), on the NUTS-0 (country level).

At this stage, one has a very large dataset; 1330 NUTS-3 regions with thousands of inundated roads each. For each inundated road, one has 5 (motorways/trunks C1-C4 + C7) or 3 (other roads C5, C6 + C7) damage curves containing an estimate of the EAD. This estimate still contains the bandwidth in uncertainty represented in (min, 25%, 50%, 75% and 100% of max damage estimates).

Post-processing (climate change impacts)
Climate change impacts are calculated in a separate post-processing module. To calculate the changes in flood hazard, we use a method proposed by Alfieri et al., 2015. In this method, the hydrological model (5*5 km) is run for all the climate scenarios. However, the inundation model is only run for the baseline scenario. The climate change impacts on inundations are represented by shifting the return periods of parts of the inundation maps, rather than calculating new inundation maps for each RCP-model-evaluation year combination. These shifted parts of the inundation maps can be recognized by a unique 'Area-of-influence' (Alfieri et al., 2015). With the shifted return periods, the expected annual damage is calculated again for each individual road segment (Figure 9). Depending on the adaptation scenario, the flood protection level is also shifted[7]. Two adaptation scenarios are considered:

1) No adaptation: this means that all dike heights are frozen on 2015-levels. This is implemented in the model by shifting the flood protection levels in a similar fashion as the return periods of the inundation maps. For increasing (decreasing) flood hazard, this will lead to a large increase (decrease) of flood risk (Figure 9).
2) BAU adaptation: this means that the dike heights are adapted to the changing flood hazard, such that the protection level remains constant. This is implemented by keeping the flood protection levels constant, also when the return periods of the inundation maps change. For increasing (decreasing) flood hazard, this will lead to a very small increase (decrease) of flood risk (Figure 9).

[7] These shifts of the flood protection levels are on a coarser resolution (5*5 km^2) than the original flood protection data for the baseline level (100 * 100 m^2). As a consequence, there are minor differences between the baseline damages calculated with the normal postprocessing module (more precise) and the baseline damages calculated with the climate-change postprocessing module (approximation).

*This project has received funding from the European Union's Horizon 2020 research and innovation programme under the Grant Agreement No **776479.***

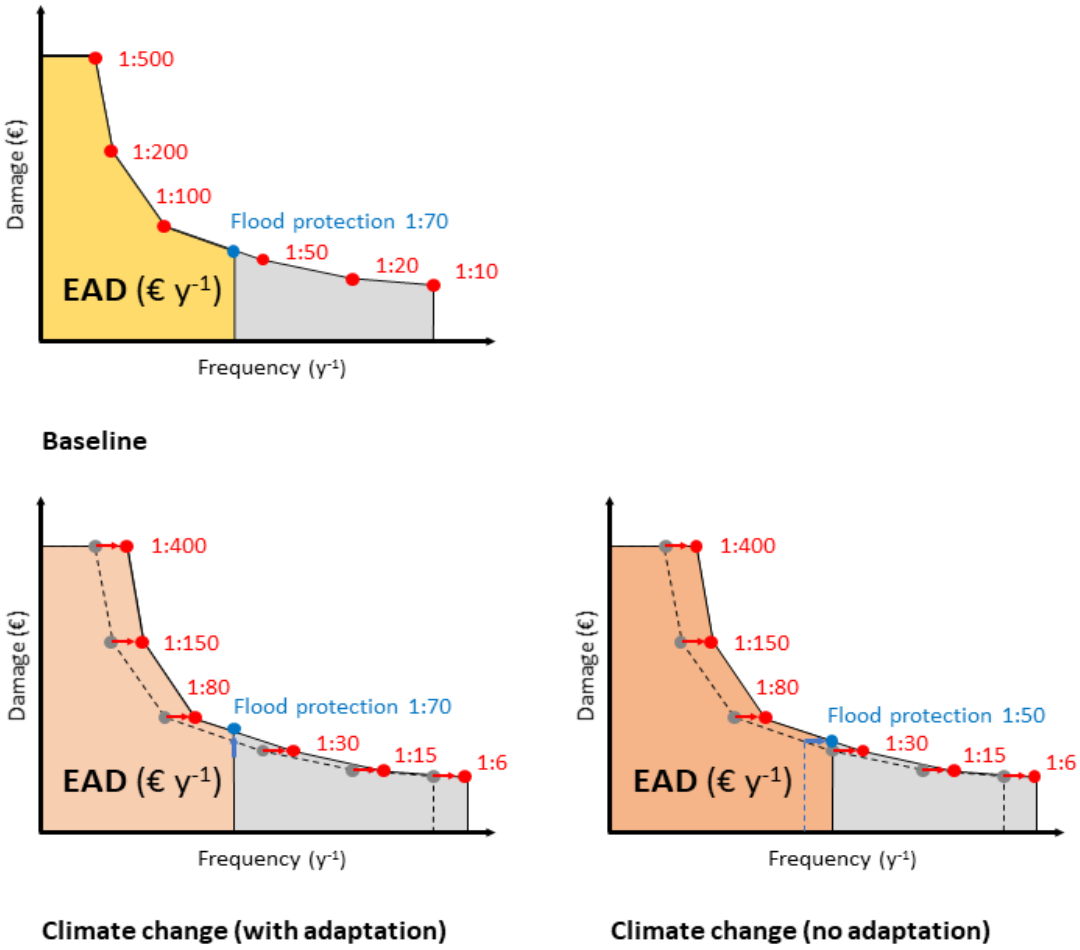

Figure 9: Risk calculation (Expected Annual Damage) for the baseline, climate change with adaptation and climate change without adaptation Axes are not to scale, shifts of return periods are for a hypothetical example

Risk

The risk calculation by integration over the damage per return period may look trivial (Figure 9). It, however, requires several assumptions, that significantly impact the EAD (Olsen et al., 2015). In the OSdaMage model, we use the trapezoidal rule to numerically integrate over six known combinations of return frequency (1:10, 1:20, 1:50, 1:100, 1:200, 1:500 y^{-1}) and damage. We assume the following:

I. The damage for events beyond the 1:500 y^{-1} event[8] (i.e. return period > 500 y, or frequency < 1/500), the damage is similar as the damage in the 1:500 year event.

[8] For climate change projections in which the return period of the 1:500 event is shifted towards a new 1:XXX event, we similarly assume the damage of the 1:XXX event for events with RP > XXX).

*This project has received funding from the European Union's Horizon 2020 research and innovation programme under the Grant Agreement No **776479.***

II. The damage for events below the 1:10 y^{-1} event (i.e. return period < 10 y), no damage will occur.

Concerning assumption (I), we recognize that one could argue that in theory, the damage for the 1:inf could go up till infinity (as suggested by the shape of some extreme value distributions), and that the corresponding damage also could go up till infinity. However, the amount of observed discharges underlying the extreme value distribution from which the water depths are sampled do not allow for accurate estimates of events beyond the 1:500. Moreover, in reality, there is a limit to the damage that can occur: when all assets reach their maximum inundation depth, and thus their maximum damage.

Concerning assumption (II), we reason that roads will usually not be constructed such that they flood every 10 years. Here, we deviate from other studies, which linearly interpolate the damage in the 1:10 event to zero damage for the 1:2 year event, which is assumed to be the bank full discharge (e.g. Alfieri et al., 2015).
Note that in the baseline scenario, the 1:10 damage is hardly used, because the return period of the flood protection is larger than 10 year almost everywhere in Europe. Therefore, the second assumption mainly starts to play a role for climate change projections, where the return periods of the flood events are shifted.

New damage curves for road infrastructure

In general, damage curves are used to determine flood damage from some known flood characteristics such as water depth, flow velocity and duration of the flood. In the continental-scale models like Lisflood and GLOFRIS, flood damage is typically a function of water depth only. In general, damage predictions may significantly improve from more complex damage functions (Schröter et al., 2014). For damage to road infrastructure in particular, this is even more important. Kreibich et al. (2009) show that flow velocity and force have a strong influence on structural damage to roads, while the water depth only has medium impact. In contrast, for structural damage to residential buildings, water depth is more important than flow velocity and flow force. This means that for a study into to road infrastructures, damage functions that only relate damage to water depth are less suitable than in studies which focus on land use classes like residential buildings.

Lisflood and GLOFRIS rely on a set of damage curves proposed by Huizinga (2007, 2017). These curves have been used in many studies (e.g. Albano et al., 2017; Amadio et al., 2019, 2016; Carisi et al., 2018; Dottori et al., 2018; Jongman et al., 2012; Prahl et al., 2018). Huizinga (2007) also proposes a 'EU-average' curve for road infrastructures, which can be applied to different member states by scaling with GDP. For our application, however, this curve has several limitations: 1) The curve is grid based, and therefore proposes a cost per m^2 rather than per m. 2) Also, it cannot distinguish between different road types, whereas expensive highways may costs much more than rural roads, even after correcting for their difference in width. 3) The curve is only depth-based, and gives no insight in the role of flood velocity in

*This project has received funding from the European Union's Horizon 2020 research and innovation programme under the Grant Agreement No **776479.***

explaining damage.

Therefore, Deltares developed a new set of damage curves for use in the OSdaMage model. We carried out an extensive literature review, looked into dozens of pictures of European flood events in which roads where hit, sent questionnaires to national road operators and finally organized a meeting with experts in the fields of flood risk modelling and road infrastructure. From this, a new set of road-specific damage curves was developed. Here, however, a reservation is to be made: the main lesson drawn from this exercise is that knowledge on flood damage to road infrastructures is still an underdeveloped and very complex field. Therefore, the proposed damage curves should be seen as a first attempt to design object-based damage curves. More research, and in particular: more comprehensive damage reporting on real-world events (like Vennapusa et al., 2013 for Iowa, USA) is required to validate and improve the proposed curves.

Concerning flow velocity, we decided to develop two separate damage functions representing low and high velocities (Figure 10). Literature indicates that under low flow velocities (< 0.2 m/s), there is hardly any structural damage to road pavements, whereas under high velocities (> 2 m/s) the damage may be very large (Kreibich et al., 2009). This is confirmed by observations of real flood events showing that under quiet flow conditions, many roads remain almost undamaged, whereas during flashfloods, roads may completely be destroyed. However, the uncertainty covered in this study is somewhat smaller than these observations suggest. The Lisflood model used is developed to simulated river floods in large river basins (Alfieri et al., 2016, 2015). For these types of floods, very high flow velocities are only found in very steep upstream areas (which are not well represented in this model) and next to dike-break locations (which is only very locally). In most of the area, the flood velocities are relatively slow; compare with the observed flood event in the next section. Therefore, we have estimated the low-flow and high-flow curve such that they span the min and max velocities occurring for these typical slow velocities.

As a first step towards new damage curves, we tabulated road construction costs from the (grey) literature (European Court of Auditors, 2013; Heralova et al., 2013; Nijland et al., 2014; Carruthers, 2013; Collier et al., 2015; Australia government, 2017; Arkansas highway, 2014; de Bruijn et al., 2014). From this, we estimated EU-average construction and max damage costs (Table 4). Secondly, we tabulated road maintenance costs (Reese, 2003; Caruthers, 2013; Archondo-Callao, 2000) as well as reported flood damage costs (Vennapusa et al., 2013). The raw tabulated data can be retrieved from Deltares on request. Thirdly, we used this data to estimate the shape of damage curves. This was done on the basis of road type, the presence of road accessories and flow velocity, and the curves were corrected for the number of lanes national GDP per capita (Figure 10).

The damage curves for motorways and trunks (C1-C4) have a different shape from the other road types (C5-C6). Motorways and trunks are usually located on

*This project has received funding from the European Union's Horizon 2020 research and innovation programme under the Grant Agreement No **776479.***

embankments (especially in flood-prone areas), which is represented by a concave section in the curve (Figure 11). This represents our assumption that relatively little damage occurs as long as the water level has not yet reached the top of the embankment. For sophisticated motorways and trunks, the damage at lower water levels is relatively large, because of damage to lighting and electronic signalling (C1, C2). This damage also occurs under low flow velocities. For simple motorways and trunks (C3, C4), which are much cheaper to construct, the damage is lower and the damage strongly depends on flow velocity (Figure 11).

Table 4: Road construction and maximum damage cost (pricelevel EU-28 average, in million 2015-Euro's)

Road type	Lanes	Construction cost range	Max damage (low flow)	Max damage (high flow)	Max dam (low flow)	Max dam (high flow)	Huizinga max damage*
Motorway	2*3	3.5 - 35	20% (a) 4% (s)	22% (a) 35% (s)	5.43 (a)* 0.46 (s)*	5.97 (a)* 3.98 (s)*	0.90
Trunk	2*2	2.5 - 7.5	idem	Idem	1.25 (a)* 0.15 (s)*	1.38 (a)* 1.31 (s)*	0.60
Primary	2*1	1 - 3	5%	35%	0.050-0.150	0.350-1.050	0.25
Secondary	2*1	0.50 - 1.5	5%	35%	0.025-0.075	0.175-0.525	0.225
Tertiary	2*1	0.20 - 0.60	5%	35%	0.010-0.030	0.070-0.210	0.175
Other	1	0.10 - 0.30	5%	35%	0.005-0.015	0.035-0.105	0.075
Track	1	0.02 - 0.05	5%	35%	0.001-0.003	0.007-0.018	0.075

Note: Huizinga max damage costs are obtained by multiplying the m^2 costs width typical road widths per road type (a) accessories road; (s) simple road

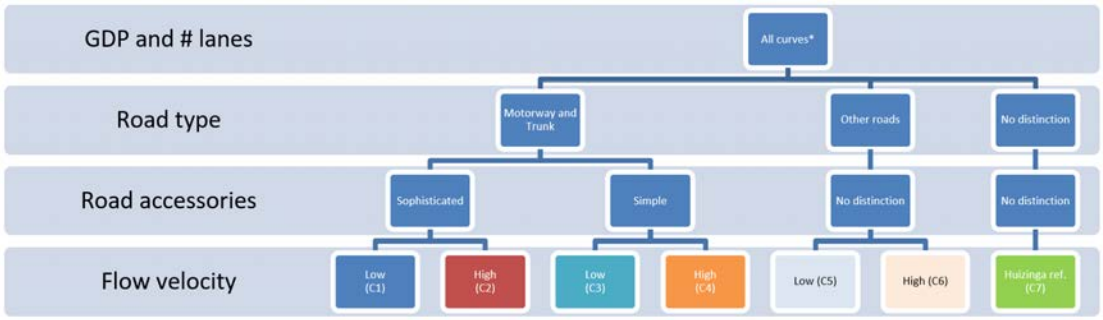

Figure 10: Dimensions to differentiate between depth-damage curves in OSdaMage

The damage curves for other roads (C5 and C6) do not have a concave section in the beginning of the curve, because they are usually not located on embankments, in

*This project has received funding from the European Union's Horizon 2020 research and innovation programme under the Grant Agreement No **776479.***

contrast to motorways and trunks. Although the relative shape of the high-flow curve is not very different from Huizinga's curve (Figure 13), the difference becomes significant when applying to different road types. For example, primary roads are more expensive than suggested by Huizinga's m^{-2} cost, therefore, the Huizinga curve is more towards our low-flow curve for this road type. In contrast, tertiary roads are relatively cheap, therefore, the Huizinga curve is more towards our high-flow curve for this road type (Figure 2.6.8).

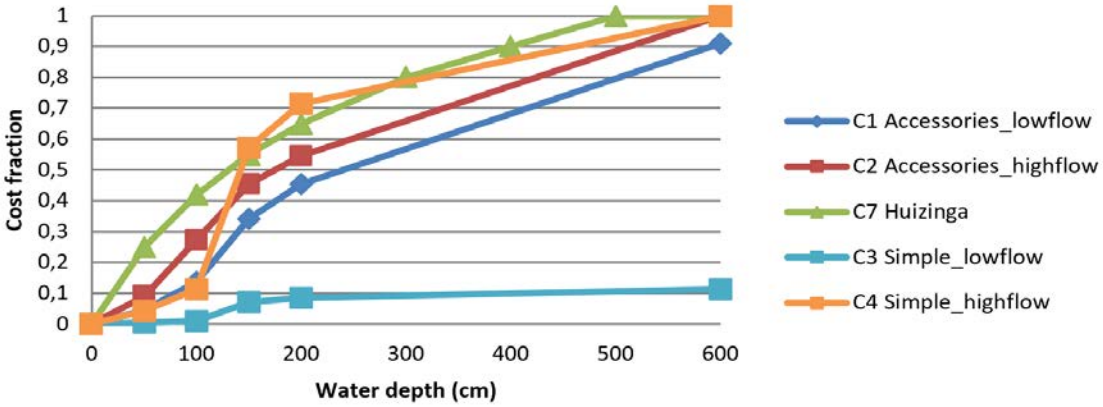

Figure 11: Relative damage curves for motorways and trunks as a percentage of maximum damage

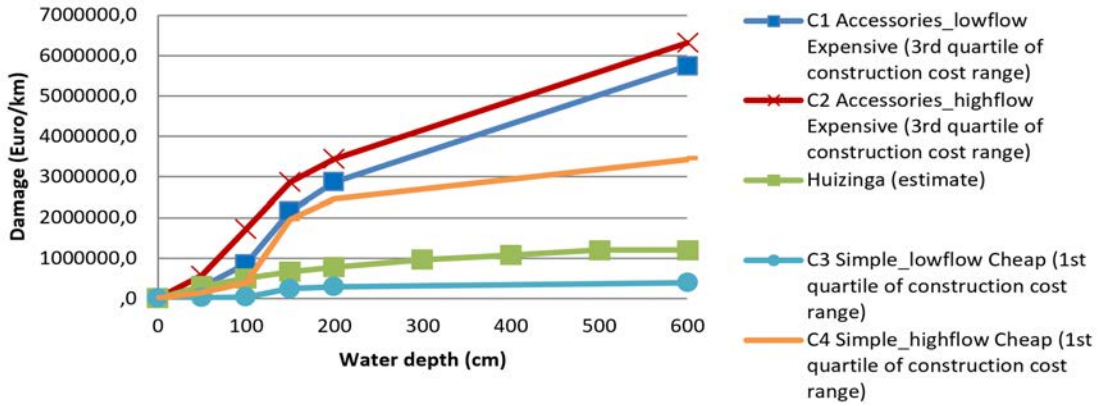

Figure 12: Absolute damage curves for illustrative combinations of damage curves and max damages of motorways (right)*

**Selection based on the assumption that the accessories curves (C1 and C2) are best applicable to more expensive roads (the upper 75% of the max damage range); whereas the simple curves (C3 and C4) are best applicable to cheaper roads (the lower 25% of the max damage range). This assumption is also referred to as 'litmix'*

*This project has received funding from the European Union's Horizon 2020 research and innovation programme under the Grant Agreement No **776479.***

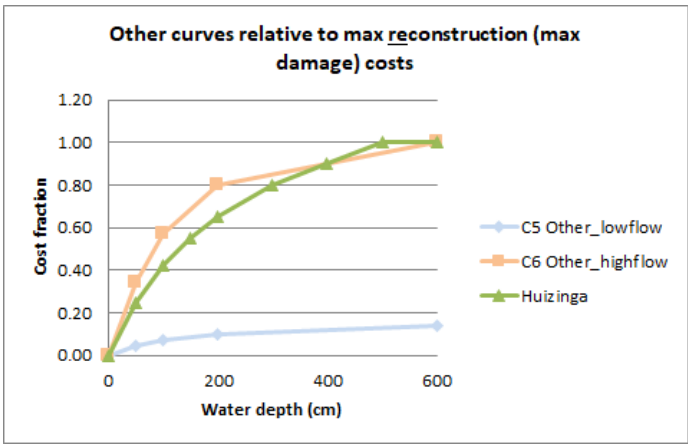

Figure 13: Relative damage curve for all other road types (not trunks or motorways).

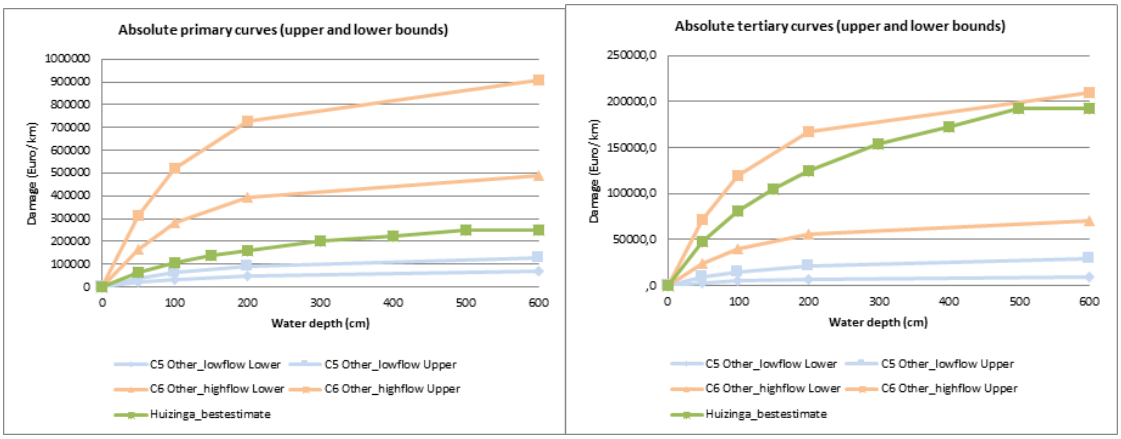

Figure 14: Absolute damage curves for all other road types (not trunks or motorways), illustrated for two road types: primary roads (left) and tertiary roads (right)

Note that the actual OSdaMage model calculates the damage relative to *new construction costs* of roads, rather than relative to *maximum damage*. The input values for the model are shown in Table 5.

*This project has received funding from the European Union's Horizon 2020 research and innovation programme under the Grant Agreement No **776479.***

Table 5: Depth-damage curves relative to total construction costs (depth in cm, damage as fraction of total construction costs)

C1		C2		C3		C4		C5		C6	
depth (cm)	*damage (-)*	*depth*	*damage*	*depth*	*damage*	*depth*	*damage*	*depth*	*damage*	*depth*	*damage*
0	0	0	0	0	0	0	0	0	0	0	0
50	0.01	50	0.02	50	0.002	50	0.015	50	0.015	50	0.12
100	0.03	100	0.06	100	0.004	100	0.04	100	0.025	100	0.2
150	0.075	150	0.1	150	0.025	150	0.2	200	0.035	200	0.28
200	0.1	200	0.12	200	0.03	200	0.25	600	0.05	600	0.35
600	0.2	600	0.22	600	0.04	600	0.35				

Model validation using Deggendorf flood

In order to validate the OSdaMage model and the new damage curves, we made a comparison of the baseline results with road repair data reported by the Bavarian Government (South-East Germany) for a flood near the down Deggendorf. On 4 June 2013, a dike breached in this region, near the confluence of the River Danube and the River Isar. This flooded two motorways (A3 and the A92) as well as their intersection: the cloverleaf junction 'Deggendorf' (Figure 15). The Bavarian State Ministry received 3.8 million for repair works on these highways (personal communication).
We estimated water depths during this event from reports (Rogowksy et al., 2016) and photos taken during the event. To validate the damage curves, we manually estimated the damage, by multiplying the average inundation depth per road with the length of the inundated section, and then applied the damage functions. The A3 submerged over the entire 6.6 km, 50 cm over the road pavement, which is about 1.5 meter above the road base. The pavement of the A92 remained dry over the entire 2.8 km, except from a small depression at an underpass with a local road. Here also, the water level was assumed 1.5 m above the road base (but apparently the pavement was a bit higher than assumed by the shape of the damage curve). Given the fairly simple road designs (no street lighting or electronic signalling), damage curves C3 (simple accessories, low-flow) and C4 (simple accessories, high-flow) are best applicable. After correction for the German 2013-GDP per capita, the total damage is estimated at €3.3 million Euro (C3, low-flow) till €26.5 million (C4, high-flow). The reported damage (€3.8 million) is therefore in the range of our damage estimates, but more towards to the low-flow than the high-flow estimate. Satellite imagery shows that only minor repair works took place after the flood, which is a strong indication that the flow conditions were indeed relatively low.

*This project has received funding from the European Union's Horizon 2020 research and innovation programme under the Grant Agreement No **776479.***

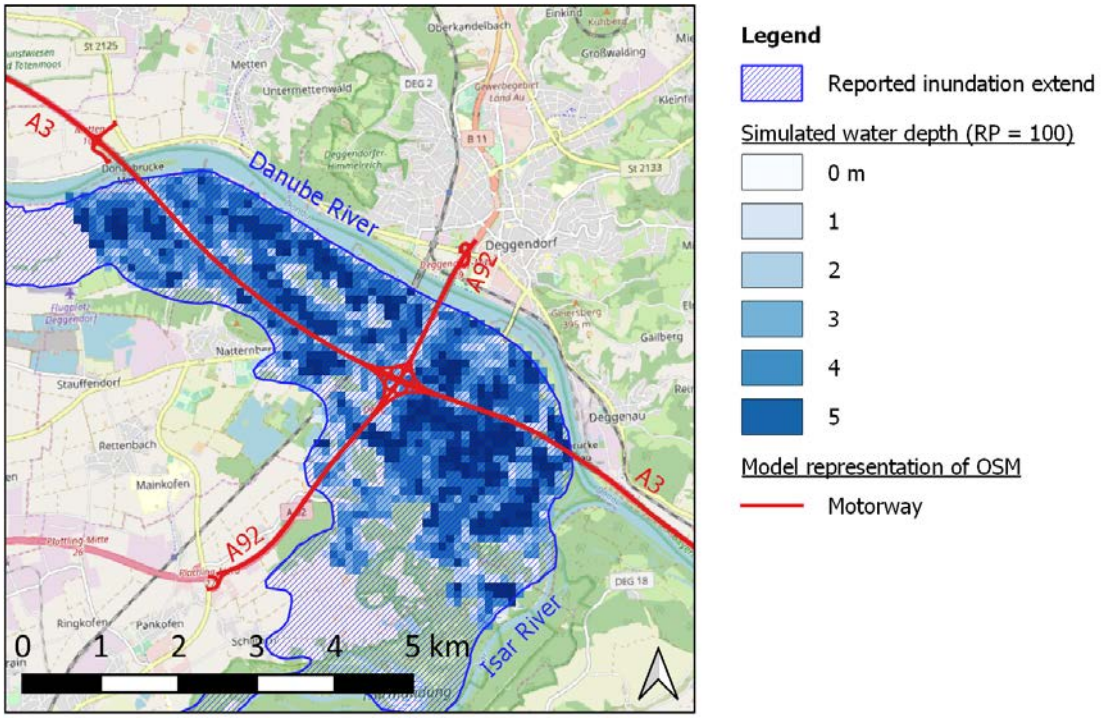

Figure 15: Reported and simulated inundation of the Deggendorf junction of the A3 and A92 in July, 2013

2.7 Data and experiment description

The experiments and the data used will follow the simulation protocol defined in D1.6 using the scenarios defined in D1.5, with a few adjustments for the coastal impact calculations. As sea-level rise has a relative small sensitivity to the climate model used, but high sensitivity to the ice-sheet melting assumptions (Hinkel, 2014), the low, average and high climate signal has been interpreted as the 5th, the 50th and the 95th ice-sheet melting quantile of RCP2.6 resp. RCP4.5 of the HadGEM2-ES sea-level rise scenarios taken from (Hinkel, 2014). These are completed with the 50th quantile of RCP 6.0 resp. RCP8.5 of the HadGEM2-ES sea-level rise scenarios. As high sea-level rise might have severe impacts, we also did a model run with a high end sea-level rise scenario, based on the 95th quantile of HadGEM2-ES from (Jevrejeva, 2016). This high-end scenario was combined with SSP5.

For the coastal impact assessment dikes are initialized according to a stylized rule based on GDP per capita and population density (Hall, 2015) and expert judgement values for the 136 coastal megacities (Hallegatte, 2013). For future protection standards two adaptation strategies have been used. “No adaptation” means that all dike heights are frozen on 2015 levels. Dikes are maintained until they are permanently overtopped, but not raised anymore. In the “BAU adaptation” (Business as usual adaptation) dikes are raised according to the rule used to initialise them, which means dikes are raised with sea-level rise and with growing wealth.

*This project has received funding from the European Union’s Horizon 2020 research and innovation programme under the Grant Agreement No **776479.***

3 Results

3.1 DIVA Sea level rise and storm surge impacts

Sea-level rise

According to the sea-level rise scenarios described in the previous section, the global coastal mean-sea-level rises between 32 cm and 75 cm until 2100 with the scenarios defined in D1.5, while in the additional high end scenario 170 cm coastal mean sea-level rise in 2100 occurs (see Figure 16). Low, medium and high scenarios for RCP2.6 and RCP 4.5 are defined in terms of the 5th, 50th and 95th quantile of the ice-sheet (Antarctica, Greenland) contributions instead of different climate models, as it has been shown that the former has bigger influence on the sea-level rise (Hinkel,2014).

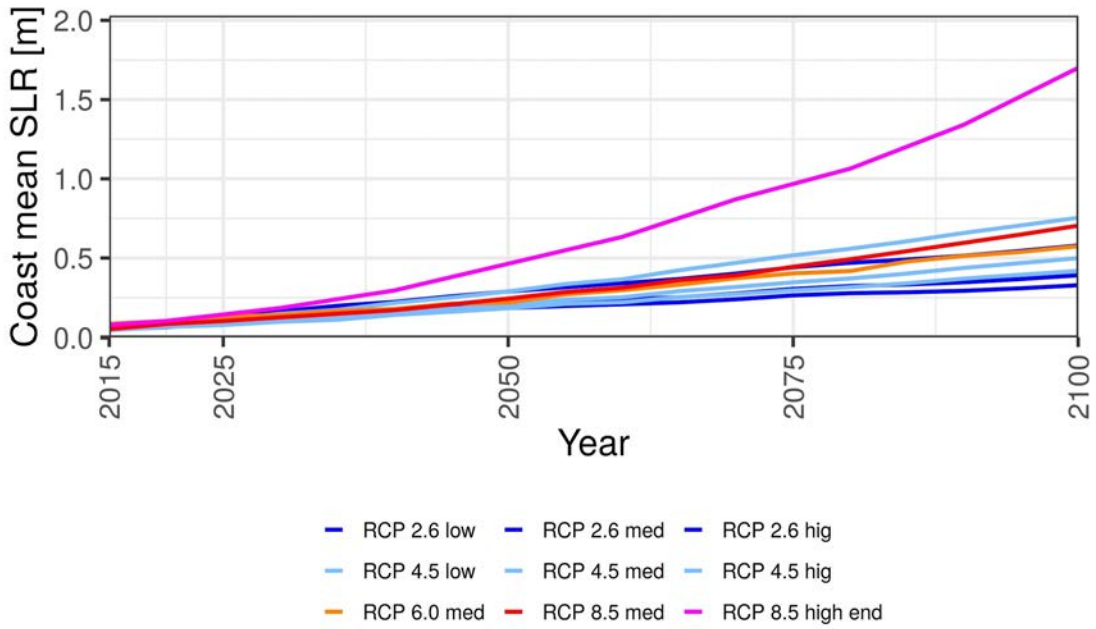

Figure 16: Coastal mean sea-level change (in meter) against the 1985-2005 average for the scenarios used in this study.

The sea-level rise uncertainty is mainly determined by the assumptions about the sensitivity of the two big ice-sheets (Greenland and Antarctica) to raising global mean temperature. That explains that the high sea-level rise scenario of RCP 4.5 produces a higher sea-level rise in 2100 than the medium scenario of RCP 8.5 and the medium scenario of RCP 6.0, and even the high sea-level rise scenario of RCP 2.6 produces a higher sea-level rise in 2100 than the medium scenario of RCP 6.0. However, while sea-level rise scenarios under RCP 2.6 and RCP 4.5 in general follow a linear trend, sea-level rise scenarios under RCP 6.0 and RCP 8.5 show acceleration over the 21st century (especially in the second half).

*This project has received funding from the European Union's Horizon 2020 research and innovation programme under the Grant Agreement No **776479.***

Local patterns of sea-level rise under the scenarios used in this study are shown in Figure 17. Sea-level rise at European coasts is not significantly higher or lower than the global average, but also difficult to model due to Europe's diverse geography (Baltic sea and Mediterranean are very raw resolved).

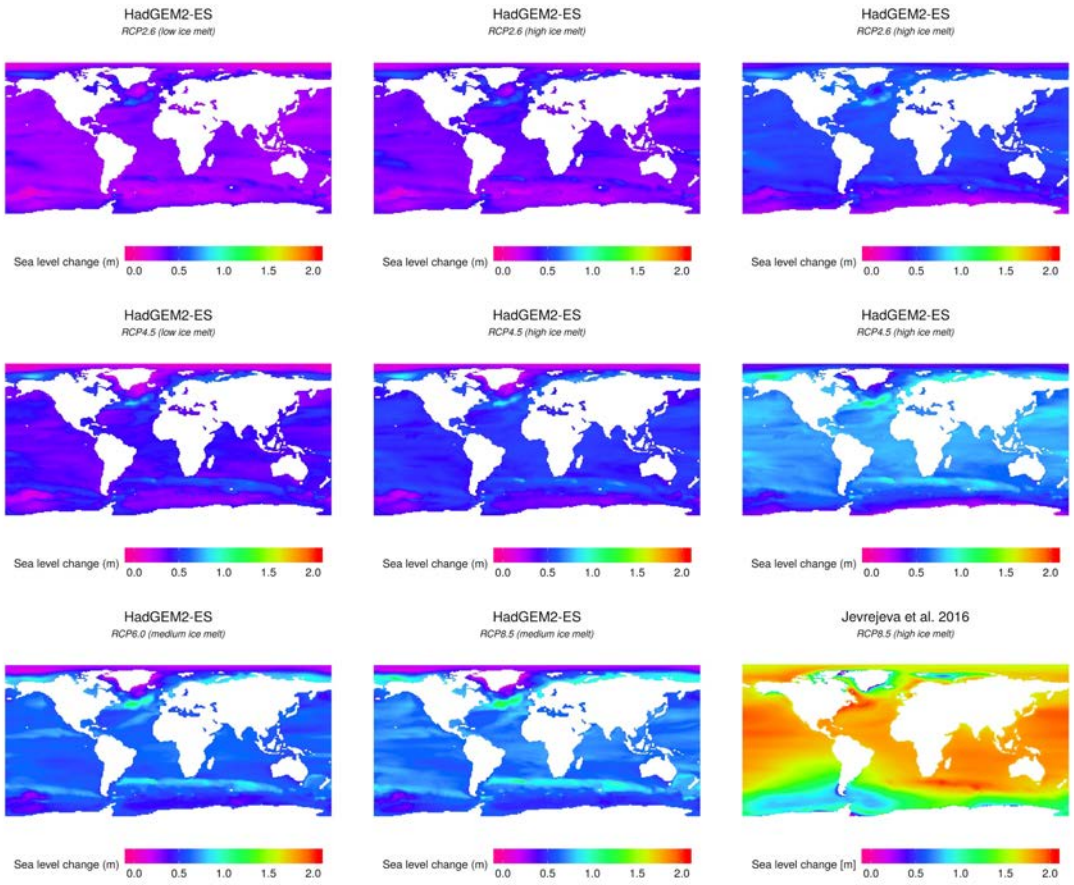

Figure 17: Local sea-level change in 2100 (in meter) against the 1985-2005 average for the scenarios used in this study.

Flood impacts and protection cost

Figure 18 shows the 21st century sea flood cost globally and in the EU28, with and without adaptation. This figure is meant to be illustrative, showing that the sea flood cost in the EU are up to 20 percent of the global cost and that adaptation might lower the cost of increased flooding by at least an order of magnitude. Without further adaptation, global annual sea flood costs could reach about €80 trillion in 2100 under RCP 8.5 high-end sea-level rise and about €40 trillion under RCP 8.5 medium sea-level rise (both combined with SSP5). Within EU28 respective values are about EUR 13 trillion in 2100 under RCP 8.5 high-end sea-level rise and about €4.5 trillion under RCP 8.5 medium sea-level rise (again both combined with SSP5). On the low end, global sea flood cost could be €440-950 billion under RCP 4.5 and €400-830 billion RCP 2.6, both including business-as-usual adaptation. For EU28 the respective values

*This project has received funding from the European Union's Horizon 2020 research and innovation programme under the Grant Agreement No **776479.***

are €23-64 billion under RCP 4.5 and €22-58 billion under RCP 2.6. With adaptation the EU28 values are roughly 5 percent of the global value showing the huge capacity and potential for coastal protection in Europe.

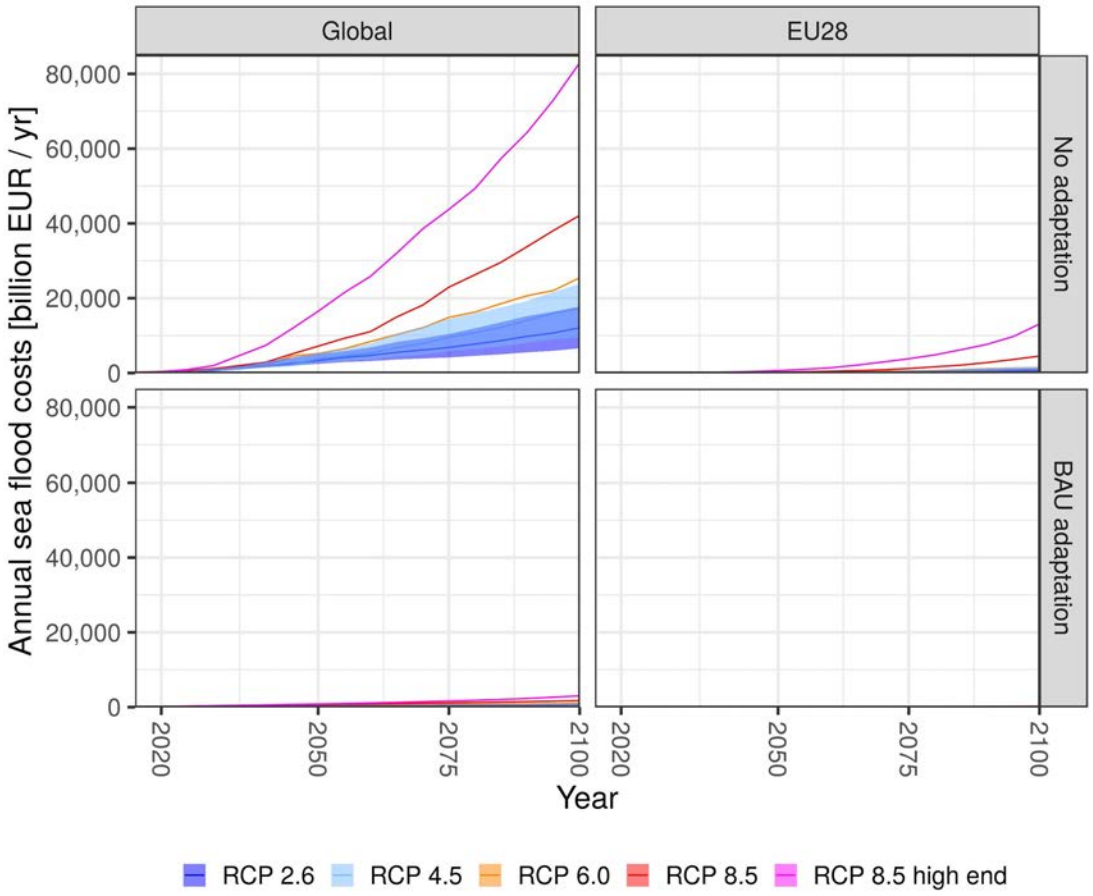

Figure 18: Sea flood cost globally and in the EU28, with and without adaptation, to illustrate the relations. The shaded areas for RCP 2.6 and RCP 4.5 show the range over all runs done for these RCPs (different SSPs and ice-sheet contributions). For the other RCPs only one model run was done. In the EU28 with BAU adaptation values are below 260 and thus not visible at the used common scale. Detailed results for all runs done are available in the COACCH database and the COACCH outputs.

The reduction of sea flood impact due to coastal protection comes at a price: protection infrastructure need to be constructed, raised and maintained. Figure 19 shows sea flood cost and protection cost for the EU28. Protection cost are about two orders of magnitude lower (in 2100 €15-40 billion) as the sea flood cost without further protection and reduce seaflood cost roughly by two orders of magnitude. Without further adaptation existing coastal protection requires annual maintenance cost of about €15 billion. Protection infrastructure is maintained until it is permanently overtopped. As no new protection infrastructure is build and no existing protection infrastructure is raised, the maintenance costs are falling over 21st century. The higher the sea-level rises the less protection stays functional and thus

*This project has received funding from the European Union's Horizon 2020 research and innovation programme under the Grant Agreement No **776479.***

the lowest protection cost in the “no adaptation” scenario occurs under RCP 8.5 high end sea-level rise. Under the RCP 2.6 low end sea-level rise scenario protection cost almost stays constant over 21st century as only very few protection infrastructures are permanently submerged.

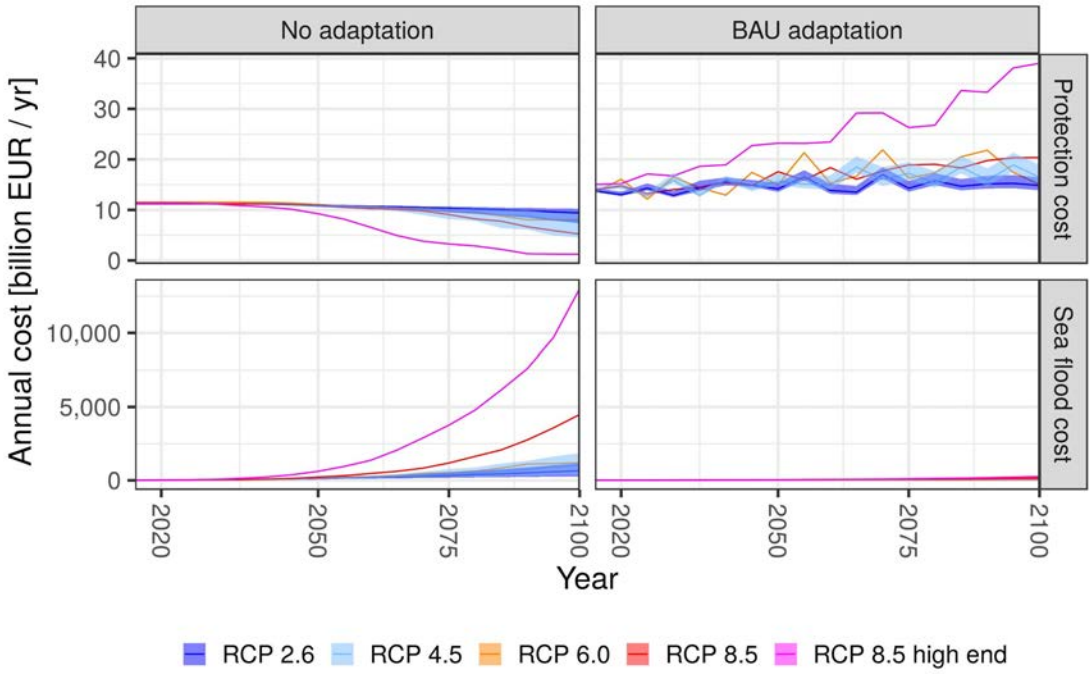

Figure 19: EU28 sea flood and protection cost over 21st century. Shaded areas for RCP 2.6 and RCP 4.5 show the uncertainty range over all runs done for these RCPs.

Accumulated country level costs are shown in Figure 21. The biggest share of the sea flood cost is on only a few countries: the United Kingdom, Germany, France, Italy, the Netherlands and Belgium. Sea flood cost are particularly high under high end sea-level rise without adaptation. For this combination sea flood cost are up to trillion €64 trillion for the United Kingdom, €38 trillion for Germany, €32 trililon for France, €28 trillion for Italy and €27 trillion for the Netherlands. For the Netherlands the sea flood costs under the high end no adaptation scenario are disproportionately high compared with the other scenarios. This is because the Netherlands has very high coastal protection standards today. These high protection standards would protect the country quite well against lower sea-level rise - even if they are not raised over 21st century. Accumulated protection cost are two orders of magnitude lower than sea flood cost, with the highest cost again for the United Kingdom. This is not surprising as the UK has the longest coastline of all EU28 countries. Protection cost for the UK under the high end sea-level rise scenario add up to €620 billion, which is three times more than the second highest cost (Denmark). For all countries the protection cost in the high-end sea-level rise scenario are highest, but the increase compared the RCP 8.5 is much lower than for instance the equivalent increase in seaflood cost. This shows, that a large proportion of the protection cost is the

*This project has received funding from the European Union’s Horizon 2020 research and innovation programme under the Grant Agreement No **776479.***

maintenance of (already) existing protection infrastructure.

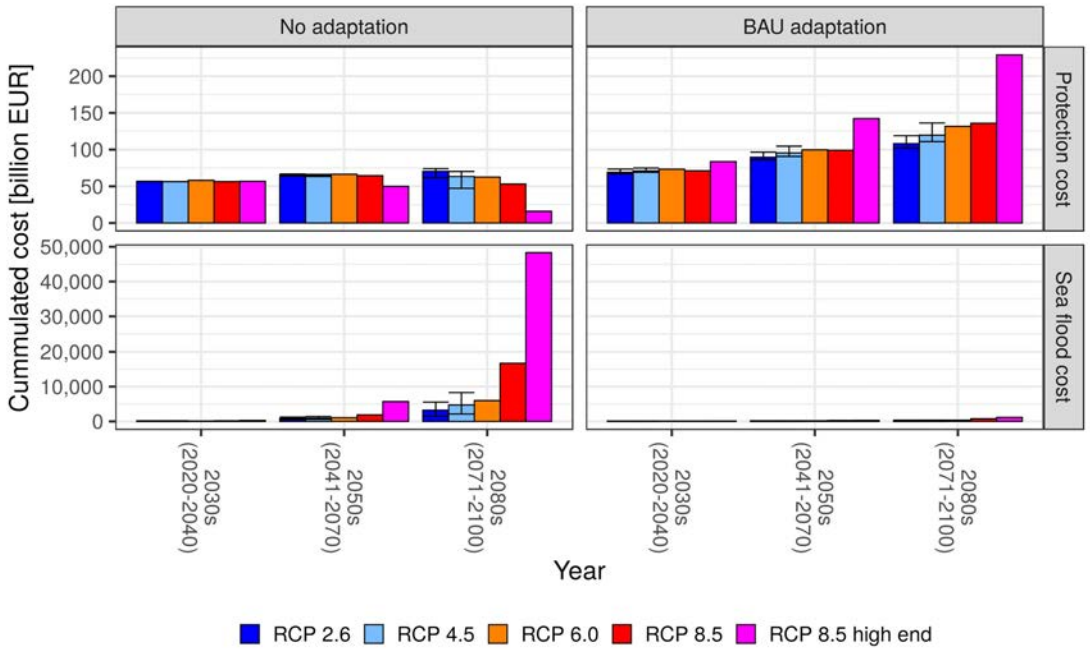

Figure 20: Accumulated EU28 sea flood and protection cost over different time periods of 21st century. Error bars for RCP 2.6 and RCP 4.5 show the uncertainty range over all runs done for these RCPs.

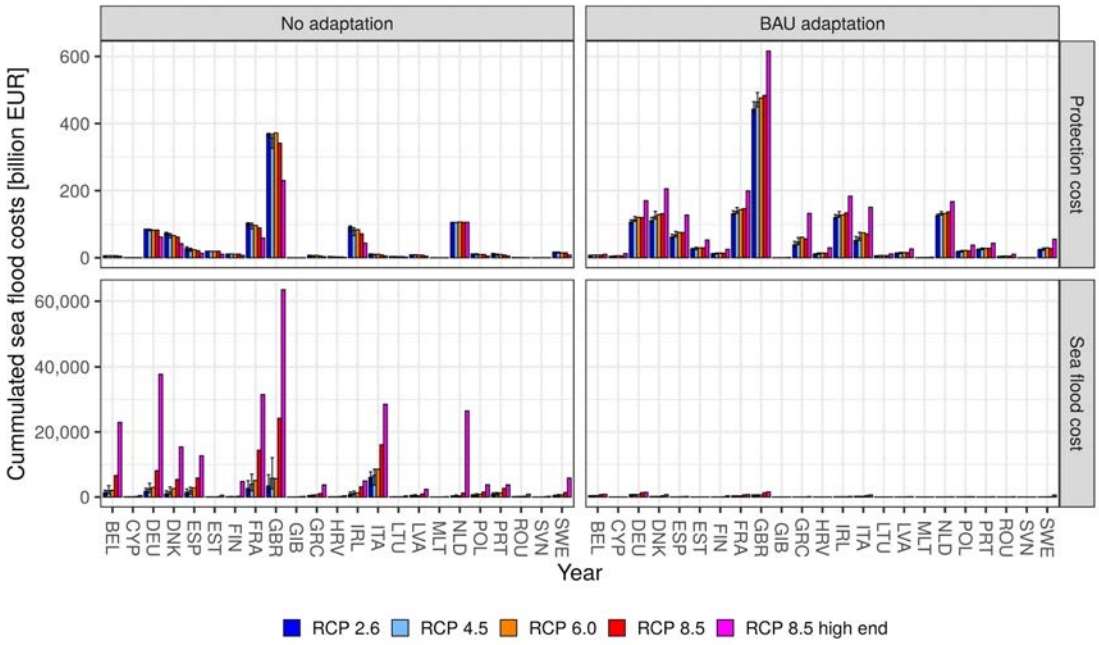

Figure 21: Accumulated national sea flood and protection cost over 21st century (2015-2100) for EU 28 countries. Error bars for RCP 2.6 and RCP 4.5 show the uncertainty range over all runs done for these RCPs.

*This project has received funding from the European Union's Horizon 2020 research and innovation programme under the Grant Agreement No **776479.***

Looking at regional results (NUTS2) we find that 135 out of 1,024 units are coastal ones. The regional sea flood cost are shown in Figure 22 and in the regional hot spots are listed in Table 6. The highest sea flood cost in the no adaptation scenario in in the Veneto region in North-east Italy (Figure 23). Other very affected regions are in Great Britain, Belgium, France and Germany. Again, the regions from the Netherlands are not amongst the most affected one as the protection standard of the Netherlands is high enough to avoid severe flood damages even if the dikes are not raised anymore.

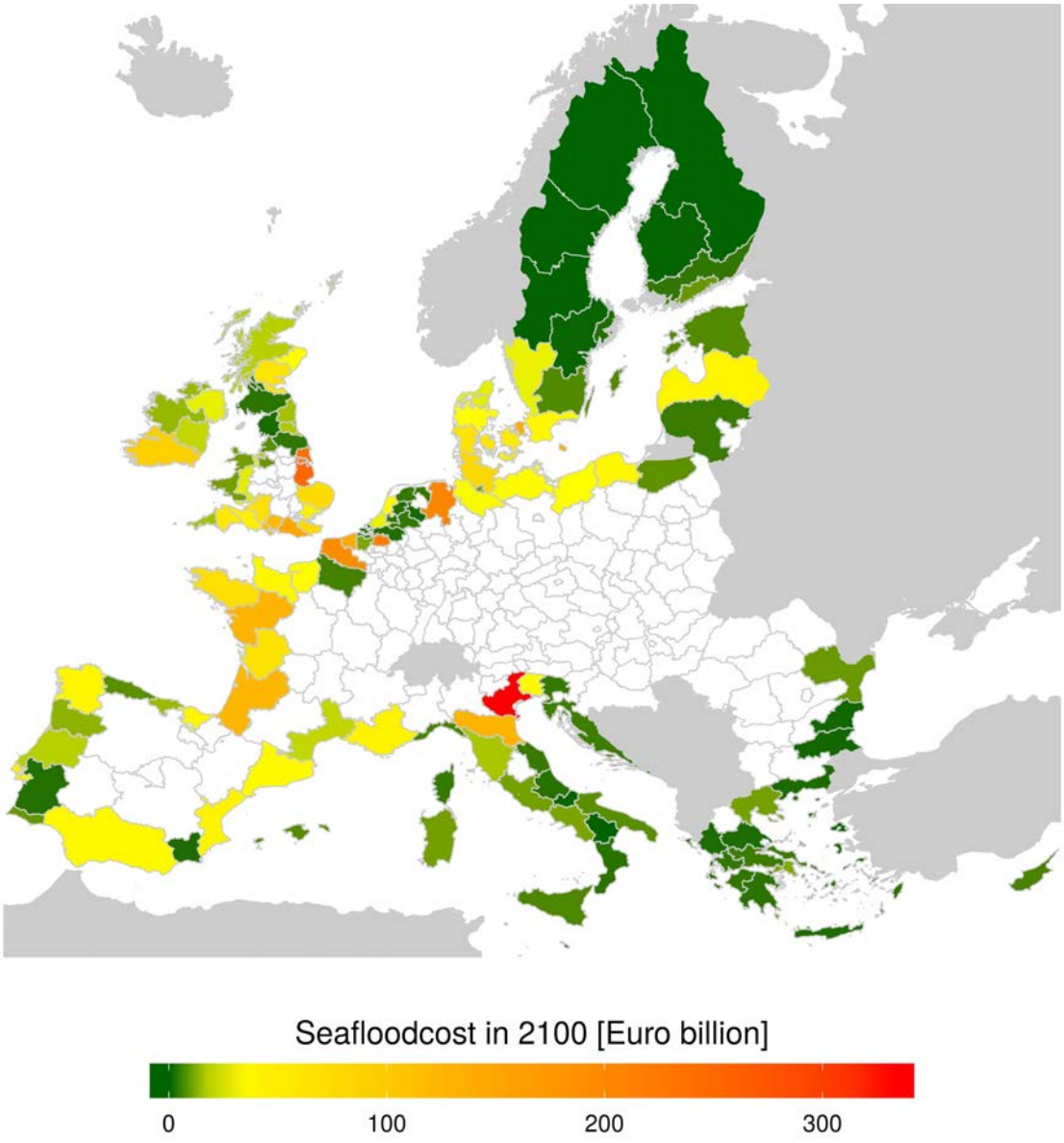

Figure 22: Sea flood cost in 2100 (RCP8.5 medium sea-level rise, SSP5) for the NUTS2-units in the EU.

*This project has received funding from the European Union's Horizon 2020 research and innovation programme under the Grant Agreement No **776479.***

Table 6: Annual expected sea flood cost in 2100 (EUR billion, without adaptation) for the 25 most affected (under RCP8.5 - also sorted for RCP8.5) regions (NUTS2) in the EU. The values for RCP2.6 and RCP4.5 refer to SSP2 and medium sea-level rise.

NUTS2 unit	Country	RCP2.6	RCP4.5	RCP6.0	RCP8.5	High end
Veneto	ITA	109.5	119.2	136.8	333.4	506.3
Lincolnshire	GBR	17.9	39.7	45.7	252.2	307.4
East Yorkshire	GBR	15.8	39.2	45.3	240	322
Antwerpen	BEL	24.7	42.6	46.8	217.9	629
Weser-Ems	DEU	22.7	38.4	40.1	202	836.9
Nord-Pas de Calais	FRA	11.9	25	30.1	191.9	303.9
Surrey East and West Sussex	GBR	10.5	22.6	22.9	147	245.4
West-Vlaanderen	BEL	13	24	27.4	141.5	294.8
Hovedstaden	DNK	5.3	12.8	59.7	136.3	320.3
Emilia-Romagna	ITA	39.6	44.4	53.2	128	202.6
Pays de la Loire	FRA	16.4	37.7	39.3	127.8	169.8
Aquitaine	FRA	18.8	36	38.2	125.5	180.4
Hampshire and Isle of Wight	GBR	7.4	17.2	14.8	120.8	273
Southern	IRL	31.1	38.8	38.3	92.6	120.5
Schleswig-Holstein	DEU	8.8	17.4	21	81.8	284.1
Kent	GBR	6.1	12.9	15.1	77.1	430.4
East Anglia	GBR	4.8	9.1	10.7	75.3	125.9
Bretagne	FRA	10.8	19.4	19.7	70.5	102.9
Gloucestershire	GBR	6.9	11.6	10.2	68.4	197.9
Poitou-Charentes	FRA	11.5	21.1	22	64.7	88.4
Eastern Scotland	GBR	3.9	11.4	6.3	63	73.4
Syddanmark	DNK	12.7	17.9	18.5	62.8	134.7
Devon	GBR	6.1	17.9	14.2	55.9	65.9
Sjaelland	DNK	10.4	17.1	19.9	53.4	92.7
Dorset and Somerset	GBR	4.4	11.2	9.5	46.6	84.5

*This project has received funding from the European Union's Horizon 2020 research and innovation programme under the Grant Agreement No **776479.***

Figure 23: Low elevation coastal zone (below 10m above mean sea-level, the darker the green the lower the elevation) in the Veneto (red) NUTS2 unit.

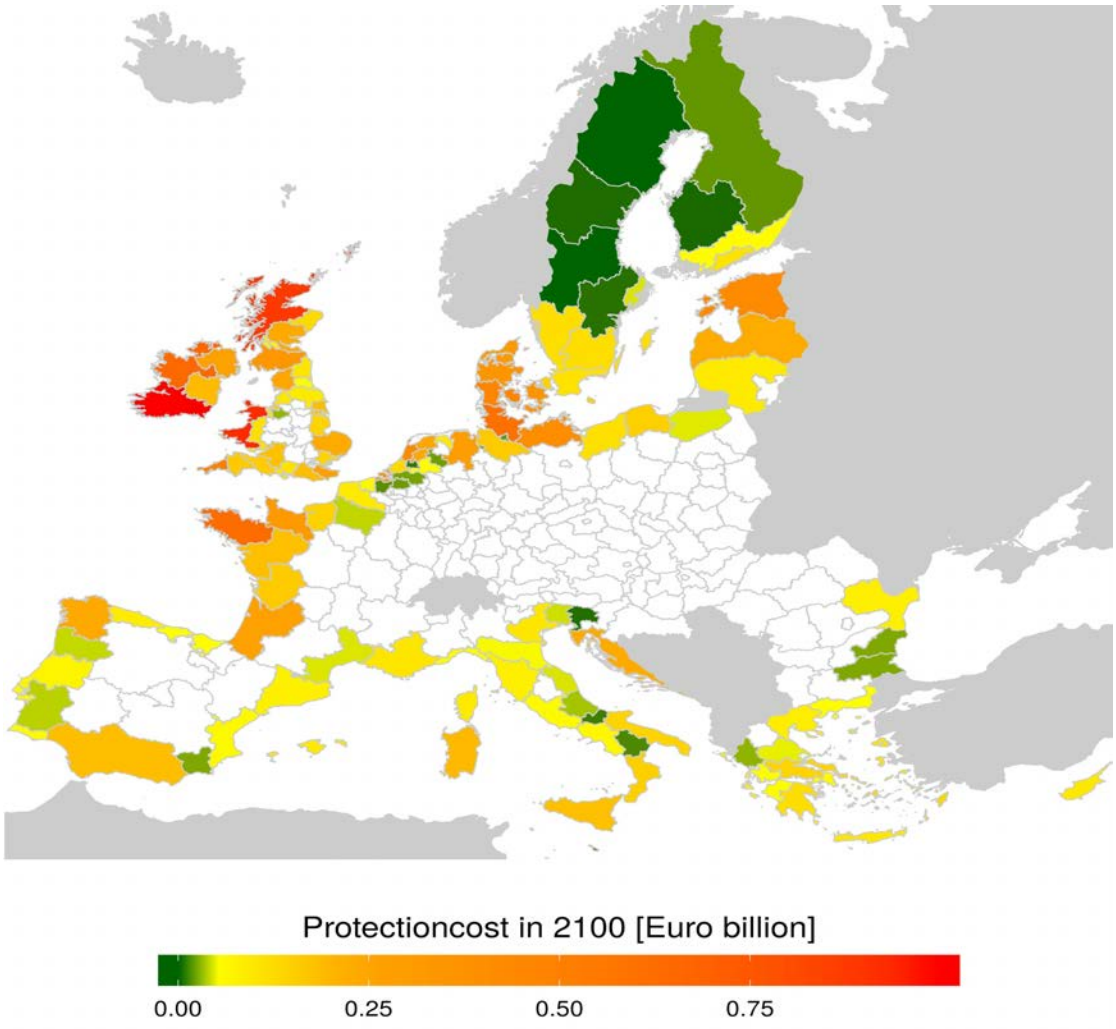

Figure 24: Protection cost in 2100 (RCP8.5 medium sea-level rise, SSP5) for the NUTS2-units in the EU

*This project has received funding from the European Union's Horizon 2020 research and innovation programme under the Grant Agreement No **776479.***

Table 7: Annual protection cost in 2100 (EUR billion, without adaptation) for the 25 most affected (under RCP8.5 - also sorted for RCP8.5) regions (NUTS2) in the EU. The values for RCP2.6 and RCP4.5 refer to SSP2 and medium sea-level rise.

NUTS2 unit	Country	RCP2.6	RCP4.5	RCP6.0	RCP8.5	High end	Dikes (km)
Southern	IRL	0.68	0.75	0.65	1.00	1.68	1125
West Wales and The Valleys	GBR	0.68	0.75	0.67	0.93	1.30	726
Highlands and Islands	GBR	0.84	0.74	0.82	0.89	1.76	1324
Northern and Western	IRL	0.54	0.53	0.52	0.65	1.09	790
Bretagne	FRA	0.46	0.53	0.47	0.63	0.94	871
Schleswig-Holstein	DEU	0.47	0.50	0.49	0.61	1.07	698
Cornwall and Isles of Scilly	GBR	0.38	0.43	0.38	0.52	0.76	412
Syddanmark	DNK	0.33	0.36	0.32	0.46	0.97	895
Eesti	EST	0.29	0.33	0.31	0.42	0.97	938
Noord-Holland	NLD	0.35	0.37	0.38	0.42	0.68	408
Mecklenburg-Vorpommern	DEU	0.28	0.32	0.27	0.41	0.94	818
Zeeland	NLD	0.36	0.37	0.38	0.41	0.62	327
Sjaelland	DNK	0.24	0.27	0.24	0.37	0.84	797
Midtjylland	DNK	0.23	0.25	0.24	0.35	0.72	635
Southern Scotland	GBR	0.30	0.28	0.29	0.34	0.56	342
Canarias	ESP	0.19	0.26	0.22	0.33	0.64	990
Nordjylland	DNK	0.22	0.23	0.23	0.32	0.76	704
Basse-Normandie	FRA	0.23	0.26	0.23	0.31	0.42	361
Weser-Ems	DEU	0.24	0.25	0.25	0.29	0.47	266
Aquitaine	FRA	0.18	0.21	0.18	0.27	0.41	440
Northern Ireland	GBR	0.23	0.2	0.21	0.27	0.51	368
Kent	GBR	0.22	0.23	0.24	0.26	0.43	228
Cumbria	GBR	0.20	0.20	0.2	0.24	0.33	161
Galicia	ESP	0.15	0.17	0.15	0.23	0.38	578
Eastern Scotland	GBR	0.20	0.20	0.21	0.23	0.44	293

Regional protection cost (Figure 24 and Table 7) in the Adaptation scenario are highest for the Southern Ireland region. Here the coastline is very long and homogenous, so that the DIVA model suggests to protect it completely (which is probably a overprotection). Other regions with high protection cost are all in North-western Europe at the atlantic coast, in Great Britain, France, Germany and the Netherlands. Protection cost for mediterranean regions are much lower.

*This project has received funding from the European Union's Horizon 2020 research and innovation programme under the Grant Agreement No **776479.***

Land loss and Migration

Cumulated land loss (caused by both - erosion and submergence) in the EU until 2100 ranges from 130 km² (RCP2.6 with Adaptation) to 6,600 km² (RCP8.5 high end sea-level rise without adaptation). In general is the land loss under higher Sea-level rise and late in the century higher than under low sea-level rise or early in the century (Figure 25).

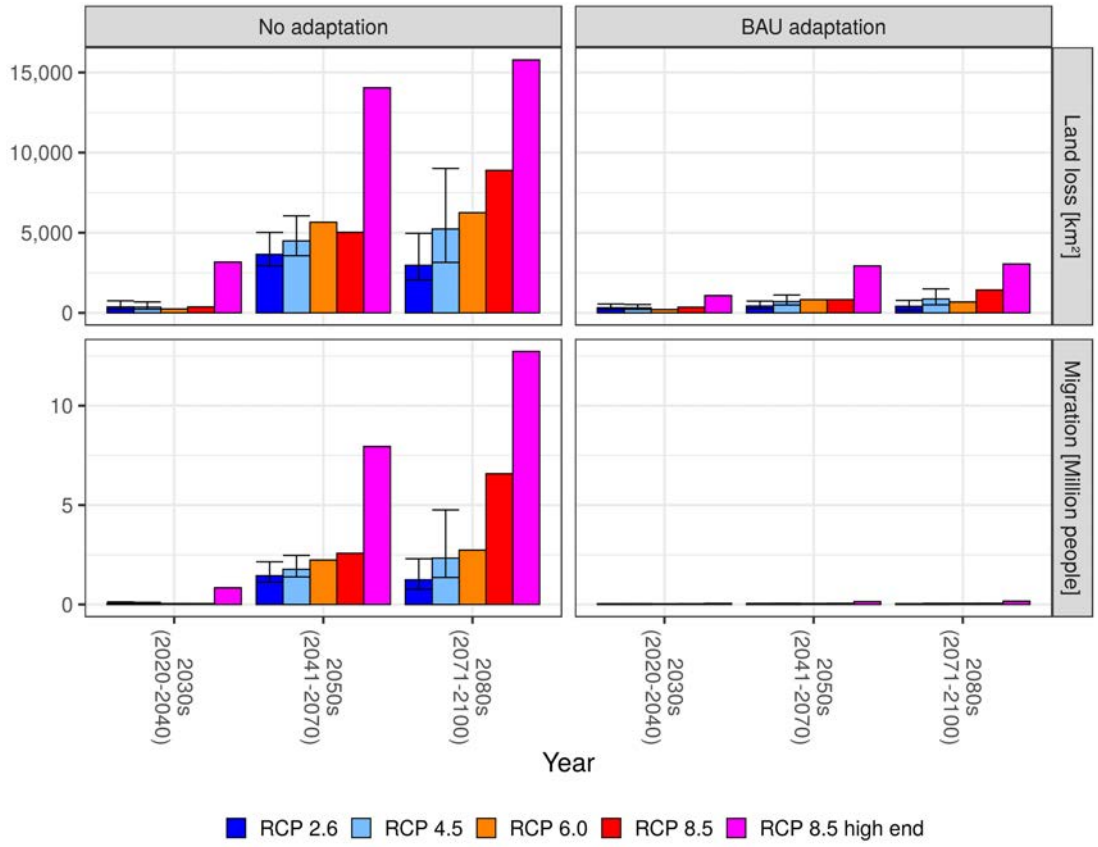

Figure 25: Accumulated EU28 land loss and migration over different time periods of 21st century. Error bars for RCP 2.6 and RCP 4.5 show the uncertainty range over all runs done for these RCPs.

The lost land forces population who lived on that land to migrate. The land loss in the EU leads to cumulated migration of 0.1 (RCP2.6 with Adaptation) to 21.5 million people (RCP8.5 high end sea-level rise without adaptation). It has to be noted that in a rich region like the EU much of the population will be protected and thus forced migration will be lower than in other regions. On Country-level, beside the North-west Atlantic coast countries, Italy and Romania suffer big land losses (Figure 26). While in Italy these losses occur in the North-east and lead to significant migration. In Romania it is mainly the unpopulated Danube-delta that loses land under sea-level rise. Thus, the land loss there does not lead to significant migration. Romania thus has the highest land loss in the adaptation scenario, as this area will likely not be

*This project has received funding from the European Union's Horizon 2020 research and innovation programme under the Grant Agreement No **776479.***

protected. The negative land loss under lower sea-level rise for Finland and Sweden is due to the isostatic rebound (Peltier,2015), which leads to raising land (as it is observed today). Only high rates of sea-level rise will overturn this effect.

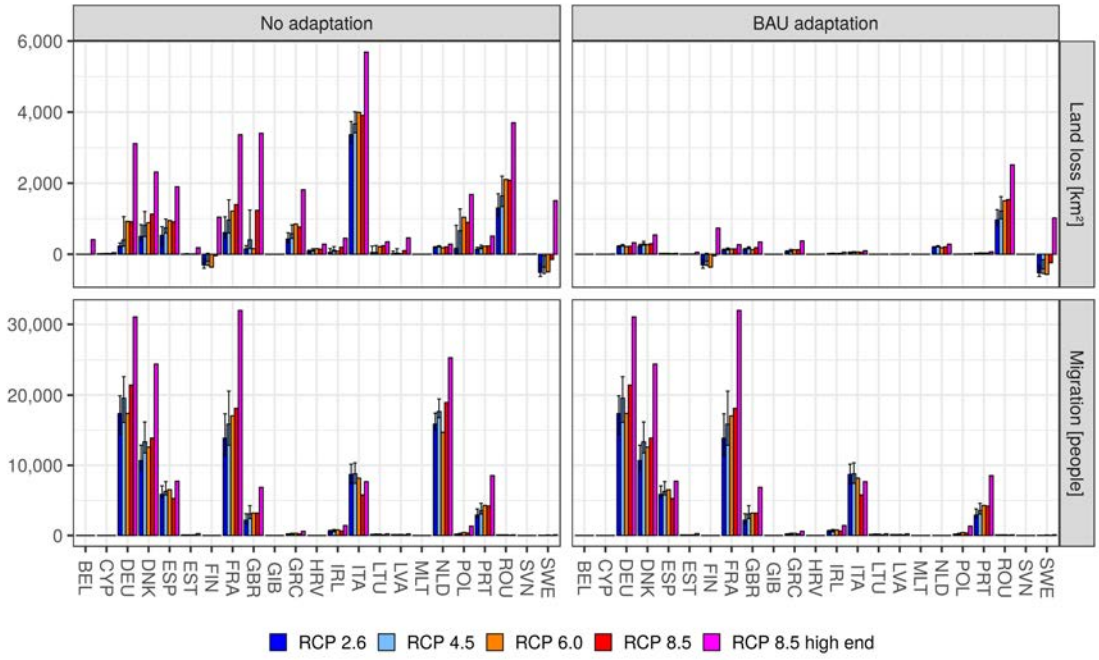

Figure 26: Accumulated national land loss and migration over 21st century (2015-2100) for EU 28 countries. Error bars for RCP 2.6 and RCP 4.5 show the uncertainty range over all runs done for these RCPs.

In terms of Migration, Germany and France are affected most. Even if the land loss is small for these two countries, they are in general densely populated so that almost every land loss leads to migration. The Netherlands lose a bit of land in the no adaptation scenario, but this land loss leads to quite some migration due to the high population density.

3.2 River floods: comparing GLOFRIS and LISFLOOD baseline

In this section, the results for river flood damage of the GLOFRIS and LISFLOOD grid-based damage models are compared. To enable the most transparent comparison, this is done for the baseline of the river discharge simulations of both models, which deviates from the COACCH baseline. In the other sections, we will correct the results to the COACCH baseline.

The GLOFRIS model projects annual riverine flood damage in the EU with a total of €9.5 billion in 2010 (with a 2015 price level). As shown in Figure 27, the highest expected damage values are found in Portugal, the Mediterranean coast of Spain and France, and regions in Croatia, Poland and Sweden.

*This project has received funding from the European Union's Horizon 2020 research and innovation programme under the Grant Agreement No **776479.***

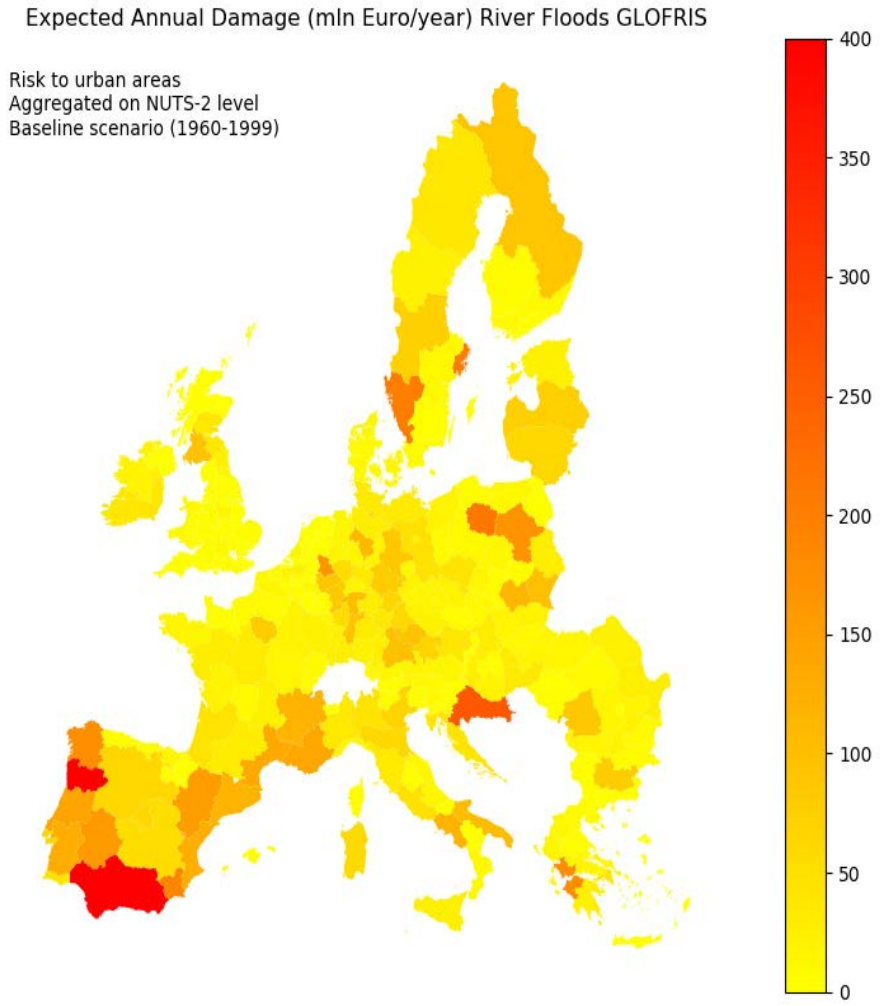

Figure 27: Expected Annual Damage from river floods for urban areas in 2010.

According to Lisflood, the baseline EAD from river floods amounts €8.8 billion per year. The spatial distribution on NUTS-2 level is shown in Figure 27. This baseline estimate is based on discharge observations from 1990-2016, for which inundation maps are simulated for the floods with return periods of 10, 20, 50, 100, 200 and 500 years. The floods extend are therefore representative for the year 2003, with a price level of 2015. For the other river flood risk results, both the flood maps and the damage estimates will be corrected in order to represent the COACCH evaluation years and the 2015 price level.

The most important differences between Lisflood and GLOFRIS are (a) the spatial resolution, (b) the exposure data and (c) the flood protection levels. (a) Lisflood's spatial resolution is 100x higher (100*100 m) than GLOFRIS' resolution (1*1 km). This

*This project has received funding from the European Union's Horizon 2020 research and innovation programme under the Grant Agreement No **776479.***

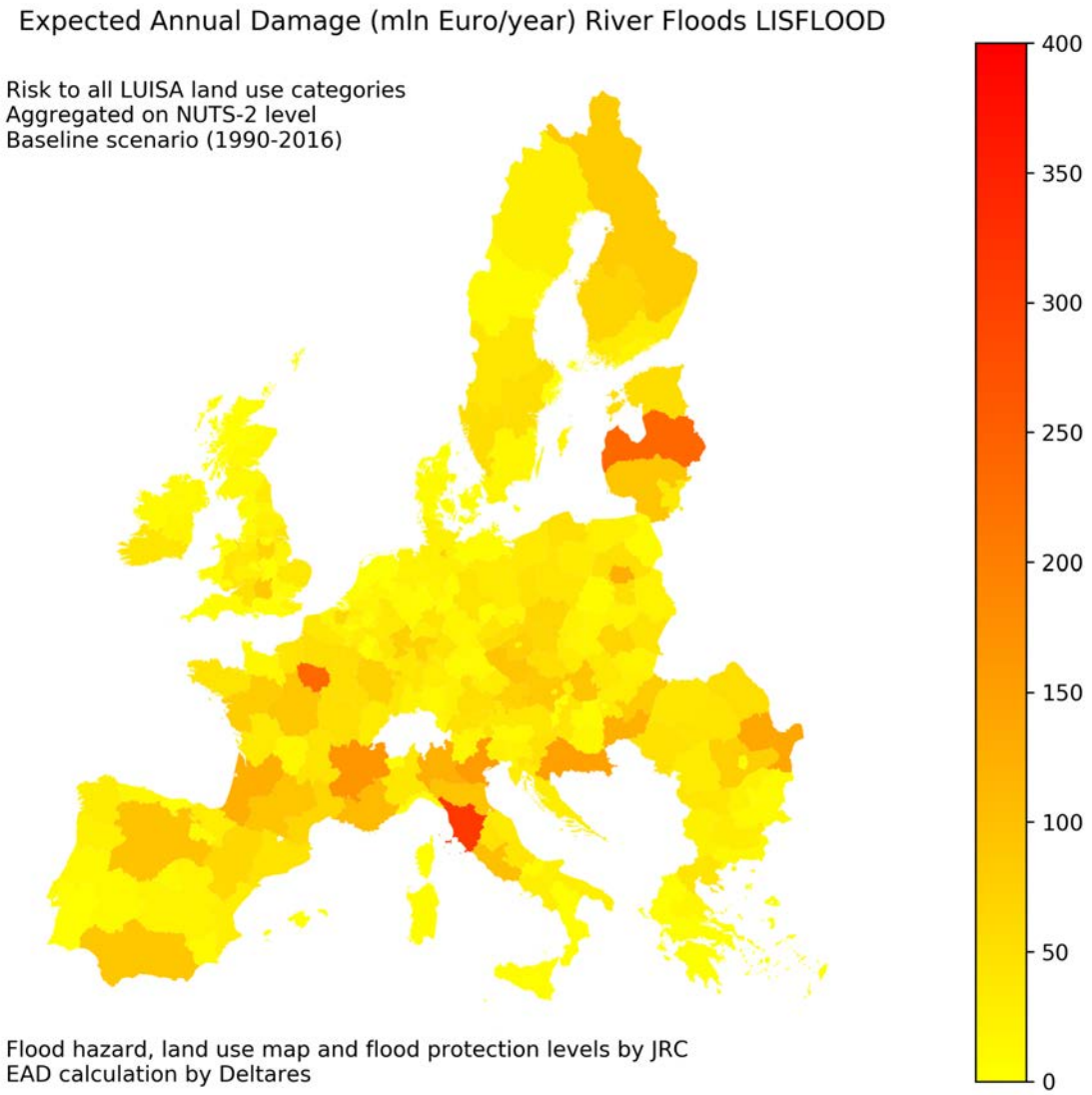

Figure 28: Baseline Expected Annual Damage from river floods for all land use categories in the LUISA landcover classification, for observed discharges in 1990-2016.

could partly explain the higher EAD estimate of GLOFRIS. GLOFRIS' coarser grid may predict certain assets to be hit by a flood, whereas Lisflood's finer grid predicts that the same assets are not hit. This difference especially matters in densely built areas, such as cities. Here, GLOFRIS sometimes overestimates the inundation extent because it needs to route the water via a 1*1 km grid. (b) The Lisflood exposure data is derived from the LUISA land use classification, which is a spatial and thematic refinement of the CORINE land cover classification, on a 100*100 km scale (Rosina et al, 2018). In contrast, the GLOFRIS exposure data is derived by multiplying the percentage of urban area per grid cell, which includes all kinds of built-up environment, by the estimated value of assets per square kilometer. The data for the current built environment per grid cell is taken from the HYDE database (Klein

*This project has received funding from the European Union's Horizon 2020 research and innovation programme under the Grant Agreement No **776479.***

Goldewijk, 2011), whereas the estimated asset value is taken from Ward et al. (2013). (c) Both Lisflood and GLOFRIS use protection levels derived from the FLOPROS database (Scussolini et al., 2016). In GLOFRIS, the modeled layer of the FLOPROS database is used, which assesses protection standards on a sub-national scale. The Lisflood flood protection data has been updated over the course of the years by the Joint Research Centre. Among these updates are corrections proposed by Jongman (2014) and various other sources. Other differences between Lisflood and GLOFRIS (as well as differences between values reported in other studies) may originate from different hydrologic input data, different methodologies to compute the expected annual damage (Olsen et al., 2015), hydrologic and hydraulic routing procedures (see the description of models in section 2.1).

Both Glofris (€9.5 billion) and Lisflood (€8.8 billion) find baseline annual damages above estimates reported by the British Insurance (€4.3 billiob) and the EEA (€8 billion) (both cited in Alfieri et al., 2015). This difference can be partly attributed to differences in baseline years and the associated corrections for inflation. They are however well within the range of other model studies reporting €5, €3, €13 and €7 billion annually for the baseline in Europe (Alfieri et al., 2018).

3.3 River floods: development of GLOFRIS built environment direct damages over the entire SSP/RCP/GCM space

In this section we show the development of EAD for NUTS2 regions over the periods 2030, 2050 and 2080 across a range of RCP-SSP combinations. For Figure 28 it can be seen that high-risk regions are similar to those shown in the baseline figure. However, amongst the highest EAD values now are regions in Northern Portugal, Croatia and Poland, whereas it can be seen that flood risk in the Po and Elbe river basin is projected to stagnate or slightly decrease compared to the baseline situation. Furthermore, the absolute difference in expected damage is larger between high- and low-risk regions compared to the baseline. For example, the lowest projected EAD for RCP4.5-SSP2 is approximately €7,000 damage per year in 2030 compared to €12,000 in 2010, whereas the maximum is €800 million in 2030 compared to €400 million in 2010. Finally, the difference across the scenarios is relatively small for 2030. For example, the average EAD across NUTS2 regions for RCP4.5-SSP2 is €64 million (SD = €100 million) , whereas this is €82 million (SD = €133 million) for RCP8.5-SSP5.

Figure 29 shows a slightly larger effect of climate- and socio-economic change on the expected annual flood risk in 2050 compared to 2030. The projected average EAD across regions under RCP4.5-SSP2 is €123 million, which remains relatively constant for scenarios plotted in panels A to E. The difference becomes particularly large for RCP8.5, the high-end carbon emission scenario, in combination with SSP5, which is a socio-economic scenario characterized by high economic growth. Under this

*This project has received funding from the European Union's Horizon 2020 research and innovation programme under the Grant Agreement No **776479.***

scenario, plotted in panel F, the average EAD across NUTS2 regions is €252 million, and the differences between high- and low-risk regions becomes greater, as the lowest observed EAD is €43,000 and the highest is €3.6 billion. The high growth of economic assets under this scenario, which is assumed to occur evenly across regions, largely causes the escalation of flood risk under this scenario. This is evident by comparing panel F with panel E, which is the outcome of the same RCP scenario, but instead includes a socio-economic scenario of low economic and population growth in Europe.

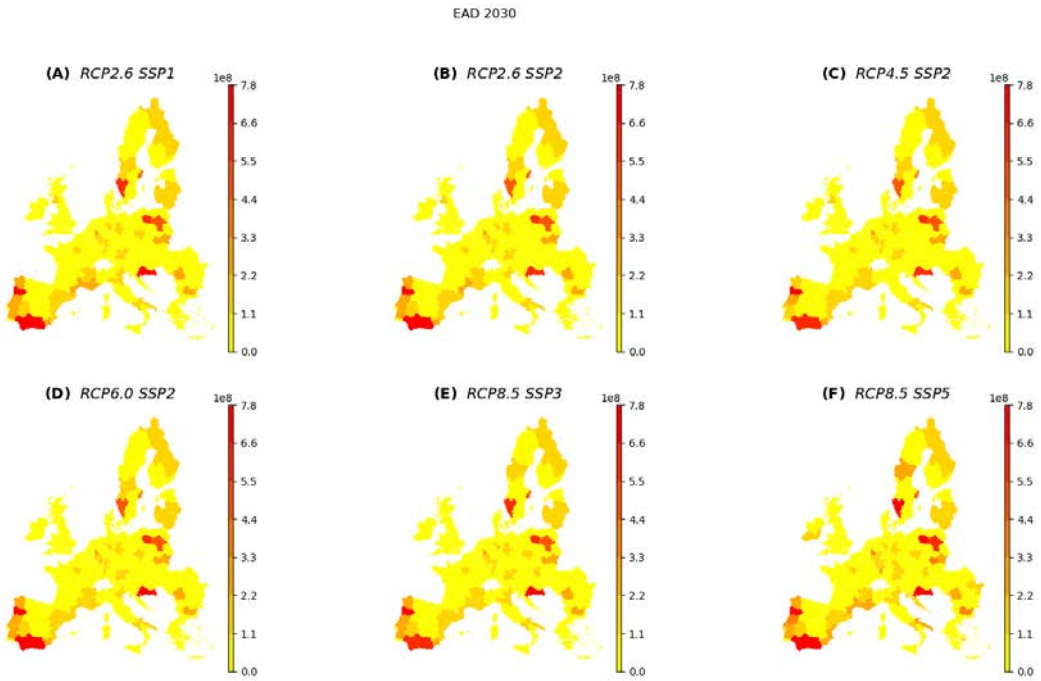

Figure 29: EAD estimates for 2030 for several RCP-SSP combinations

*This project has received funding from the European Union's Horizon 2020 research and innovation programme under the Grant Agreement No **776479.***

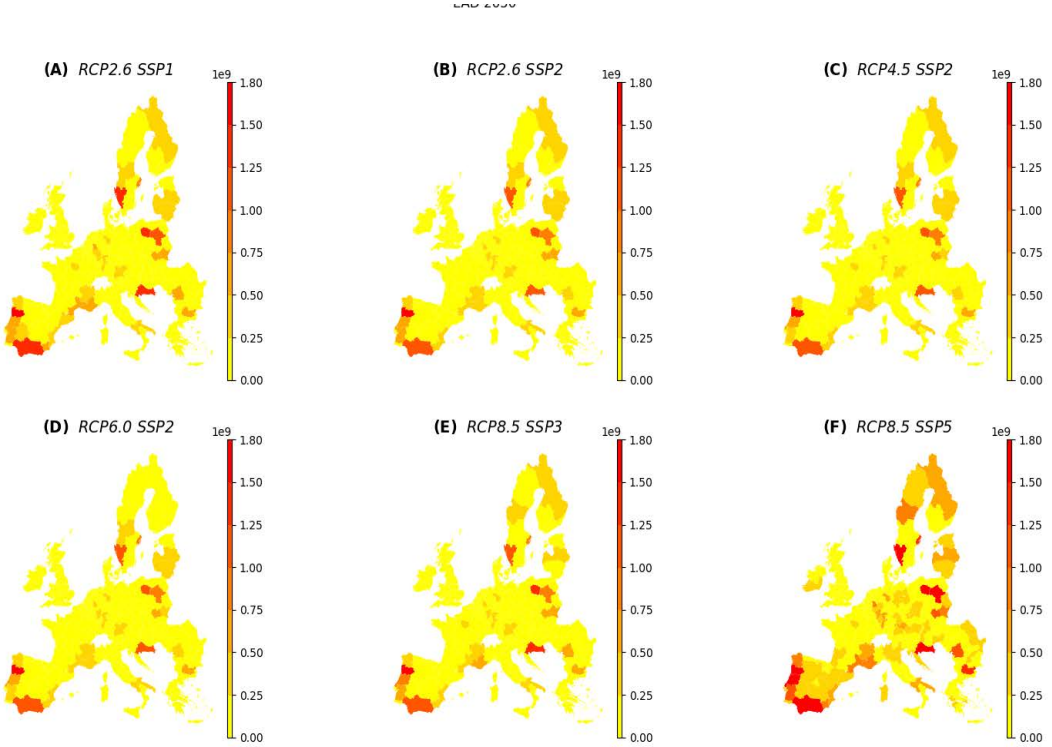

Figure 30: EAD estimates for 2050 for several RCP-SSP combinations

The developments observed in Figure 30 are further extended towards 2080, as shown in Figure 31 below. In addition to the regions already shown to have high expected damage in earlier projections, large parts of Germany, France, Sweden and Finland now show high levels of risk under the high-end scenario plotted in panel F. For scenarios plotted in panels A to E, the projected cumulative damage is in the range of €70-80 billion, whereas this is estimated to be €255 billion under RCP8.5-SSP5 projected in panel F.

The large difference observed between panels E and F, which share the same climate scenario, is caused by the projected socio-economic development towards 2080, which affects the exposure to flood hazard. Under SSP3, which represents the bleakest future in terms of economic growth out of the SSP-scenarios, GDP over the period 2010-2080 is expected to grow with a factor 1.5 on average over the NUTS2 regions, whereas for the same period this growth factor is projected at 5.6 under SSP5. The population, under SSP3, is projected to decline on average in the EU by 26.6%, whereas under SSP5 it is expected to rise with 45% compared to 2010.

*This project has received funding from the European Union's Horizon 2020 research and innovation programme under the Grant Agreement No **776479.***

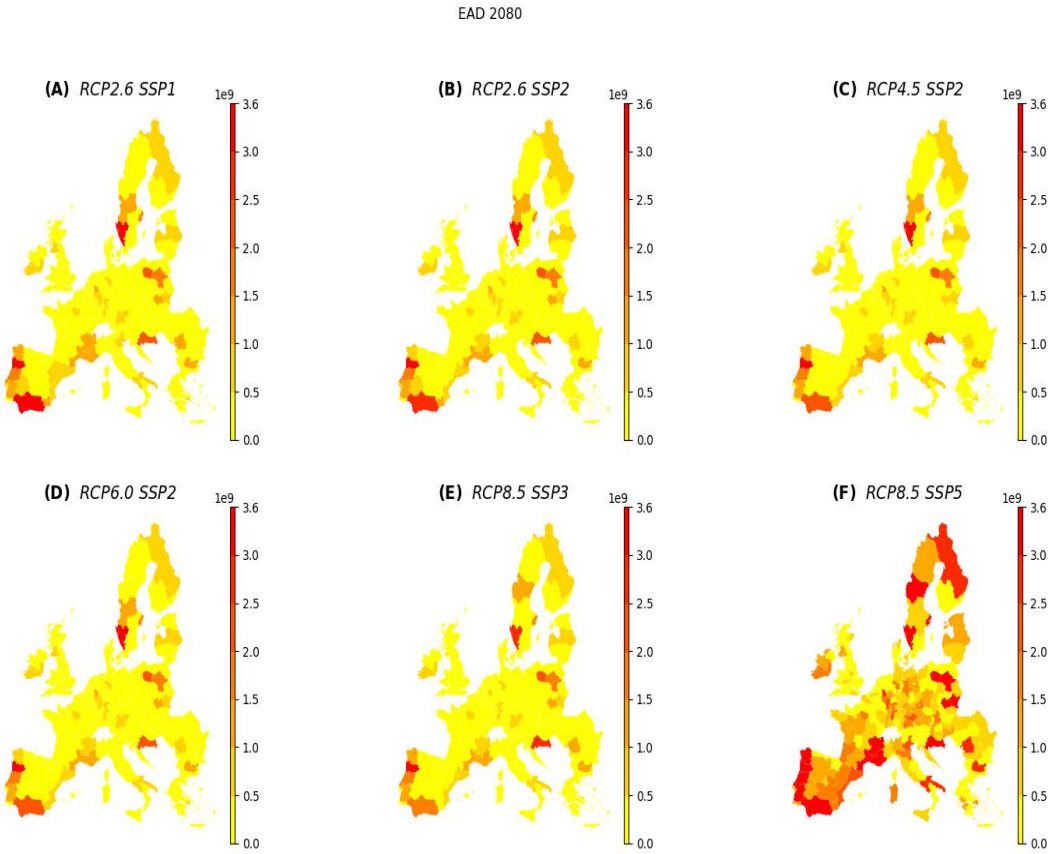

Figure 31: EAD estimates for 2080 for several RCP-SSP combinations

3.4 River floods: CLIMRISK-RIVER

In this section, we present some key results from the CLIMRISK-RIVER model. First, the model is validated using in-sample and out-of-sample GLOFRIS Δ*EAD* estimates. Next, the flood damage estimates produced by the model are presented on an aggregate level for Europe. Here, we also present some key country-level results. Finally, particularly interesting local damage estimates are presented to illustrate the relevance of estimating climate impacts at a spatially explicit level.

Model Validation

The model fit to GLOFRIS data is shown in Figures 32 below for CLIMRISK-RIVER model (Model 6) and an alternative, Model 2. Please note that we assess performance of the model on the global scale here. Two main conclusions can be drawn from these figures. First, Model 6 has a better fit to actual data than Model 2 as is measured by the mean-normalized RMSE and adjusted R^2. The variance of the mean-normalized adjusted R^2 is lower under Model 6. Whereas Model 2 only accounts for GDP and first order temperature change, Model 6 also accounts for precipitation and the squared and interaction terms of temperature and

*This project has received funding from the European Union's Horizon 2020 research and innovation programme under the Grant Agreement No **776479.***

precipitation. Second, Model 6 is able to predict future projected GLOFRIS estimates reasonably well with the majority of predictions not over or underestimating by more than 1.5 times the mean value of the projected GLOFRIS damage.

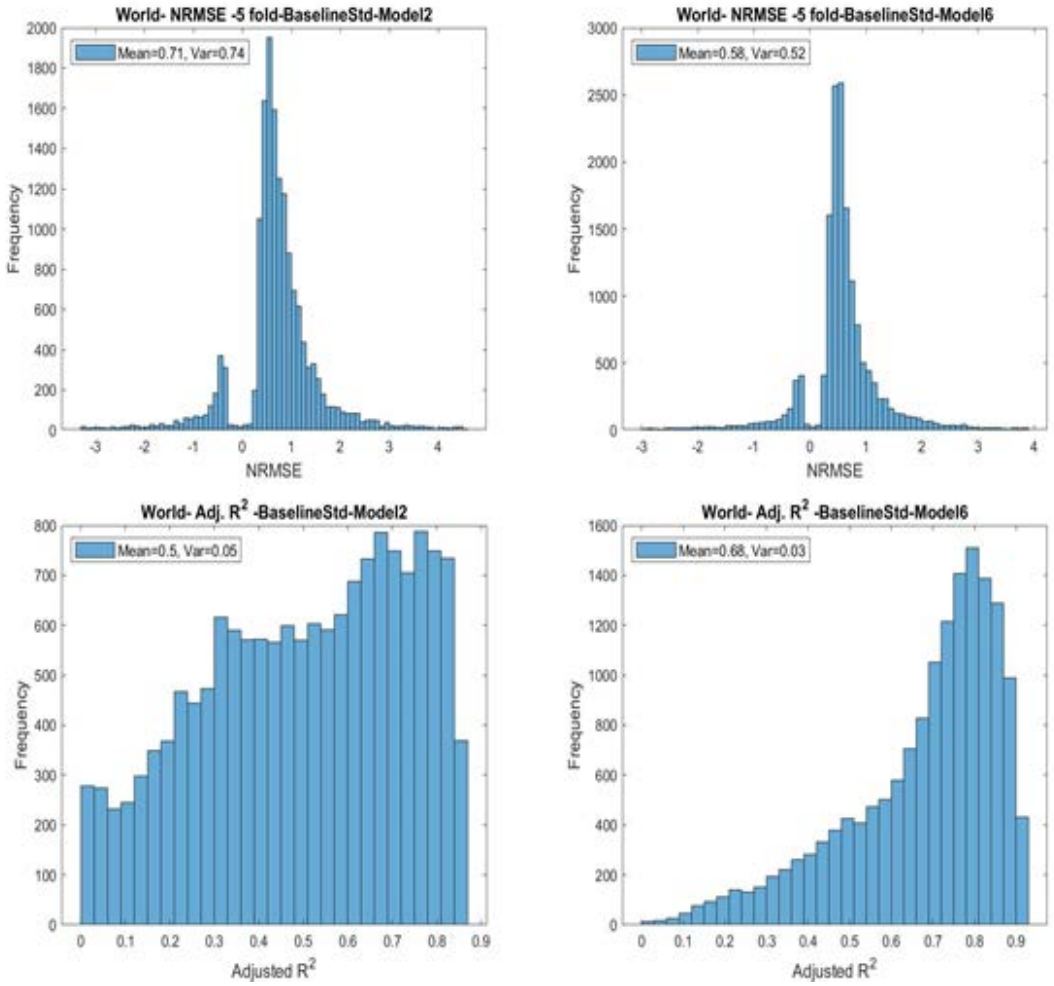

Figure 32: Model fit and forecasting performance of models 2 and 6: The CLIMRISK-RIVER Model 6 (right panel) has a better model fit and forecasting performance than Model 2 (left panel) measured by both.

The spatial distribution of adjusted R2 and NRMSE in Europe is shown in Figure 33 along with their respective histograms in Figure 34. In Europe, the adjusted R2 is higher in central and western parts than in eastern Europe and the Baltic region. These figures confirm that overall the CLIMRISK-RIVER model also performs well in Europe.

*This project has received funding from the European Union's Horizon 2020 research and innovation programme under the Grant Agreement No **776479.***

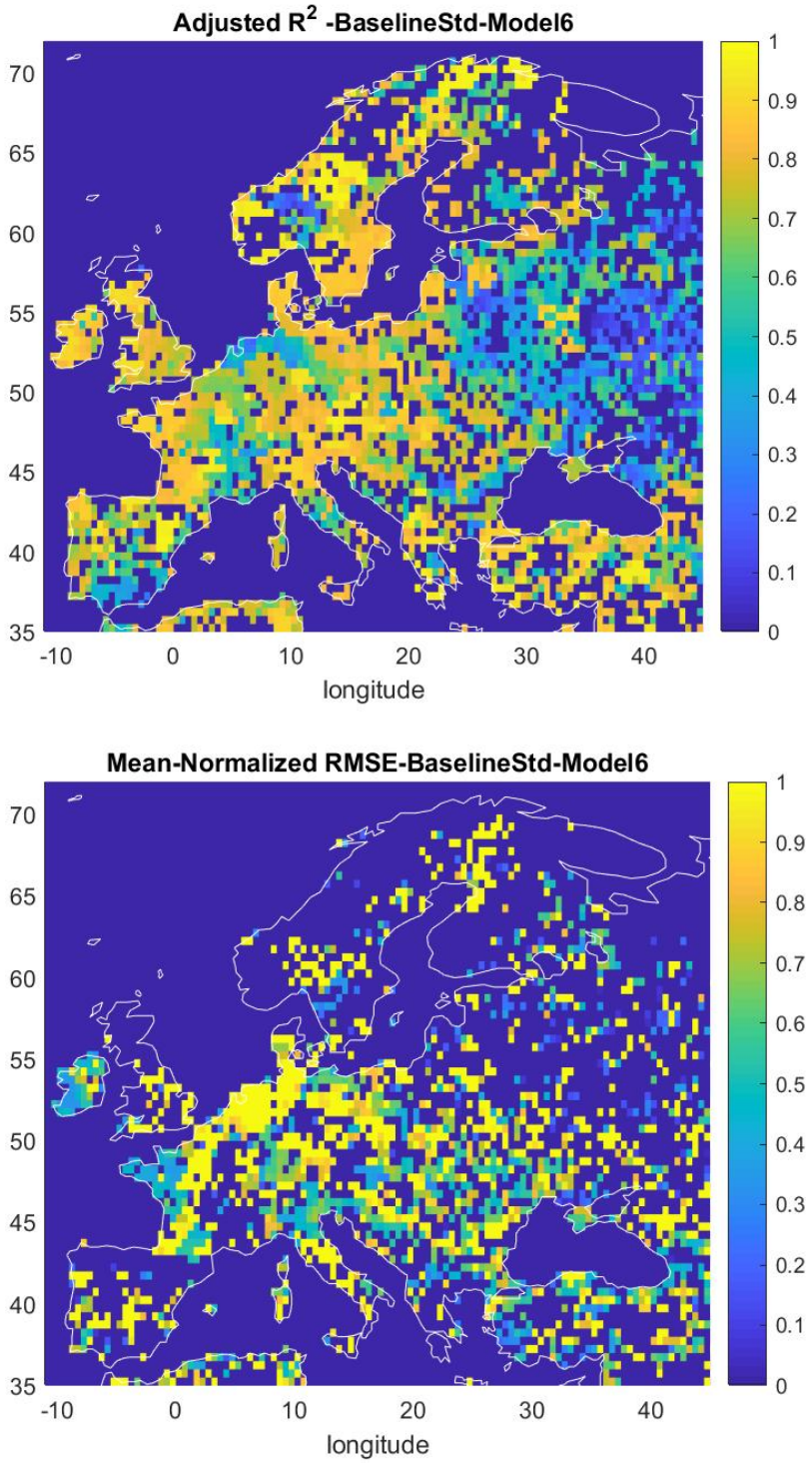

Figure 33: Adjusted R^2 and NRMSE: Measures of model fit and forecasting performance in Europe. When NRMSE=1 for a given cell, the model makes a forecasting error equal to the mean value of ΔEAD_{GF}

*This project has received funding from the European Union's Horizon 2020 research and innovation programme under the Grant Agreement No **776479.***

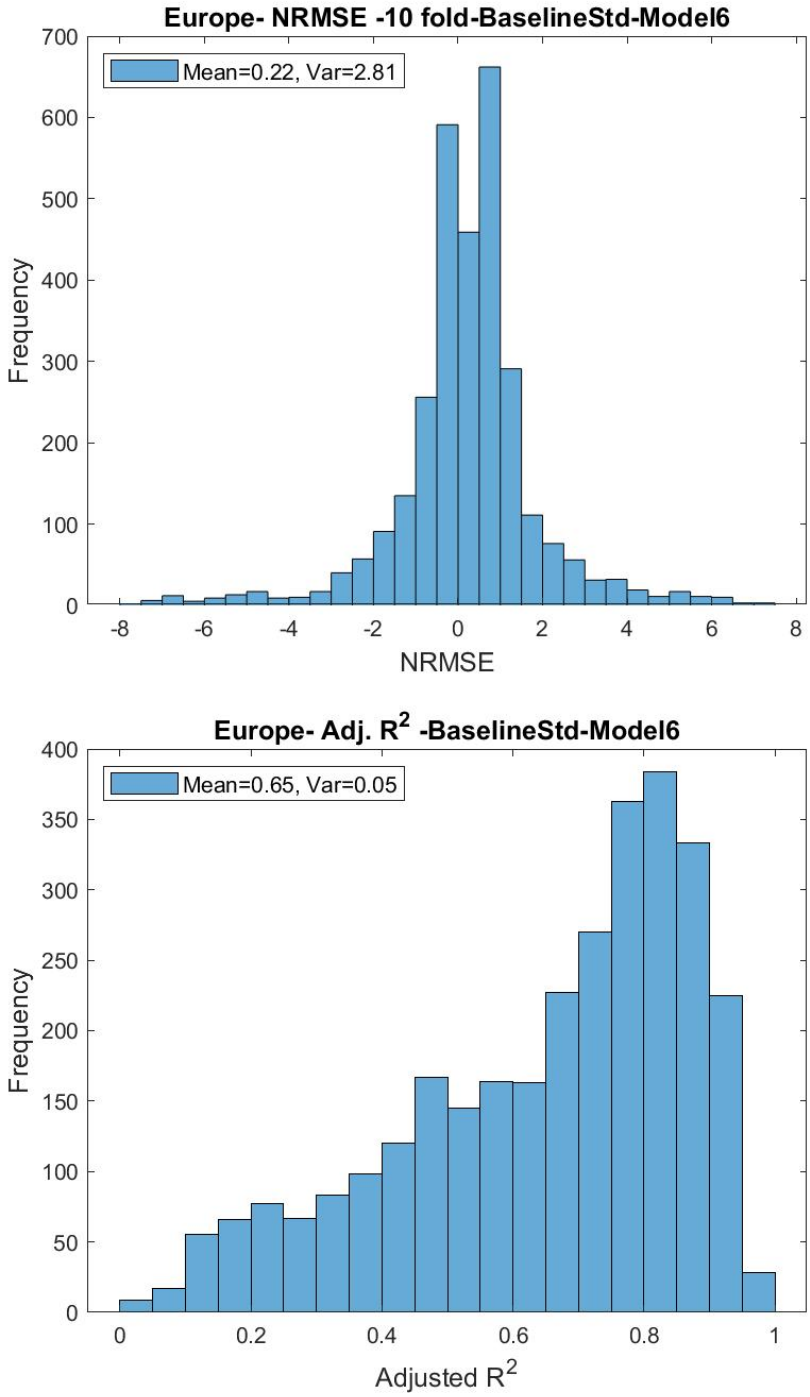

Figure 34: Forecasting performance of CLIMRISK-RIVER (Model 6) as measured by the distribution of NRMSE and adjusted R^2 in Europe.

*This project has received funding from the European Union's Horizon 2020 research and innovation programme under the Grant Agreement No **776479.***

Aggregate Flood Risk

Next, we look at the development of climate change related flood risk on an aggregate level, firstly on a regional and continental and then on a country level. Figure 35 shows the evolution of river flood risk on a global scale in Europe. The results do not vary significantly between different RCP scenarios in the first half of the century but start to diverge in the second for both adaptation assumptions. The reduction in river flood risk is much greater with the upkept protection standards (*CurrentStd*) than with a more strict emission reduction policy, regardless of the RCP scenario or region. This is evident from the spread between the red and blue lines corresponding to *BaselineStd* and *CurrentStd*. The evolution of climate related river flood damage is similar in Europe, with discounted (3%) damage reaching €22-30 billion in 2100.

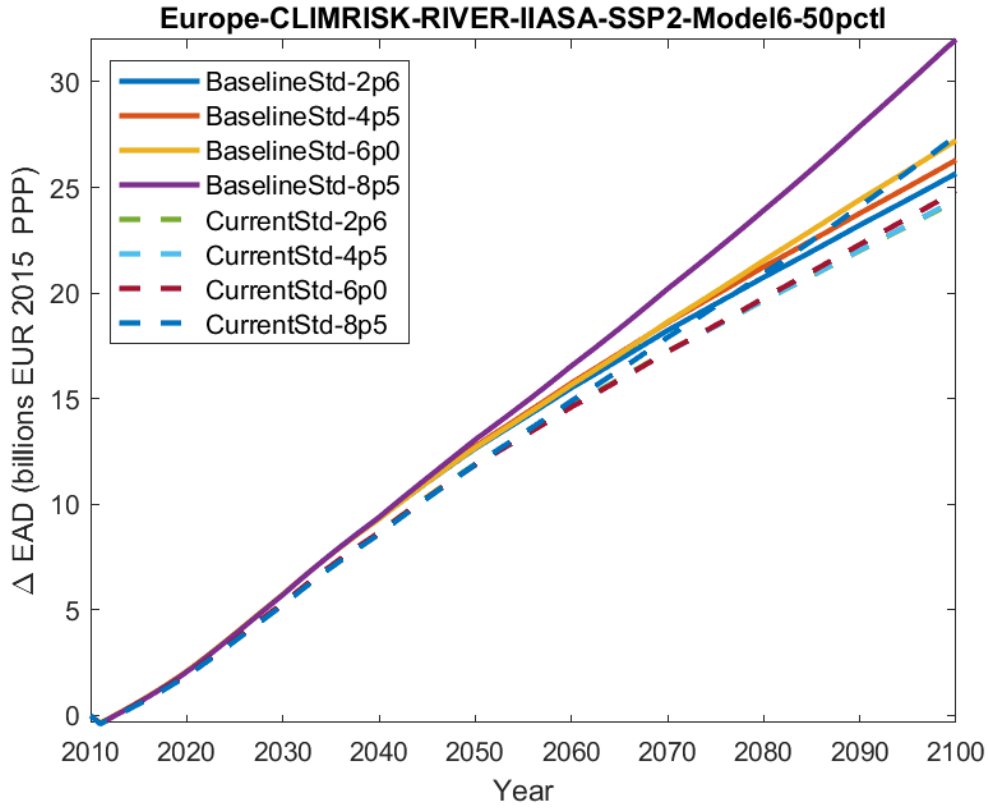

Figure 35: Evolution of ΔEAD in Europe for BaselineStd and CurrentStd flood adaptation assumptions for different RCP scenarios (2.6, 4.5, 6.0 and 8.5) under the SSP2 socioeconomic scenario.

However, when modelled river flood risk is put into perspective of the total damage from climate change in Europe in Figure 36, then the results are not all too worrying. The total damage estimates in CLIMRISK exceed €1.5 trillion under RCP 6.0 - SSP2 and reach €800 billion under RCP 2.6 - SSP2 in 2100. However, the CLIMRISK-RIVER estimates in Europe never exceed €35 billion by 2100 under any RCP scenario.

*This project has received funding from the European Union's Horizon 2020 research and innovation programme under the Grant Agreement No **776479.***

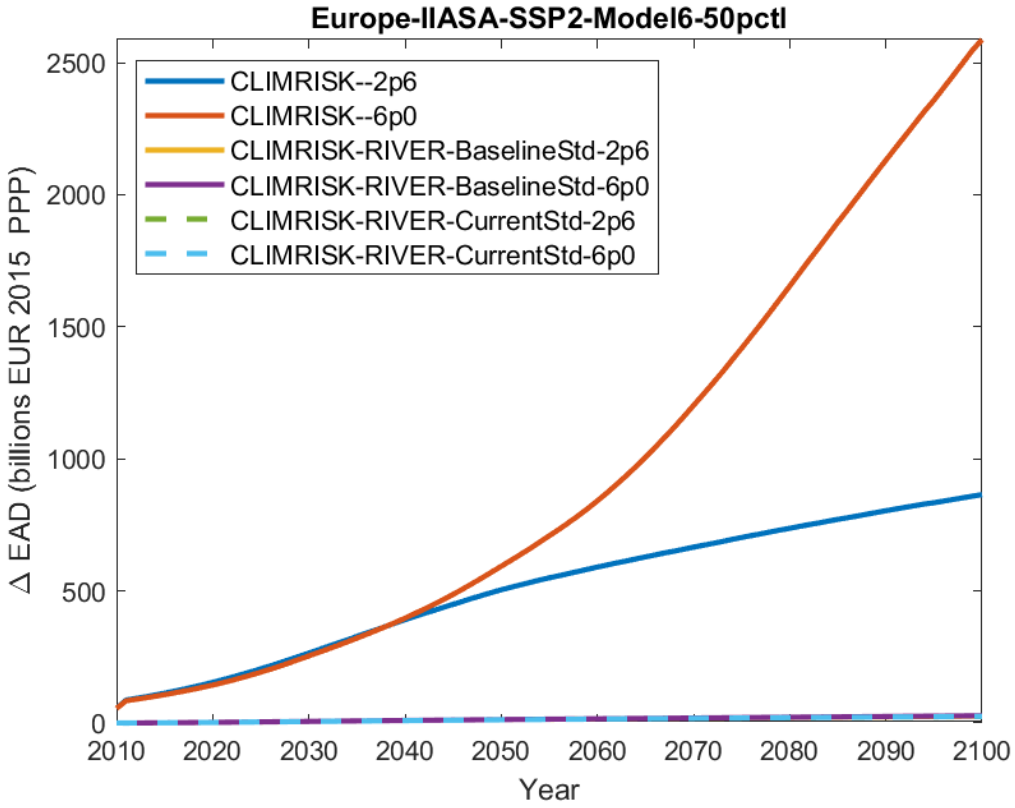

Figure 36: River flood risk makes for a small portion of aggregate risk of climate change in Europe

Next, we wish to present the CLIMRISK-RIVER damage estimates on a country level. The damage estimates are presented in terms of total discounted Δ*EAD*. Figure 37 below presents a european map of country-level damage estimates. The discounted total damage in Europe is relatively low compared to the rest of the world since many developed countries already have high river flood protection standards in place. Nevertheless, economically leading european countries with a lot of exposed assets tend to have the highest modelled flood risk. Some notable EU28 examples include Germany with €29 billion, Portugal with €18 billion, Italy with €14 billion and France with €12 billion in discounted total ΔEAD under the RCP6.0 - SSP2 scenario.

*This project has received funding from the European Union's Horizon 2020 research and innovation programme under the Grant Agreement No **776479.***

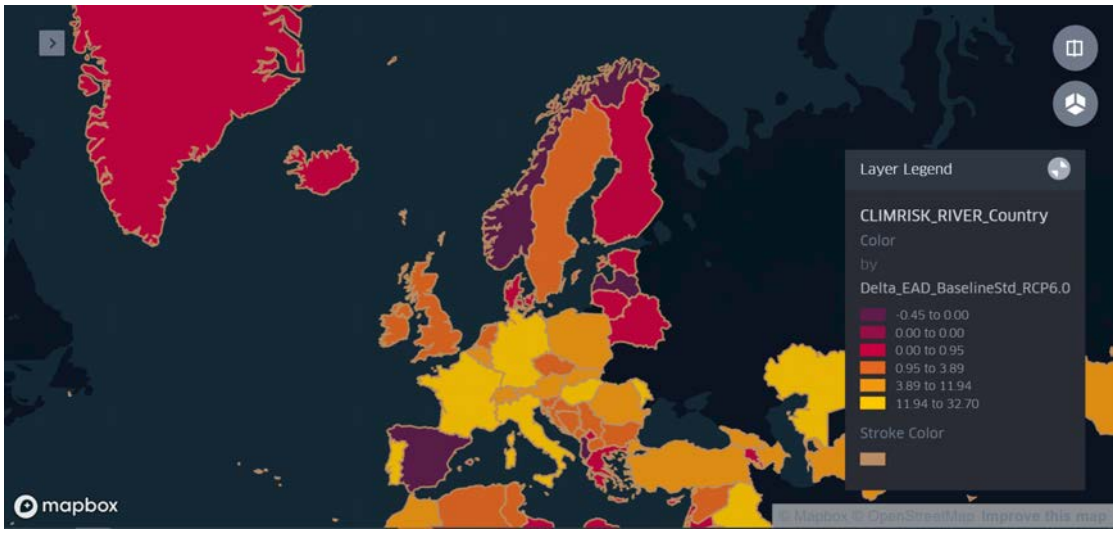

Figure 37: Discounted change in EAD of river flooding in Europe per country. Scenario combination: RCP 6.0 - SSP 2

Local Flood Risk

In this section, we analyze the local impacts of river flooding due to climate change. Figure 38 illustrates the flood risk in Europe under *BaselineStd* and *CurrentStd* scenarios. The selected scenario combination in this figure is RCP 6.0 - SSP2. In Europe, the area around the Rhine river basin and the Black Sea is expected to be most affected by climate change related river flooding, with many cells exceeding €500 million in discounted total EAD over the twenty-first century. The lowest flood risk is expected in the Baltic countries in North-Eastern Europe. It is important to notice that, although small compared to many areas in the world, river flood risk in Europe can locally be relatively high. Some cells in Central Europe, around the Rhine river basin in Germany, are expected to experience over €2 billion in discounted total flood damage which is very high relative to the other parts of Europe considering the cell-size. This result highlights the importance of modelling local-level flood risk as country-level and other aggregate results fail to provide information on the spatial distribution of risk.

*This project has received funding from the European Union's Horizon 2020 research and innovation programme under the Grant Agreement No **776479.***

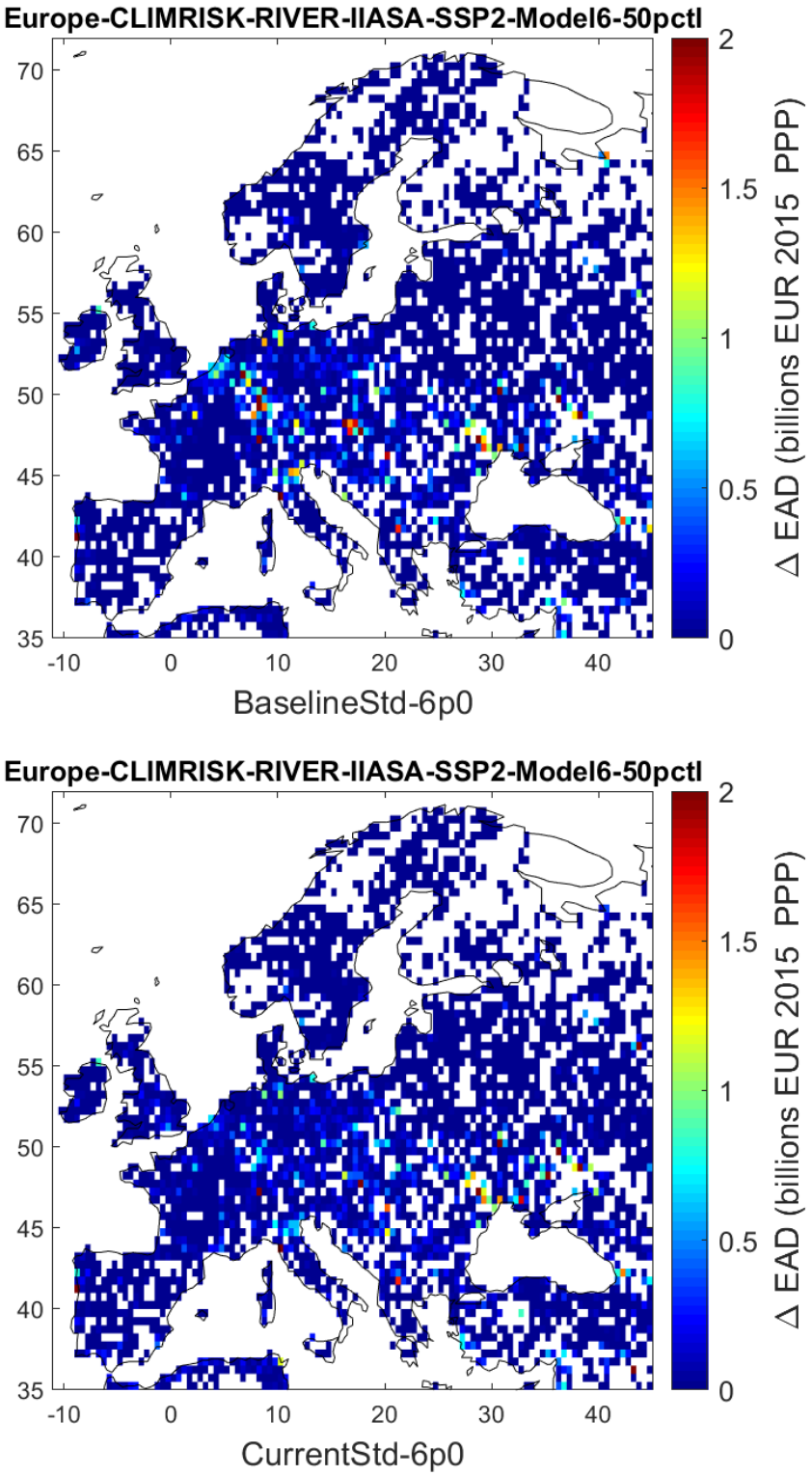

Figure 38: Discounted change in EAD of river flooding in the twenty-first century for Europe for RCP 6.0 - SSP2 - BaselineStd and CurrentStd adaptation assumptions

*This project has received funding from the European Union's Horizon 2020 research and innovation programme under the Grant Agreement No **776479.***

3.5 River floods: impacts on road transport infrastructure

In this section, the flood risk to road infrastructure in the EU-28 is described. First, the expected annual damage (EAD) in the baseline scenario is described, from road segment level up till the total damage in the EU-28. Then, we describe how this flood risk may change as a result from climate change, irrespective of socio-economic changes. Finally, we address the effects of climate change (RCPs) and socio-economic development (SSPs) combined.

Baseline

In the baseline scenario, the expected annual damage (EAD) to road infrastructure is calculated using two methods. The first method is grid-based and overlays the Lisflood hazard maps with the LUISA land use categories containing infrastructural land use (see method section 2.6). According to this method, the EAD is €276 million per year for the EU-28 (Figure 39, left-hand panel). This includes damages to road and rail networks, as well as road and rail assets found in urban and industrial areas. The second method uses the line-based OSdaMage model and a new set of damage curves (See section 2.6.3). According to this method, the EAD is €205 million per year for the EU-28 (Figure 39, central panel). This only includes direct damage to road infrastructure. It includes damage to the roads itself, but not any additional damage to tunnels and bridges. In the remainder of this section, we restrict ourselves to these direct costs to the road infrastructures, as determined with the OSdaMage model.

The EAD estimates in OSdaMage visualize a large uncertainty band, originating from two factors. The first factor is uncertainty in flow velocity. For damage to road infrastructure, flow velocity is at least as important as water depth (Kreibich et al., 2019). Under low flow velocities, road pavements may remain almost undamaged, whereas under high velocities, complete reconstruction may be required for the same water depths. The low flow and high flow bound of the velocities that can be found in the Lisflood model are represented by the two boxplots (Figure 39, central panel). The second factor is uncertainty in the economic value of the road assets. Within Europe, there is large variability in road design practices, which is reflected in large range of potential max damages per road (Table 9). The box-and-whisker plots represent the min, 25%, 50%, 75 and maximum potential damage of this range (Figure 39, right-hand panel). Of course, the grid-based 'reference' model also has this very large uncertainty band, the range of this uncertainty is however not known.

Additional metadata from OSM is used to give a best estimate within this range of uncertainty, referred to as the 'Litmix' estimate (Table 9). As discussed in the method section, separate damage curves were developed for motorways and trunk roads with sophisticated accessories (like street lighting and electronic signalling) in contrast to simple roads that lacking these accessories. In OSM, data on the presence of street lighting is available for parts of the road network. From this data, a specific mix of damage curves, max damage range and flow conditions was made, further referred to as the 'Litmix': For motorway and trunk roads with street lighting, the

*This project has received funding from the European Union's Horizon 2020 research and innovation programme under the Grant Agreement No **776479.***

'sophisticated accessories' damage curves (C1 and C2) were used; the 3rd quartile of the max damage range (corresponds to upper part of boxes in Figure 39, center panel) was taken; and the average of the upper and high flow curves were taken. For motorway and trunk roads without street lighting, the simple (no accessories) curves (C3 and C4) were used, in combination with the 1rd quartile of the max damage range (the bottom part of the boxes in Figure 39); and again the average of the upper and high flow curves were taken. For all other road types, the average of the upper and high flow curves is taken.

Table 8 Parameter settings for the 'Litmix' estimate

	If road type is motorway or trunk		Other road types
	If street lighting is not present	If street lighting is present	n.a.
Damage curve	Simple roads (C3 and C4) Average of low-flow (C3) and high-flow curve (C4)	Accessories roads (C1 and C2) Average of low-flow (C1) and high-flow curve (C2)	Average of low-flow (C5) and high-flow curve (C6)
Max damage estimate	1st quartile	3rd quartile	Average value of max damage range

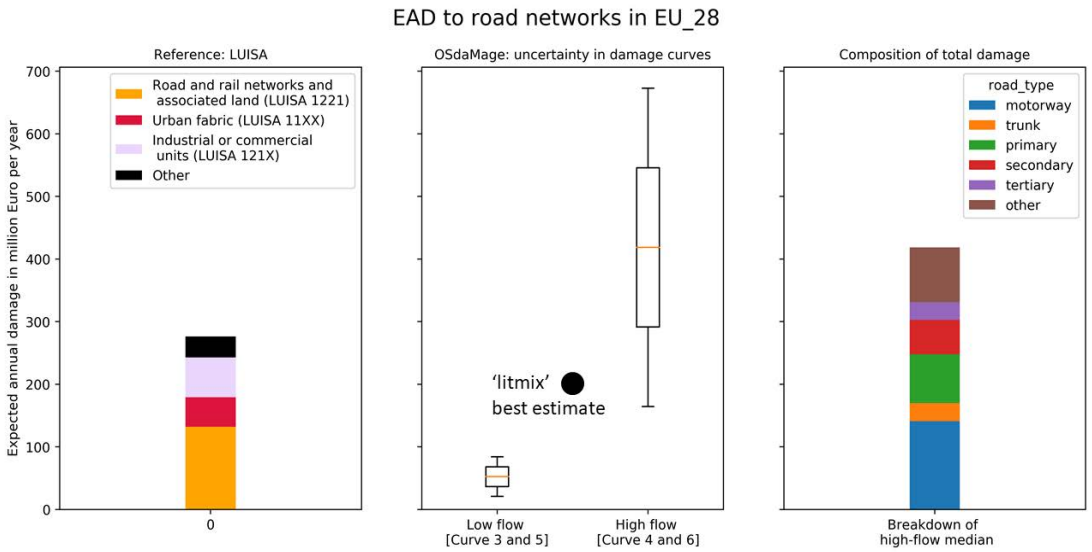

Figure 39: Expected Annual Damage (EAD) to road infrastructure in the EU-28, in the grid based reference model (left-hand panel); according to the OSdaMage model (central panel) and break-down of OSdaMage result by road type (right-hand panel)

The right-hand panel shows of Figure 39 shows how the damage is composed of contributions from different road types.

The spatial distribution of the EAD is shown on the NUTS-3 (Figure 40) and NUTS-2 (Figure 41) level. Germany, France and Italy are exposed to the highest flood risk

*This project has received funding from the European Union's Horizon 2020 research and innovation programme under the Grant Agreement No **776479.***

(resp. €45, €43 and €23 millionn). The risk is concentrated around the rivers that spring in the Alps and then flow through regions with dense road networks, such as the Danube and Rhine in Germany; the Rhône in France and the Po in Italy. Germany has an additional flood hotspot in the Elbe River basin, Franch in the Garonne River basin and Italy in the Tiber River basin. Two remarkably high-risk NUTS-2 regions are Pohjois- ja Itä-Suomi (Finland) and Kontinentalna Hrvatska (Croatia), see Table 10.

Besides the region-aggregated results as outlined above, the new OSdaMage model also allows for a road-specific representation of the results. Figure 42 gives an overview of the flood risk for the EU-28 motorway and trunk network, highlighting some particular high-risk areas.

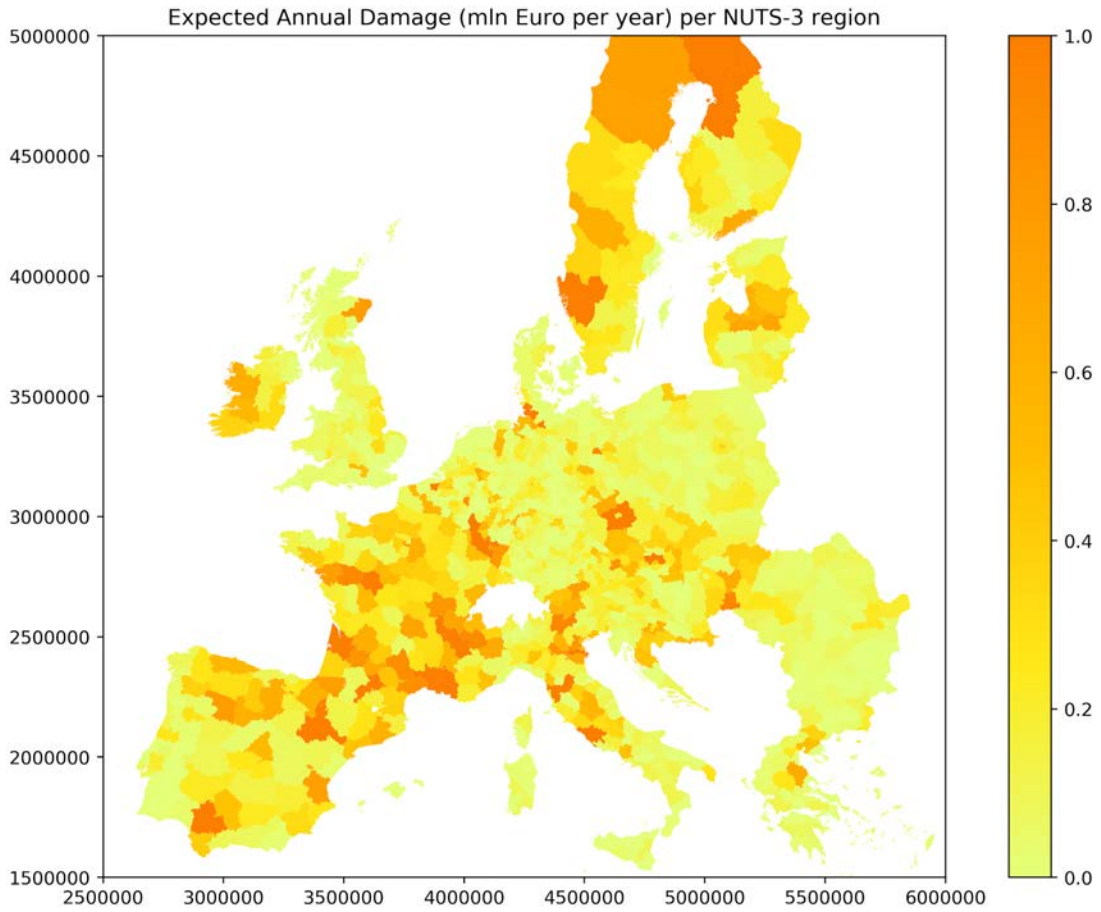

Figure 40: ***Expected Annual Damage (EAD) to road infrastructure in the baseline scenario, aggregated on the NUTS-3 level, according to the OSdaMage model***
x and y coordinates according to the ETSR89/EPSG:3035 projection

This project has received funding from the European Union's Horizon 2020 research and innovation programme under the Grant Agreement No ***776479.***

Table 9: Top-10 NUTS-3 regions with highest EAD

NUTS-3 code	Name	EAD (million Euro)
FI1D7	Lappi	2.3
FRK26	Rhône	2.1
ITI14	Firenze	1.8
ITI17	Pisa	1.7
DE600	Hamburg	1.7
ITI43	Roma	1.6
FRI12	Gironde	1.6
SE232	Västra Götalands län	1.5
ES243	Zaragoza	1.4
FRJ23	Haute-Garonne	1.4

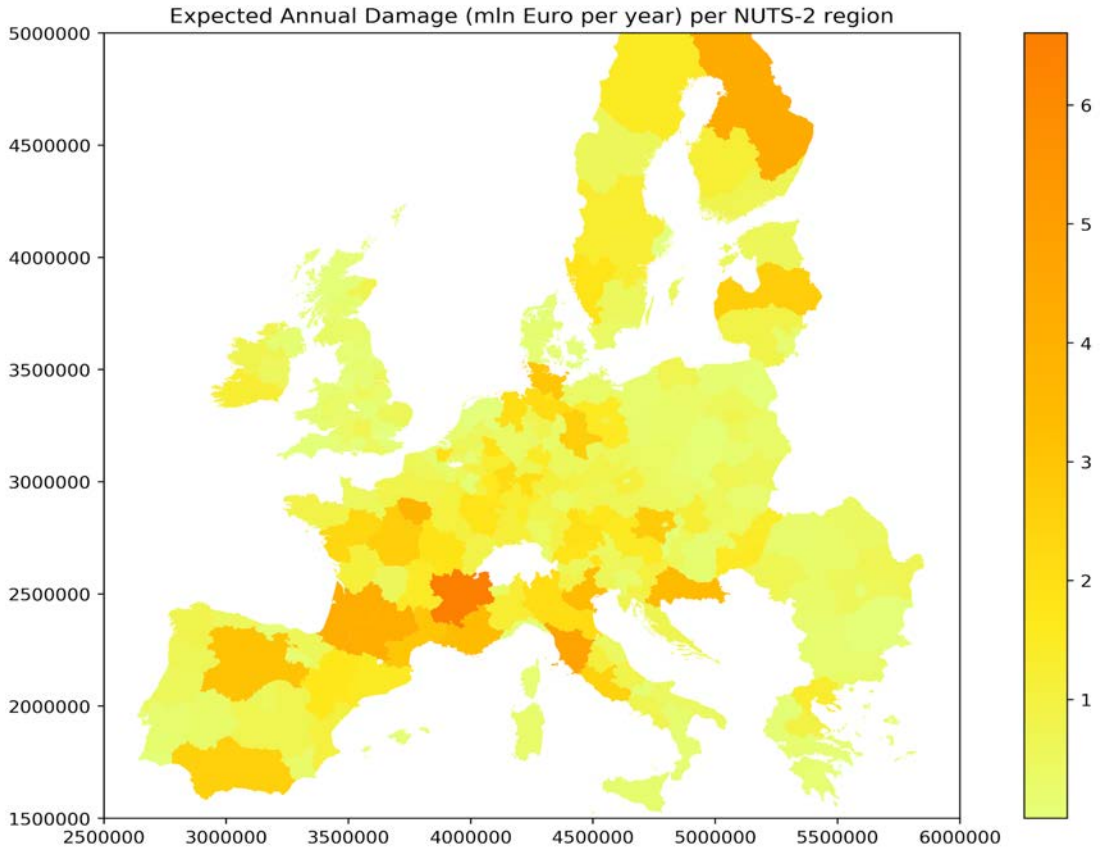

Figure 41: Expected Annual Damage (EAD) to road infrastructure in the baseline scenario, aggregated on the NUTS-2 level, according to the OSdaMage model (x and y coordinates according to the ETSR89/EPSG:3035 projection)

*This project has received funding from the European Union's Horizon 2020 research and innovation programme under the Grant Agreement No **776479.***

Table 10: Top-10 NUTS-2 regions with highest EAD

NUTS-2 code	Name	EAD (million Euro)
FRK2	Rhône-Alpes	6.6
ITI1	Toscana	4.7
FI1D	Pohjois- ja Itä-Suomi	4.4
FRI1	Aquitaine	4.1
FRJ2	Midi-Pyrénées	4.1
FR10	Ile-de-France	3.8
HR04	Kontinentalna Hrvatska	3.4
FRL0	Provence-Alpes-Côte d'Azur	3.3
ITH3	Veneto	3.3
ES41	Castilla y León	3.1

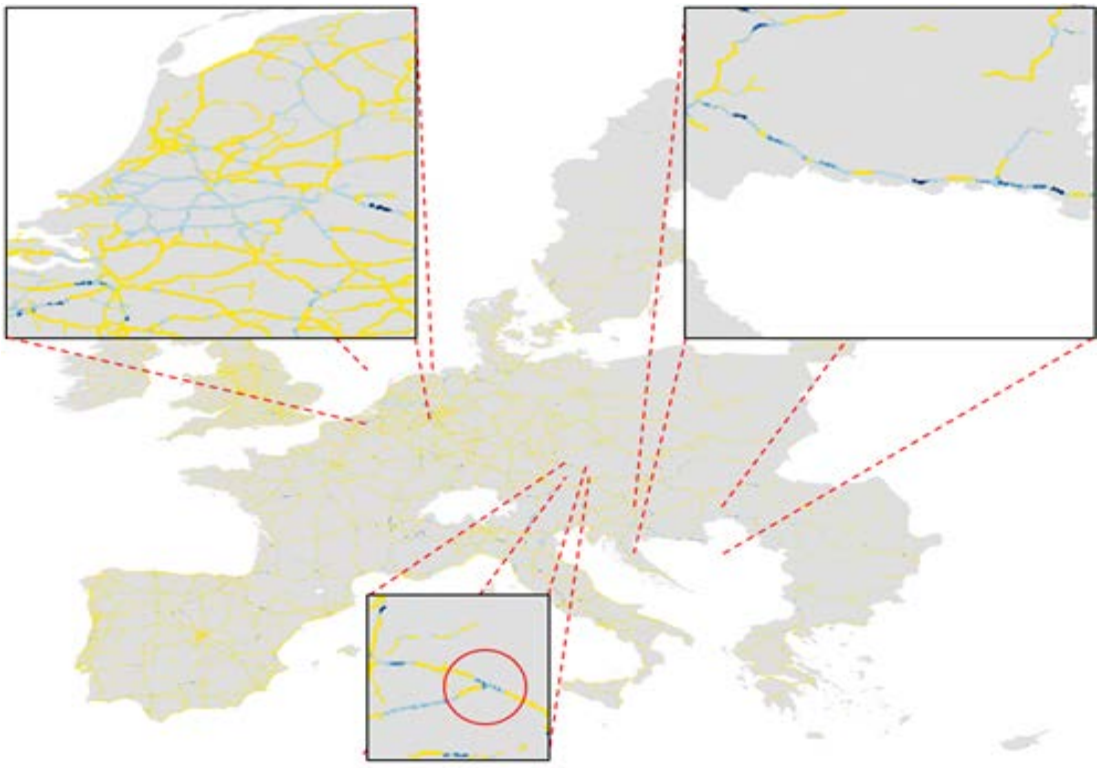

Figure 42: ***EAD to motorways and trunks in the EU-28 main road network*** *(a high resolution image, as well as country-level figures, can be retrieved from Deltares upon request). Red circle indicates the location of the Deggendorf flood event, which is recognized as a high-risk area by the OSdaMage model.*

This project has received funding from the European Union's Horizon 2020 research and innovation programme under the Grant Agreement No ***776479.***

To illustrate the richness of Figure 42 we now present an illustrative list of 10 high-risk motorway/trunk sections, which could lead to considerable direct- and indirect impacts of river flooding.

- Germany: the North-Western Estuaries (Eems-Dollard, Wezer River, Elbe River); threatening roads around the towns of Leer, Bremen and Hamburg.
- Scandinavia: Götenburg (notably the E20); as well as many trunk roads in Northern Sweden and Finland
- Lithuania: key trunk roads connecting Riga
- Poland: the S7 between Gdànsk and Elbląg
- Austria-Slowakia: roads from Vienna-Bratislava at risk from Danube River; and from the Morava River (border) and Váh River (Slowakia)
- Croatia: A3/E70 highway from Zagreb all the way to Serbia (See frame Figure 42)
- Italy: Po River crossing big motorways: A13 (Padua-Bologna); E45/A22 (Verona-Modana); E70 and E35 around Piacenza
- Austria: the A93 from Raubling to Innsbrück; the E60 from Innsbrück to Landeck
- French Alps: A41 and A43 near Grenoble and Chambéry along Isère River; A6 from Mâcon to Lyon along Saône River
- The Netherlands: floods in the Delta of Rhine-Meuse Rivers could cause severe disruptions of the countries' motorway networks; although the likelihood (and thus the EAD) of such events is small because of very high flood protection levels.

Note that this overview is not complete. Also note that this approach helps to get a first impression of high-risk areas, but is not suitable for accurate forecasting of flood risks on a high spatial level. Although the quality of the OSM-data would be good enough to do this, the inaccuracy of the flood risk data (notably the elevation map behind this data) and uncertainty about local measures to reduce flood risks is considerable. This overview, however, can be used as a starting point for local investigations. Also, it will be used to study the relation between direct- and indirect costs of road disruptions and if these indirect effects could have 'tipping point' characteristics (COACCH Work Package 3).

Climate change results: only RCPs

In this section, the development of damage to road infrastructures due to river flooding under scenarios for climate change is presented. Here we restrict ourselves to the development of damage as a result of climate change (RCPs), irrespective of socio-economic development (SSPs). Figure 43 shows that, without adaptation, there is a very strong increase of flood risk under by 2086, under RCP8.5. Figure 44 shows that these projections are very sensitive to the used combination of global climate models and regional circulation models. As a best estimate, we take the EU-28 summed, median results of the model runs (Table Error: Reference source not found). Without adaptation, the EAD increases by 165% to €537 million per year by 2086 under RCP4.5. Under RCP8.5, the increase is 365% to €825 million per year by

*This project has received funding from the European Union's Horizon 2020 research and innovation programme under the Grant Agreement No **776479.***

2086. With adaptation, the increase is only 2% for both RCPs (Table 3.5.3).

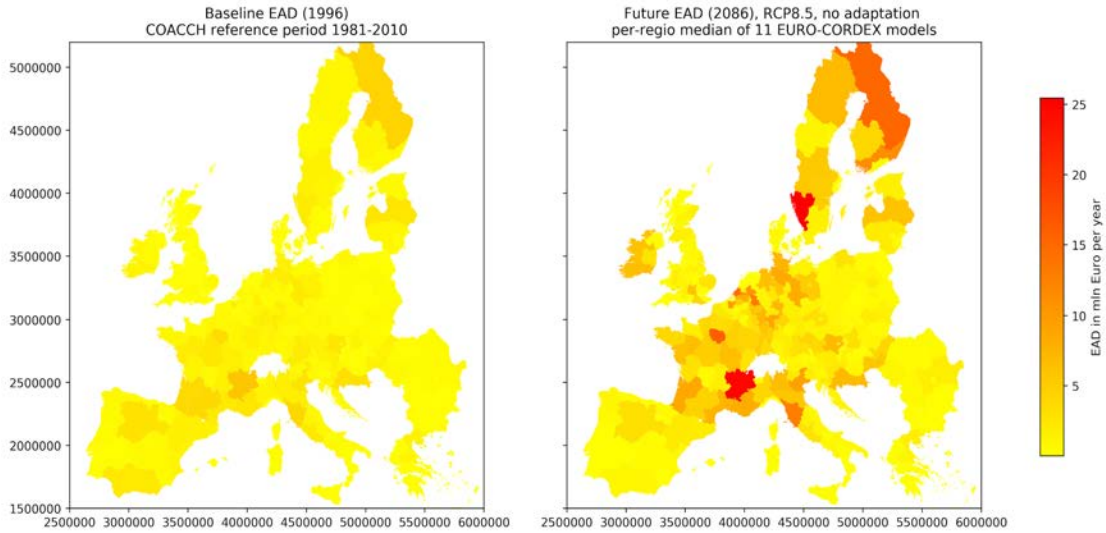

Figure 43: EAD to road infrastructure in 1996 and 2086, aggregated on NUTS-2 level

x and y coordinates according to the ETSR89/EPSG:3035 projection

Figure 45 shows how the results spatially differ over the 11 climate models. In all these figures, the price level of the damages is 2015, irrespective of the evaluation year. These values are not discounted, and also not corrected for the development of GDP in the year of evaluation. So the damage is calculated as if the floods took place in the socio-economic conditions of 2015.

*This project has received funding from the European Union's Horizon 2020 research and innovation programme under the Grant Agreement No **776479.***

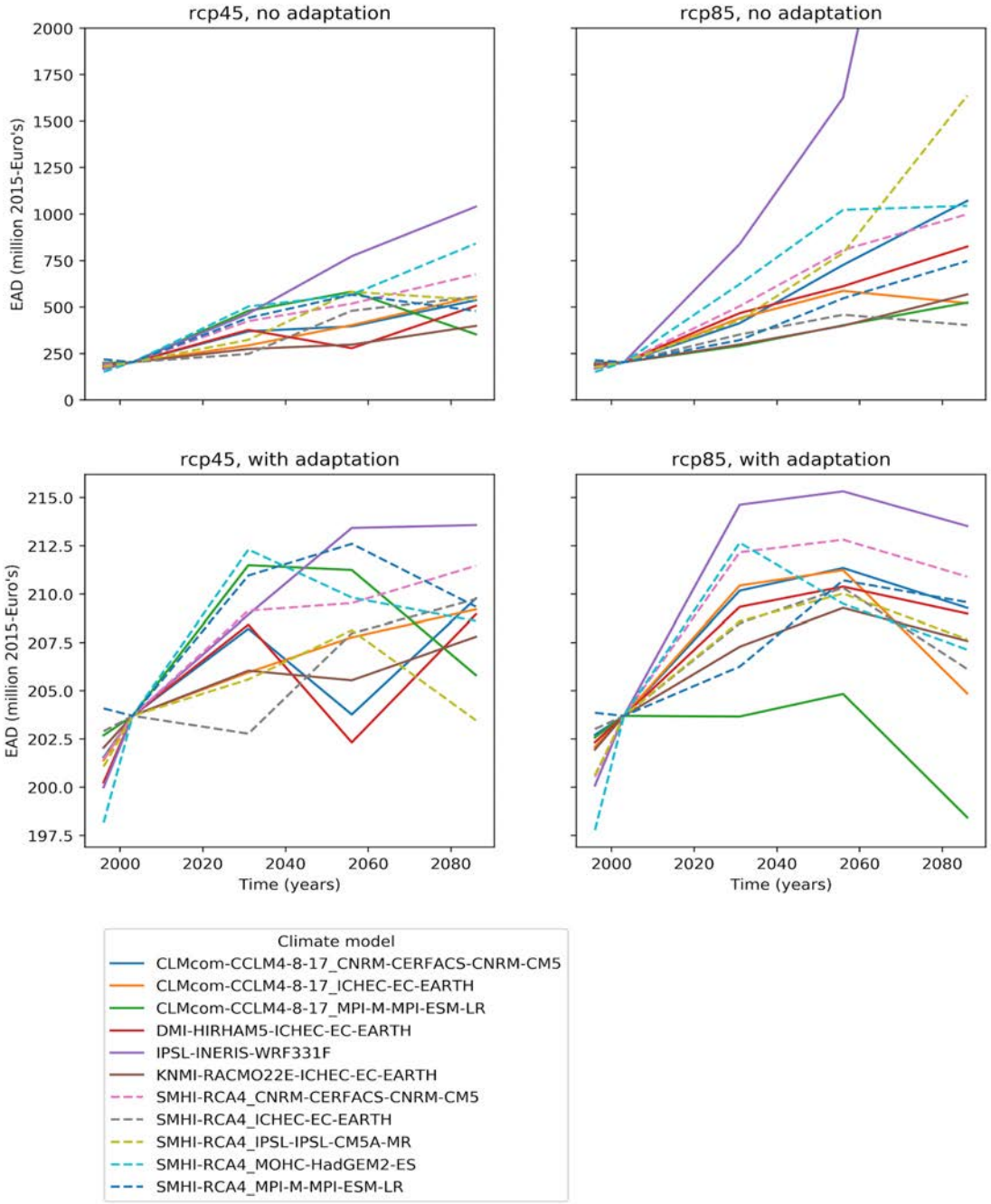

Figure 44: ***Development of flood risk over time, for EUROCORDEX combinations of regional atmospheric models and global climate models***

This project has received funding from the European Union's Horizon 2020 research and innovation programme under the Grant Agreement No ***776479.***

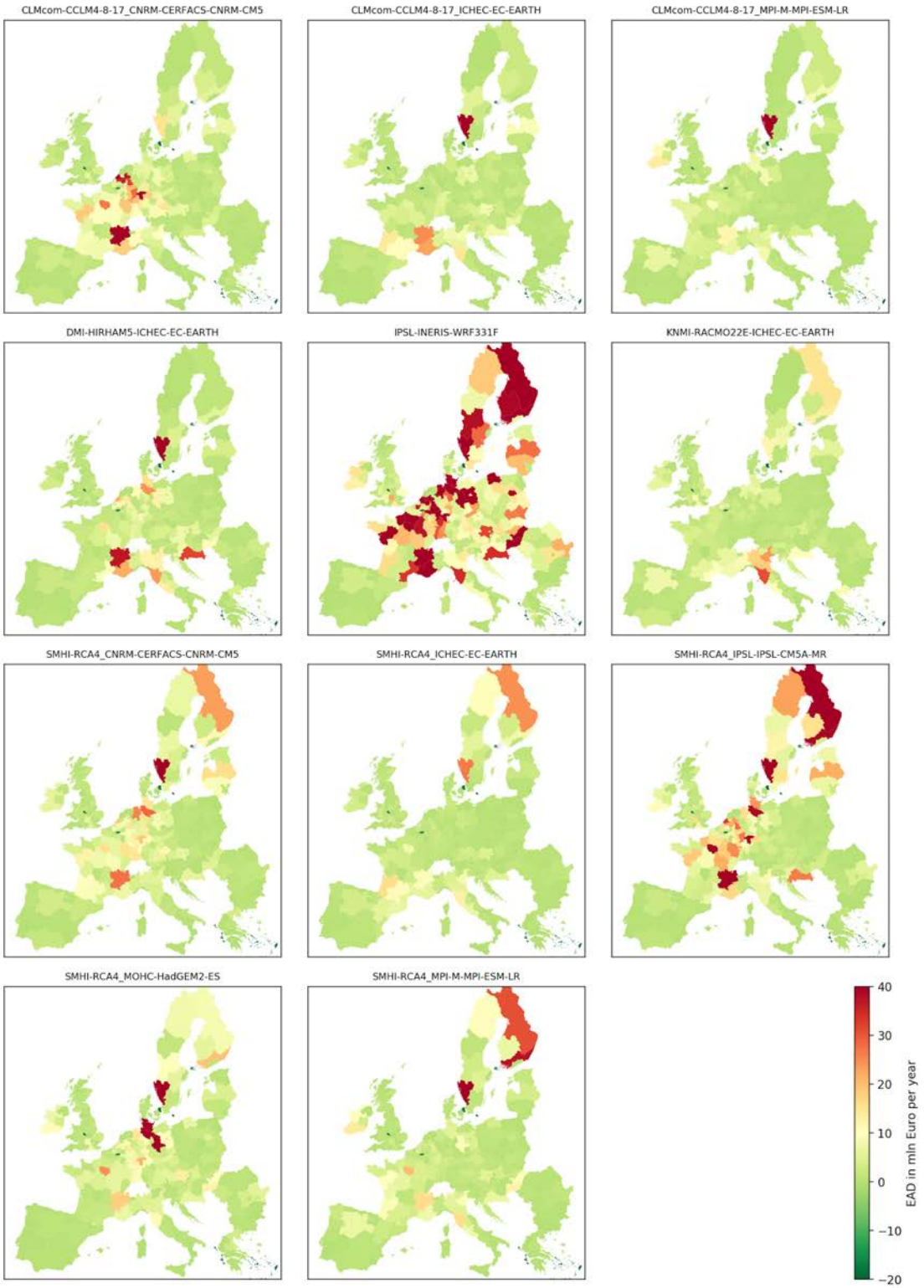

Figure 45: ***Flood risk to road infrastructure per NUTS-2 region for different climate models, RCP8.5, evaluation year 2086, no adaptation***

This project has received funding from the European Union's Horizon 2020 research and innovation programme under the Grant Agreement No ***776479.***

Climate change results: RCPs and SSPs

In this section, the development of river flood risk to road infrastructure is described for climate change (RCPs) combined with socio-economic development. The damage was linearly scaled with national development of GDP per capita according to the illustrative OECD dataset ('OECD Env-Growth') in the Shared Socioeconomic Pathways (SSPs) database of IIASA[9]. Note that these damages are not discounted.

Figure 46 shows how the flood risk develops according to 2 different RCPs for the SSP2 'Middle of the Road'. In RCP4.5, the median flood risk will increase from €158 million/year in the COACCH baseline (1996), to €494 million (2031), €954 million (2056) and €1,469 million (2086). In RCP8.5, this increase is larger, from a baseline of €162 million (1996) to €563 million (2031), €1,147 million (2056) and €2,286 million (2086). For RCP8.5, this is a change of a factor 7.1 (2056) and 14.1 (2086) respectively. These factors compare well to the estimates of Alfieri et al. (2015): 3.8-7.5 (2050) and 5.7-19 (2080).
Figure 47 shows how for RCP4.5, the flood risk differs for the SSPs.

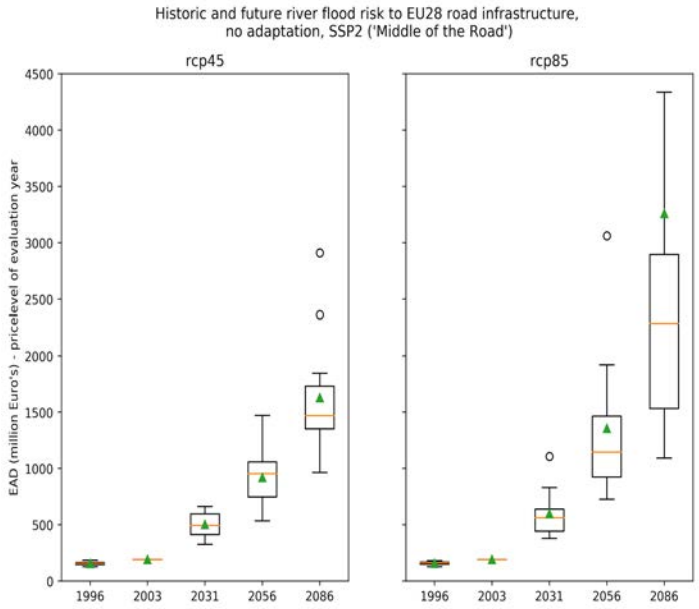

Figure 46: ***Historic and future EAD to EU28 road infrastructure****, shown for the price level in the year the floods occur (not discounted to the 2015 price level). Boxplots show the spread of the results within the EUROCORDEX model ensemble. The outliers of rcp85, evaluation year 2086, are beyond the graph.*

[9] The data of 2003 was scaled with a factor 0.895 (Eurostat, 2019), representing the difference between the EU-28 average GDP per capita in 2015 (pricelevel of damage curves OSdaMage model) and 2003 (baseline of discharge simulations). Similarly, the data of 1996 was scaled by a factor 0.801, with the help of an estimate of GDP per capita annual growth rate (1.6%) in the period 1990–2003 (European Commission, 2004).

This project has received funding from the European Union's Horizon 2020 research and innovation programme under the Grant Agreement No ***776479.***

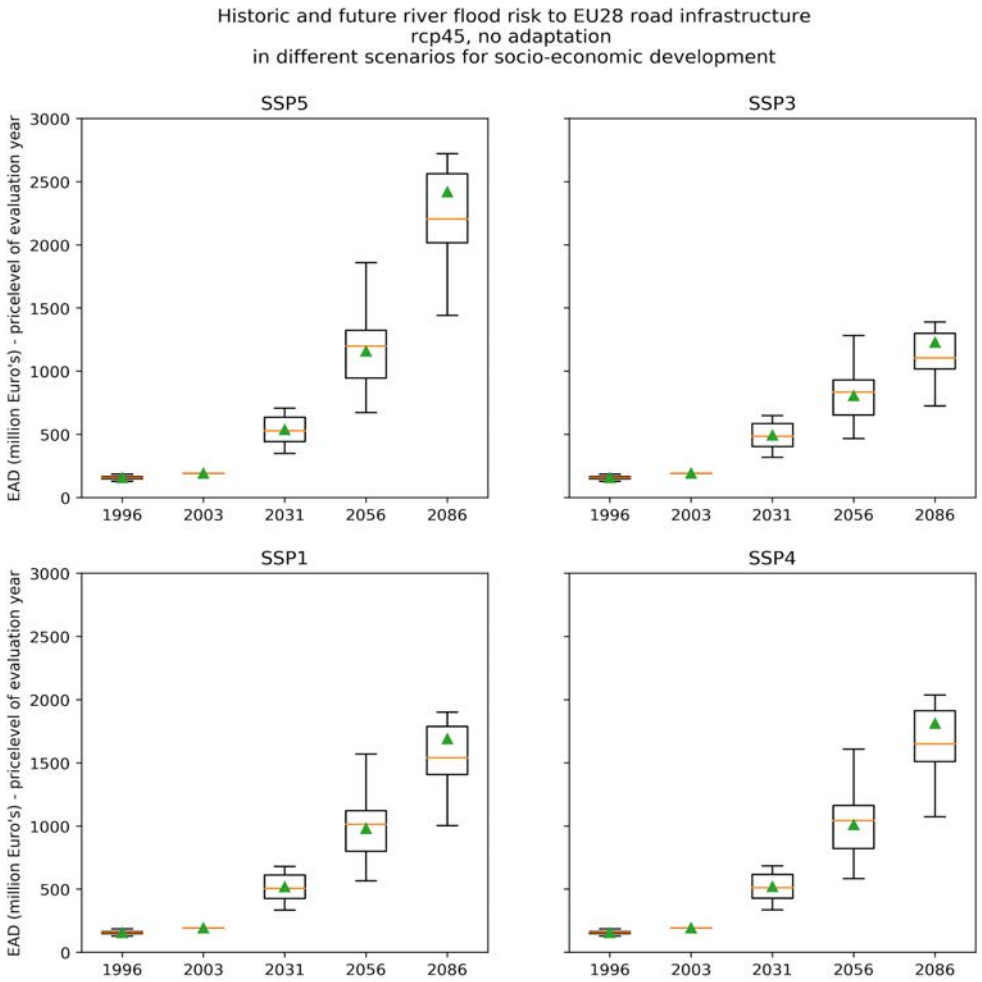

Figure 47: ***Historic and future EAD to EU28 road infrastructure****, shown for the price level in the year the floods occur (not discounted to the 2015 price level). Boxplots show the spread of the results within the EUROCORDEX model ensemble.*

This project has received funding from the European Union's Horizon 2020 research and innovation programme under the Grant Agreement No ***776479.***

4 Conclusions

This deliverable aimed at presenting the climate risks from river and coastal floods to the built environment in general, with special attention to road transport infrastructure.

Coastal floods could have the biggest effects to infrastructure, if adaptation measures are not continued and intensified. Under a (low probability) high end sea-level rise scenario with a global average mean sea-level rise of 1.7m in 2100 the annual cost of coastal floods for the European Union could reach €13 trillion in 2100 (in combination with SSP5), under the (unrealistic) assumption that there no investments into raising of existing and construction of new dikes. A medium RCP 8.5 sea-level scenario in combination with SSP5 leads to €4.5 trillion annual coastal flood cost in 2100. Regionally the impacts are highest in the north-west of Europe (North sea coast). In the Baltic sea or the Mediterranean the impacts are in general lower, with the exception of the Veneto region in northern Italy. There, large low-lying areas are combined with high surges in the northern Adria.
The investment into coastal adaptation can lower these cost to €0.16 (RCP8.5, SSP5) to €0.27 (high-end) billion, with annual investments of €15 and €40 billion. However, the investment cost are about two orders of magnitude lower than the sea flood cost without adaptation. Thus, it seems to be crucial to invest into coastal adaptation in densely populated areas in the EU.

For river floods, the GLOFRIS model estimates that expected annual damage is steadily rising over the period 2010-2080 for the EU as a whole. In 2010, expected annual damage is €9.5 billion, which increases to between €71-80 billion in 2080 for the first five scenarios given in section 3.3, while under RCP8.5-SSP5 this estimate is projected to rise as high as €255 billion. Therefore, the variability across climate- and socio-economic scenarios is quite low for all except RCP8.5-SSP5, which shows significantly higher damage estimates as a result of high growth of population and assets. Highest expected damage is seen for coastal regions on the Iberian Peninsula, southern France, Croatia, Poland and Sweden. This is mainly because the land in coastal regions is often quite flat, and thus potentially bigger areas are flooded. It is important to detect areas that are particularly vulnerable to rising risk of river flooding, as decisions have to be made early on regarding optimal adaptation strategies, such as raising protection standards, as well as household-level risk reduction.

The direct costs of river floods to road infrastructure are estimated at €205 million per year for the baseline of LISFLOOD-OSdaMage. This translates to €168 million per year in the COACCH baseline of 1996. Under RCP 4.5, and SSP2, this will increase to €504 million, €920 million and €1,630 million per year in 2031, 2056 and 2086 respectively, assuming no adaptation. Under RCP 8.5, the increase is to €598 million, €1,356 million and €3,260 million per year respectively. So without adaption, damage in SSP2 may increase by a factor 10.4 for RCP4.5 and a factor 20.6 for RCP8.5. With

*This project has received funding from the European Union's Horizon 2020 research and innovation programme under the Grant Agreement No **776479.***

adaptation, this increase in damage can be almost completely avoided. This however comes at large investment costs mainly to wide-scale improvement of the river flood protection infrastructure.

Road damage only contributes a small percentage (2.3 %) to the total river flood damage observed in the European Union (€0.205 billion of €8.8 billion annually). Still, the development of the line-based OSdaMage model has been a very useful. First of all, because the most important impact of road disruptions is not in the direct damage to the physical assets, but rather in the travel delay costs and indirect damage to trade flows. This has an impact on the economy well beyond the direct infrastructural damages. Having developed a line-based model, we can now study these effects in Work Package 3. Second, our method has identified a list of flood hot-spots in the EU road network, which could be a starting point for new investigations on the local level. This hot-spot identification was not possible with the traditional grid-based approach and gives more perspective of action to road operators. The new approach is therefore more tailored towards actual stakeholder demands. Third, it was unknown that the direct contribution of roads to overall damage was so small before we actually did this study. In several studies, higher values were found, usually in the order of 5-10% of total damage, but sometimes even up till 50-60% (Jongman et al., 2012). In a recent study, Bubeck et al. (2019) find that damage to railway infrastructure only already contributes to 10.8%-13.8% of overall flood losses. In this context, an interesting conclusion is that the new JRC grid-based approach, in which the LUISA land cover map is used rather than the CORINE land cover map, performs fairly good compared to the new line-based approach. Fourth, we found that for damage to road networks in particular, the uncertainty in the damage estimates is relatively large. This is so because flood damage to roads depends more on flow velocity than on water depth, whereas all continental-scale studies work with depth-damage functions rather than damage function that incorporate flow velocity.

Unfortunately, we were not able to combine OsdaMage with DIVA. A prototype implementation of coupling failed because of poor data availability. However, we will continue to work on the coupling beyond this deliverable.

Finally, it is interesting to compare the increase in flood damage according to the two different river flood models used in this deliverable: GLOFRIS and LISFLOOD. Note that making an absolute comparison of total damage is not very helpful, because GLOFRIS calculates the damage to the built environment, whereas LISFLOOD-OSdaMage calculates damage to road infrastructure. Therefore, we compare the relative increase in damage under climate change, for RCP 4.5, SSP2, without adaptation and for all COACCH future evaluation years relative to the model baselines. For LISFLOOD-OSdaMage, the factor change in damage is 2.5; 4.5 and 7.9 for 2031, 2056 and 2086 respectively. For GLOFRIS, the factor change is 1.7, 3.4 and 7.9 for 2030, 2050 and 2080 respectively. Therefore, the two models compare reasonably well.

*This project has received funding from the European Union's Horizon 2020 research and innovation programme under the Grant Agreement No **776479.***

Recommendations

Concerning damage to road infrastructure with the OSdaMage model, we have the following recommendations for further research. First of all, we recommend to put the direct damage in perspective of indirect estimates. This will be done in work package 3, as part of the tipping point analysis. Second, more research has to be done on the damage functions to road infrastructure. An interesting exercise is to run a more detailed inundation model which can also accurately calculate the flow velocity. However, in this context it is also important to collect more field data on actual road damage after major river flood events. Third, the effect of structural failure of bridges and tunnels on networks should be further investigated. This is a potential source of much additional flood damage. Fourth, we recommend applying the line-based method to other types of line-infrastructure, such as railways and electricity lines. Fifth, it could be interesting to create an exposure map completely on the basis of OpenStreetMap, and compare the results of these to the LUISA and CORINE land cover maps. The extra amount of detail that can be gained from vector-based datasets such as OpenStreetMaps points to a final recommendation for further research. Since vector-based datasets are nearly complete and we have shown that computational power does no longer limit the processing of these datasets, high resolution exposure and vulnerability analysis can be done. This however also requires high resolution hazard modelling, beyond the 100*100 m^2 inundation maps that can be produced at this moment. For this purpose, we recommend the development of a high resolution digital elevation model for Europe as well as further investigations into the river flood protection levels. Finally, in the future OsdaMage should and will be applied to coastal floods in order to assess the coastal flood damages due to temporary inundation and due to permanent loss of parts of the transportation networks.

*This project has received funding from the European Union's Horizon 2020 research and innovation programme under the Grant Agreement No **776479.***

5 References

Albano, R., Mancusi, L., Sole, A., & Adamowski, J. (2017). FloodRisk: a collaborative, free and open-source software for flood risk analysis. Geomatics, Natural Hazards and Risk, 8(2), 1812–1832. https://doi.org/10.1080/19475705.2017.1388854

Amadio, M., Mysiak, J., Carrera, L., & Koks, E. (2016). Improving flood damage assessment models in Italy. Natural Hazards, 82(3), 2075–2088. https://doi.org/10.1007/s11069-016-2286-0

Amadio, M., Rita Scorzini, A., Carisi, F., Essenfelder, H. A., Domeneghetti, A., Mysiak, J., & Castellarin, A. (2019). Testing empirical and synthetic flood damage models: The case of Italy. Natural Hazards and Earth System Sciences, 19(3), 661–678. https://doi.org/10.5194/nhess-19-661-2019

Alfieri, L., Feyen, L., Dottori, F., & Bianchi, A. (2015). Ensemble flood risk assessment in Europe under high end climate scenarios. Global Environmental Change, 35, 199–212. https://doi.org/10.1016/j.gloenvcha.2015.09.004

Alfieri, L., Feyen, L., & Di Baldassarre, G. (2016a). Increasing flood risk under climate change: a pan-European assessment of the benefits of four adaptation strategies. Climatic Change, 136(3–4), 507–521. https://doi.org/10.1007/s10584-016-1641-1

Alfieri, L., Feyen, L., Salamon, P., Thielen, J., Bianchi, A., Dottori, F., & Burek, P. (2016b). Modelling the socio-economic impact of river floods in Europe. Natural Hazards and Earth System Sciences, 16(6), 1401–1411. https://doi.org/10.5194/nhess-16-1401-2016

Bruijn, K. de, Wagenaar, D., Slager, K., Bel, M. de, & Burzel, A. (2014). Updated and improved method for flood damage assessment. Delft.

Carisi, F., Schröter, K., Domeneghetti, A., Kreibich, H., & Castellarin, A. (2018). Development and assessment of uni- and multivariable flood loss models for Emilia-Romagna (Italy). Natural Hazards and Earth System Sciences, 18(7), 2057–2079. https://doi.org/10.5194/nhess-18-2057-2018

Carruthers, R (2013). What prospects for transport infrastructure and impacts on growth in southern and eastern Mediterranean countries? MEDPRO Report No. 3.

Collier, P., Kirchberger, M., & Soderbom, M. (2015). The Cost of Road Infrastructure in Low and Middle Income Countries.

Doll, C., & Van Essen, H. (2008). Road infrastructure cost and revenue in Europe Produced within the study Internalisation Measures and Policies for all external cost of Transport (IMPACT) – Deliverable 2. Retrieved from https://ec.europa.eu/

*This project has received funding from the European Union's Horizon 2020 research and innovation programme under the Grant Agreement No **776479.***

transport/sites/transport/files/themes/sustainable/studies/doc/2008_road_infrastructure_costs_and_revenues.pdf

Dottori, F., Martina, M. L. V., & Figueiredo, R. (2018). A methodology for flood susceptibility and vulnerability analysis in complex flood scenarios. Journal of Flood Risk Management, 11, S632–S645. https://doi.org/10.1111/jfr3.12234

Estrada, F., Botzen, W. W., & Tol, R. S. (2017). A global economic assessment of city policies to reduce climate change impacts. Nature Climate Change, 7(6), 403.

Estrada, F., Botzen ,W. (2018). Economic impacts and risks of climate change and benefits of current climate negotiations. Working paper.

European Commission (2004). The European Union economy: 2003 review. European Commission, Directorate-General for Economic and Financial Affairs. Retrieved from https://ec.europa.eu/economy_finance/publications/pages/publication7694_en.pdf

European Court of Auditors. (2013). Are EU Cohesion Policy funds well spent on roads? Special Report No 5/2013. https://doi.org/10.2865/71435

Hempel, S., Frieler, K., Warszawski, L., Schewe, J., Piontek, F., 2013. A trend-preserving bias correction – The ISI-MIP approach. Earth Syst. Dyn. https://doi.org/10.5194/esd-4-219-2013

Heralova, R. S., Hromada, E., & Johnston, H. (2014). Cost structure of the highway projects in the Czech Republic. Procedia Engineering, 85, 222–230. https://doi.org/10.1016/j.proeng.2014.10.547

Hinkel, J., Klein R. J. T. (2009). Integrating knowledge to assess coastal vulnerability to sea-level rise: The development of the DIVA tool. Global Environ Change 19(3), p. 384-395. DOI: 10.1016/j.gloenvcha.2009.03.002

Hinkel, J., Nicholls, R. J., Tol, R. S., Wang, Z. B., Hamilton, J. M., Boot, G., Vafeidis, A. T., McFadden, L., Ganopolski, A. and Klein; R. J. T. (2013). A global analysis of coastal erosion of beaches due to sea-level rise: An application of DIVA. In: Global and Planetary Change 111, p. 150-158. DOI: 10.1016/j.gloplacha.2013.09.002.

Hinkel, J., Lincke, D., Vafeidis, A.T., Perrette, M., Nicholls, R. J., Tol, R. J. S., Marzeion, B., Fettweis, X., Ionescu, C. and Levermann, A. (2014). Coastal flood damage and adaptation cost under 21st century sea-level rise. Proceedings of the National Academy of Sciences 111(9), p. 3292-3297. DOI: 10.1073/pnas.1222469111

Hoozemans, F.M.J., Marchand, M. and Pennekamp; H. A. (1993). A Global Vulnerability Analysis: Assessment for Population, Coastal Wetlands and Rice Production on a Global Scale, 2nd Edition. Delft Hydraulics, the Netherlands.

*This project has received funding from the European Union's Horizon 2020 research and innovation programme under the Grant Agreement No **776479.***

Huizinga, H. J. (2007). Flood damage functions for EU member states. Lelystad, The Netherlands.

Huizinga, J., Moel, H. de, Szewczyk, W., 2017. Global flood depth-damage functions. Methodology and the database with guidelines. EUR 28552 EN. doi: 10.2760/16510

Jongman, B., Kreibich, H., Apel, H., Barredo, J. I., Bates, P. D., Feyen, L., … Ward, P. J. (2012). Comparative flood damage model assessment: Towards a European approach. Natural Hazards and Earth System Science, 12(12), 3733–3752. https://doi.org/10.5194/nhess-12-3733-2012

Jongman, B., Hochrainer-Stigler, S., Feyen, L., Aerts, J. C. J. H., Mechler, R., Botzen, W. J. W., … Ward, P. J. (2014). Increasing stress on disaster-risk finance due to large floods. Nature Climate Change, 4(4), 264–268. https://doi.org/10.1038/nclimate2124

Kebede, A.S., R.J. Nicholls, S. Brown and S. Hanson (2010). Coastal zone. In Mozambique: Economics of Adaptation to Climate Change, World Bank, Washington DC, pp. 47-58.

Klein Goldewijk, K., Beusen, A., Van Drecht, G. & De Vos, M. (2011). The HYDE 3.1 Spatially Explicit Database of Human-Induced Global Land-use Change over the Past 12,000 Years. *Global Ecology and Biogeography, 20, pp. 73-86.*

Koks, E. E., Rozenberg, J., Zorn, C., Tariverdi, M., Vousdoukas, M., Fraser, S. A., … Hallegatte, S. (2019). A global multi-hazard risk analysis of road and railway infrastructure assets. Nature Communications, 10(1), 1–11. https://doi.org/10.1038/s41467-019-10442-3

Kreibich, H., Piroth, K., Seifert, I., Maiwald, H., Kunert, U., Schwarz, J., … Thieken, A. H. (2009). Is flow velocity a significant parameter in flood damage modelling? Natural Hazards and Earth System Science, 9(5), 1679–1692. https://doi.org/10.5194/nhess-9-1679-2009

Lincke, D., Hinkel J. (2018). Economically robust protection against 21st century sea-level rise. Global Environmental Change 51, p. 67-73. DOI: 10.1016/j.gloenvcha.2018.05.003

Meinshausen, M., Raper, S. C., & Wigley, T. M. (2011). Emulating coupled atmosphere-ocean and carbon cycle models with a simpler model, MAGICC6–Part 1: Model description and calibration. Atmospheric Chemistry and Physics, 11(4), 1417-1456.

Messner F, et al. (2007) .Evaluating flood damages: Guidance and recommendations on principles and methods. FLOODsite Project Deliverable D9.1. Available at http://www.floodsite.net/html/partner_area/project_docs/T09_06_01_Flood_damage_guidelines_d9_1_v2_2_p44.pdf.. Accessed August 26, 2019.

*This project has received funding from the European Union's Horizon 2020 research and innovation programme under the Grant Agreement No **776479.***

Muis, S., Verlaan, M., Winsemius, H., Aerts, J. C. J. H., Ward, P. (2016). A global reanalysis of storm surges and extreme sea levels. Nat Communications 7. DOI: 10.1038/ncomms11969.

Nicholls, R.J., S. Brown, S. Hanson, and J. Hinkel (2010). Economics of coastal zone adaptation to climate change, Climate and Development, World Bank Discussion Papers, 10, World Bank, Washington DC, 48pp.

Nicholls, R.J., S. Hanson and J. Hinkel (2013). The economics of adaptation in the coastal sector - In Economics of Climate Change in East Asia - Westphal, Michael L., Hughes, Gordon A. and Brömmelhörster, Jörn (eds.) Asian Development Bank, Manila, p. 60-83.

Nicholls, R.J., D. Lincke, J. Hinkel, T.v.d. Pol (2018). Global Investment Costs for Coastal Defence Through the 21st Century. In: Rozenberg, J. and M. Fay (2019). Beyond the Gap : How Countries Can Afford the Infrastructure They Need while Protecting the Planet. Sustainable Infrastructure;. Washington, DC: World Bank. https://openknowledge.worldbank.org/handle/10986/31291

Nijland, H., Wortelboer-van Donselaar, P. M., Korteweg, J. A. C., & Snellen, D. (2010). 'Met de kennis van nu': leren van evalueren Een casestudy: A5 Verlengde Westrandweg. The Hague: Netherlands Environmental Assessment Agency.

Nordhaus, W. D., & Yang, Z. (1996). A regional dynamic general-equilibrium model of alternative climate-change strategies. The American Economic Review, 741-765.

Nordhaus, W. D. (2014). A question of balance: Weighing the options on global warming policies. Yale University Press.

Nordhaus, W. D. (2017). Revisiting the social cost of carbon. Proceedings of the National Academy of Sciences, 114(7), 1518-1523.

Olsen, A. S., Zhou, Q., Linde, J. J., & Arnbjerg-Nielsen, K. (2015). Comparing methods of calculating expected annual damage in urban pluvial flood risk assessments. Water (Switzerland), 7(1), 255–270. https://doi.org/10.3390/w7010255

OpenStreetMap contributors. (2019). Europe dump of OpenStreetMap. Downloaded January 7, 2019.

Peltier, W. R., Argus, D. F., and Drummond, R. (2015). Space geodesy constrains ice age terminal deglaciation: The global ICE-6G_C (VM5a) model, J. Geophys. Res. Solid Earth 120, p. 450-487, DOI:10.1002/2014JB011176.

Prahl, B. F., Boettle, M., Costa, L., Kropp, J. P., & Rybski, D. (2018). Damage and protection cost curves for coastal floods within the 600 largest European cities.

*This project has received funding from the European Union's Horizon 2020 research and innovation programme under the Grant Agreement No **776479.***

Scientific Data, 5(1), 180034. https://doi.org/10.1038/sdata.2018.34

Riahi, K., Van Vuuren, D. P., Kriegler, E., Edmonds, J., O'neill, B. C., Fujimori, S., ... & Lutz, W. (2017). The shared socioeconomic pathways and their energy, land use, and greenhouse gas emissions implications: an overview. Global Environmental Change, 42, 153-168.

Rogowsky, W. (2013). Erfahrungsbericht vor Ort beim Hochwasser 2013 in Bayern. Deggendorf.

Rosina, K., Batista e Silva, F., Vizcaino, P., Marín Herrera, M., Freire, S., & Schiavina, M. (2018). Increasing the detail of European land use/cover data by combining heterogeneous data sets. International Journal of Digital Earth, 8947. https://doi.org/10.1080/17538947.2018.1550119

Sadoff, C.W., Hall, J.W., Grey, J.C.J.H., Aerts, Dan., Ait-Kadi, M., Brown, C., Cox, A., Dadson, S., Garrick, D., Kelman, J., McCornick, P., Ringler, C., Rosegrant, M., Whittington, D., Wiberg, D. (2015). Securing Water, Sustaining Growth: Report of the GWP/OECD Task Force on Water Security and Sustainable Growth.

Schröter, K., Kreibich, H., Vogel, K., Riggelsen, C., Scherbaum, F., & Merz, B. (2014). How useful are complex flood damage models? Water Resources Research, 50(4), 3378–3395. https://doi.org/10.1002/2013WR014396

Scussolini, P., Aerts, J. C. J. H., Jongman, B., Bouwer, L. M., Winsemius, H. C., de Moel, H., and Ward, P. J. (2016). FLOPROS: an evolving global database of flood protection standards, Nat. Hazards Earth Syst. Sci. 16, 1049-1061, DOI: 10.5194/nhess-16-1049-2016.

Spencer, T., M. Schuerch, R. J. Nicholls, J. Hinkel, D. Lincke, A.T. Vafeidis, R. Reef, L. McFadden, S. Brown (2016). Global coastal wetland change under sea-level rise and related stresses: The DIVA Wetland Change Model. Global and Planetary Change 139, p. 15-30. DOI: 10.1016/j.gloplacha.2015.12.018

Stehfest, E., van Vuuren, D., Kram, T., Bouwman, L., Alkemade, R., Bakkenes, M., Biemans, H., Bouwman, A., Den Elzen, M., Janse, J., Alkemade, R., Bakkenes, M., Biemans, H., Bouwman, A., Den Elzen, M., Janse, J., Lucas, P., van Minnen, J., Muller, C., Prins, A.G., 2014. Integrated assessment of global environmental change with IMAGE 3.0, Model description and policy applications, The Hague: PBL Netherlands Environmental Assessment Agency.

Stocker, T. F., Qin, D., Plattner, G. K., Tignor, M., Allen, S. K., Boschung, J., ... & Midgley, P. M. (2013). Climate change 2013: The physical science basis.

Sutanudjaja, E. H., Van Beek, R., Wanders, N., Wada, Y., Bosmans, J. H., Drost, N., ... & Karssenberg, D. (2018). PCR-GLOBWB 2: a 5 arcmin global hydrological and water resources model. Geoscientific Model Development,

*This project has received funding from the European Union's Horizon 2020 research and innovation programme under the Grant Agreement No **776479.***

11(6), 2429-2453.

Taylor, K. E., Stouffer, R.J., Meehl, G.A., 2012. An overview of CMIP5 and the experiment design. Bull. Am. Meteorol. Soc. https://doi.org/10.1175/BAMS-D-11-00094.1

UNISDR (2015). Proposed Updated Terminology on Disaster Risk Reduction: A Technical Review. Community, Environ. Disaster Risk Manag. https://doi.org/10.1108/S2040-7262(2011)0000007007

Yohe, G. and R.S.J. Tol (2002). Indicators for social and economic coping capacity: moving toward a working definition of adaptive capacity. Global Environmental Change 12, p. 25-40.

Vafeidis, A. T., R. J. Nicholls, L. McFadden, R. S. J. Tol, J. Hinkel, T. Spencer, P. S. Grashoff, G. Boot, and R. J. T. Klein (2008). "A New Global Coastal Database for Impact and Vulnerability Analysis to Sea-Level Rise." Journal of Coastal Research 24(4). p. 917-24. DOI: 10.2112/06-0725.1

Van Beek, L. P. H., Bierkens, M.F.P., 2009. The Global Hydrological Model PCR-GLOBWB: Conceptualization, Parameterization and Verification, Report Department of Physical Geography, Utrecht University, Utrecht, The Netherlands

Van Beek, L. P. H., Wada, Y., Bierkens, M.F.P., 2011. Global monthly water stress: 1. Water balance and water availability. Water Resour. Res. https://doi.org/10.1029/2010WR009791

Van Vuuren, D. P., Lucas, P.L., Hilderink, H., 2007. Downscaling drivers of global environmental change: Enabling use of global SRES scenarios at the national and grid levels. Glob. Environ. Chang. https://doi.org/10.1016/j.gloenvcha.2006.04.004

Vennapusa, P. K. R., White, D. J., & Miller, D. K. (2013). Western Iowa Missouri River Flooding — Geo-Infrastructure Damage Assessment, Repair and Mitigation Strategies. Retrieved from http://trid.trb.org/view.aspx?id=1261618

Ward, P. J., Jongman, B., Aerts, J.C.J.H., Bates, P.D., Botzen, W.J.W., DIaz Loaiza, A., Hallegatte, S., Kind, J.M., Kwadijk, J., Scussolini, P., Winsemius, H.C., 2017. A global framework for future costs and benefits of river-flood protection in urban areas. Nat. Clim. Chang. https://doi.org/10.1038/nclimate3350

Ward, P. J., Jongman, B., Weiland, F.S., Bouwman, A., Van Beek, R., Bierkens, M.F.P., Ligtvoet, W., Winsemius, H.C., 2013. Assessing flood risk at the global scale: Model setup, results, and sensitivity. Environ. Res. Lett. https://doi.org/10.1088/1748-9326/8/4/044019

Weedon, G. P., Gomes, S., Viterbo, P., Shuttleworth, W.J., Blyth, E., Österle, H., Adam, J.C., Bellouin, N., Boucher, O., Best, M., 2011. Creation of the WATCH

*This project has received funding from the European Union's Horizon 2020 research and innovation programme under the Grant Agreement No **776479.***

Forcing Data and Its Use to Assess Global and Regional Reference Crop Evaporation over Land during the Twentieth Century. J. Hydrometeorol. https://doi.org/10.1175/2011jhm1369.1

Winsemius, H. C., Aerts, J. C., van Beek, L. P., Bierkens, M. F., Bouwman, A., Jongman, B., ... & Ward, P. J. (2016). Global drivers of future river flood risk. Nature Climate Change, 6(4), 381.

Winsemius, H. C., Van Beek, L.P.H., Jongman, B., Ward, P.J., Bouwman, A., 2013. A framework for global river flood risk assessments. Hydrol. Earth Syst. Sci. https://doi.org/10.5194/hess-17-1871-2013

*This project has received funding from the European Union's Horizon 2020 research and innovation programme under the Grant Agreement No **776479.***